ABSTRACT

DYNAMIC SIMULATIONS OF PARTICLE SUSPENSIONS SUBJECTED TO AN EXTERNAL ELECTRIC FIELD

by
Xianjin Jiang

A numerical method is performed to study the suspension of polarizable particles in nonconductive solvents subjected to external electric fields. Such particles experience both hydrodynamic and electrostatic interactions. The hydrodynamic force acting on the particles is determined using the Stokesian dynamics method under the assumption that the Reynolds number is much smaller than 1, while the electrostatic force is determined by differentiating the electrostatic energy of the suspension, which is computed from the induced particle dipoles. In addition, the multiple image method is used to compensate for the electrostatic force when two particles are close to each other. Because the electrostatic energy accounts for both far- and near-field interactions, so does the corresponding force.

In this thesis, a monodisperse suspension of hard, dielectric spheres in a Newtonian fluid contained in a channel and subjected to an electrical field due to energized electrodes embedded in the channel walls was considered. The transient particles motion is studied both under static conditions and when a pressure driven flow is applied, and in the case of a uniform and non-uniform electric field. The results show that the electrostatic energy method applied in the past to the case of a uniform electric field only can be extended to the situation where the electric field is non-uniform.

DYNAMIC SIMULATIONS OF PARTICLE SUSPENSIONS SUBJECTED TO AN EXTERNAL ELECTRIC FIELD

by
Xianjin Jiang

A Dissertation
Submitted to the Faculty of
New Jersey Institute of Technology
In Partial Fulfillment of the Requirements for the Degree of
Doctor of Philosophy in Mechanical Engineering

Department of Mechanical Engineering

January 2006

APPROVAL PAGE

DYNAMIC SIMULATIONS OF PARTICLE SUSPENSIONS SUBJECTED TO AN EXTERNAL ELECTRIC FIELD

Xianjin Jiang

Dr. Nadine Aubry, Dissertation Advisor — Date
Distinguished Professor of Mechanical Engineering, New Jersey Institute of Technology

Dr. Ernest S. Geskin, Committee Member — Date
Professor of Mechanical Engineering, New Jersey Institute of Technology

Dr. Peter Petropoulos, Committee Member — Date
Professor of Mathematical Sciences, New Jersey Institute of Technology

Dr. Pushpendra Singh, Dissertation Co-Advisor — Date
Professor of Mechanical Engineering, New Jersey Institute of Technology

Dr. Chao Zhu, Committee Member — Date
Associate Professor of Mechanical Engineering, New Jersey Institute of Technology

BIOGRAPHICAL SKETCH

Author: Xianjin Jiang

Degree: Doctor of Philosophy

Undergraduate and Graduate Education:

- Doctor of Philosophy in Mechanical Engineering,
  New Jersey Institute of Technology, Newark, NJ, 2006
- Master of Engineering in Mechanical Engineering,
  Institute of Mechanics, CAS, Beijing, P. R. China, 2000
- Bachelor of Engineering in Engineering Mechanics,
  Tsinghua University, Beijing, P. R. China, 1992

Major: Mechanical Engineering

Presentations and Publications

Xianjin Jiang, N. Aubry, P. Singh. Numerical Study of Suspensions of Particles in Electrorheological Fluids. To be submitted.

Xianjin Jiang, N. Aubry, P. Singh. Dielectrophoretic Manipulation of Spherical Particles. In preparation.

Xianjin Jiang, N. Aubry, P. Singh. Dynamic Simulation of Dielectrophoresis in Colloidal Suspensions. 58th annual meeting of the division of fluid dynamics, APS, Chicago, IL.

To my beloved daughter, Rachel Yue; son, Edward Yue; husband, Baohua Yue; my parents, Zhongmin Jiang and Fengrong Wang; in-laws, Guangxing Yue and Jiaying Sun.

ACKNOWLEDGMENT

My sincere gratitude goes to my advisors, Dr. Nadine Aubry and Dr. Pushpendra Singh, who not only gave me utmost freedom in my research and opened up a new area of interest, but also provided constant support, valuable discussions, guidance and encouragement. They have been more than advisors, mentors whom I learned so much from.

I gratefully acknowledge the support of the Department of Mechanical Engineering, New Jersey Institute of Technology, and the support of the New Jersey Center for Micro flow Control during this work.

I would also like to thank Dr. Ernest S. Geskin, Dr. Chao Zhu, and Dr. Peter Petropoulos for actively participating in my committee. And I would like to thank Dr. Demetrius Papageorgiou for participating in my proposal presentation.

During my graduate study, I was fortunate to receive help from Sharyn Serafin, Quan Jin, Dr. Linjin Zhu, Dr. Arnaud Goullet and many other NJIT friends.

I am deeply indebted to my parents, Zhongmin Jiang and Fengrong Wang, my husband, Baohua Yue, children Rachel and Edward for their sacrifices and support during my many years of study. Special thanks are also given to Prof. Zhichi Zhu and Prof. Zhu Ruan for their help and constant encouragement.

TABLE OF CONTENTS

Chapter	Page
1 INTRODUCTION	1
1.1 Overview	1
1.1.1 Dielectric Material	2
1.1.2 Dielectric Constant	2
1.1.3 Dipole Moment	3
1.2 Background and Theory	3
1.2.1 Hydrodynamics Force	3
1.2.2 Brownian Force	4
1.2.3 Buoyancy Force	4
1.3 Electorheological Fluid	5
1.3.1 Fundamentals and Mechanisms	6
1.3.2 Electrostatic Force	8
1.3.3 Applications of ER Fluid	13
1.4 Dielectrophoresis	14
1.4.1 Theory	14
1.4.2 Dielectrophoresis (DEP) Force	16
1.4.3 Applications of Dielectrophoresis	17
1.5 Objectives and Outline of This Thesis	20
1.5.1 Objectives	20
1.5.2 Outlines	21

TABLE OF CONTENTS
(Continued)

Chapter	Page
2 PHYSICS MODELS AND GOVERNING EQUATIONS	23
2.1 Physical Model	23
2.2 Governing Equations	24
2.2.1 Electric Field	24
2.2.2 Fluid Flow	25
2.2.3 Particle Motion	26
2.2.4 Repulsive Force	27
2.3 Numerical Method	28
2.3.1 Electric Field	28
2.3.2 Fluid Flow	29
3 ELECTROSTATIC FORCE	31
3.1 Exact Electrostatic Force for Two Particles in a Uniform Field	32
3.1.1 Electrical Potential of the Particles	33
3.1.2 Electrostatic Force on the Particles	36
3.2 Two Particles Multiple Image Method	38
3.2.1 Image Method for a Uniform Electric Field	39
3.2.2 Dipole Moment in Particles in the Case of a Non-uniform Field	44
3.3 Multi-Particles Electrostatic Force	46
3.3.1 Taylor Expansion	47
3.3.2 Electrostatic Force	48

TABLE OF CONTENTS
(Continued)

Chapter **Page**

3.3.3 Electrostatic Force with Near-field Effects 51

3.3.4 Electrostatic Force without the Near-field Effects 52

4 TWO PARTICLES PROBLEM 56

4.1 Two Particles in Uniform Field 56

4.1.1 Convergence of the Multiple Image Method 56

4.1.2 Comparison of the Force Computed with Different Methods 58

4.1.3 Comparison of Particles Trajectories 62

4.1.4 Attraction, Repulsion, and Alignment 64

4.1.5 Discussion 67

4.2 Two Particles Suspension with Non-Uniform Electric Field 68

4.2.1 Positive DEP ($\beta > 0$) 69

4.2.2 Discussion 79

4.3 Conclusions 80

5 MULTI-PARTICLES PROBLEM 81

5.1 Negative DEP 82

5.1.1 Electrical Field 84

5.1.2 Negative DEP with dp/dx=0 86

5.1.3 Negative DEP with dp/dx≠0 92

5.14 Discussion 96

5.2 Positive DEP 96

TABLE OF CONTENTS
(Continued)

Chapter	Page
5.2.1 Electrical Field	97
5.2.2 Positive DEP with dp/dx=0	98
5.2.3 Positive DEP with dp/dx≠0	102
5.2.4 Discussion	105
5.3 Conclusions	105
6 CONCLUDING REMARKS AND RECOMMENDATIONS FOR FUTURE WORK	107
REFERENCES	109

LIST OF TABLES

Table		Page
4.1	Convergence of Multiple Image Method	58
4.2	Comparison of the Force Functions for a Two-particle Suspension in a Uniform Electric Field	60
4.3	Comparison of Two-particle Force Components in Non-uniform Electric Field	74

LIST OF FIGURES

Figure **Page**

1.1 Diagram of a charged particle and a neutral particle in a non-uniform electric field. The positively charged body moves towards the negative electrode. The neutral body, on another hand, is polarized and therefore attracted towards areas where the electric field is the strongest (when the body is more polarizable than the surrounding medium) or the weakest (if the body is less polarizable)..... 15

2.1 Sketch of the diagram of two polarizable particles suspended in a fluid and subjected to an electric field..... 23

2.2 Schematic of the imposed near field repulsive force between two particles..... 27

3.1 Schematic of two dielectric particles suspended in a dielectric fluid. Two systems of spherical coordinates are considered: A right-hand one whose origin coincides with the center of Particle 1, and a left-hand one whose origin coincides with the center of Particle 2..... 34

3.2 Illustration of the interaction between Particle a and Particle b through multiple images of the dipole moments..... 40

3.3 Two equal-sized dielectric spheres in a uniform electric field..... 42

4.1 Force versus the particle-to-fluid dielectric constant ratio β when the distance between the two particles is (a) $r = 3a$; (b) $r = 6a$..... 61

4.2 (a) Trajectory of Particle 1 in a two-particle motion computed with four methods. The x-coordinate of Particle 1 as a function of time, computed with four different methods. (c) The y-coordinate of Particle 1 as a function of time, computed with the four different methods. (■ NF refers to the energy method with the inclusion of the near-field effects; • FF refers to the energy method in which the near-field effects have been neglected; × DD refers to the dipole-induced-dipole method; Δ IM refers to the image method where fifteen terms have been retained.)..... 63

LIST OF FIGURES
(Continued)

Figure **Page**

4.3 Electrostatic interactions between two particles, denoted by 1 ( ) and 2 (▲), suspended in a uniform electric field: (a) two particles attract each other when the line joining their centers is parallel to the electric field; (b) two particles repulse each other when the line joining their centers is perpendicular to the electric field; (c) two particles rotate and align with the applied electric field when the line joining their centers is neither parallel nor perpendicular to the electric field..... 66

4.4 Sketch of the domain, showing the electrodes in the x-y plane outside the fluid box for positive dielectrophoresis ($\beta > 0$). A, B indicate the electrodes, A being the energized electrode, B being the grounded electrode..... 69

4.5 Solution of the Laplace equation. (a) Electric field **E** lines; (b) Force ($\mathbf{E} \cdot \nabla \mathbf{E}$) lines..... 70

4.6 The y-coordinate of the first particle as a function of time, computed using four different time steps: (a) ▲ ; (b) ■ $1.25*10^{-4}$; (c) ○ $2.5*10^{-4}$; (d) $5.0*10^{-4}$..... 71

4.7 Comparison of the trajectories of two particles in the case of positive dielectrophoresis obtained with the image method and the DEP force only. (a) Full view of the trajectories; (b) close view of the two particles as the latter are close to each other, near x = 1.28mm..... 76

4.8 Comparison of the first particle's y coordinate as a function of time in the case of positive dielectrophoresis computed with the image method and the DEP force only. (a) Full view; (b) close view as the particles get close to each other..... 76

4.9 Comparison of the trajectories of the two particles in the case of positive dielectrophoresis computed with the image method, the energy method without near-field interaction, and the point-dipole method. (a) General view of the trajectories; (b) closer view as the particles get close to each other, near x = 1.22mm..... 77

4.10 Comparison of the trajectory of the two particles in the x-y plane, computed with various methods..... 78

4.11 Comparison of the y coordinate of the first particle as it evolves in time, computed with various methods..... 79

LIST OF FIGURES
(Continued)

Figure **Page**

5.1 Sketch of the domain considered for the manipulation of particles by means of dielectrophoresis, where the location of electrodes (green and red) along the walls and various dimensions are specified..... 83

5.2 Particle array in 3-D view consisting of two layers with 20 particles in each layer..... 84

5.3 Contours of the (dimensionless) electric potential φ..... 84

5.4 Solution of Laplace's equation. (a) Electric field (**E**) lines; (b) Electric force ($\mathbf{E}\cdot\nabla\mathbf{E}$) lines..... 85

5.5 Trajectory of Particle 1 in a nonuniform electric field. (a) x-y plot; (b) x-t plot..... 87

5.6 Instantaneous snapshots of the suspension computed by using the image method including the near-field interactions at the various times: (a) t = 0s; (b) t = 0.1s; (c) t = 0.25s; (d) t = 1s; (e) t = 2s. There is no pressure driven flow in this simulation..... 90

5.7 Instantaneous snapshots of the suspension computed by using the image method excluding the near-field interaction at the various times: (a) t = 0s; (b) t = 0.1s; (c) t = 0.25s; (d) t = 1s; (e) t = 2s. There is no pressure driven flow in this simulation..... 91

5.8 Instantaneous snapshots of the suspension structure with the inclusion of near-field interactions (image method) with pressure driven flow (dp/dx = 10 pas./m), at various times: (a) t = 0.1s; (b) t = 0.25s; (c) t = 0.5s; (d) t = 1s..... 93

5.9 Instantaneous snapshots of the suspension structure with the inclusion of near-field interactions (image method) with pressure driven flow (dp/dx = 20 pas./m) at various times: (a) t = 0.1s; (b) t = 0.25s; (c) t = 0.5s; (d) t = 1s. 94

5.10 Instantaneous snapshots of the suspension structure with the inclusion of the near-field interactions (image method) with pressure driven flow (dp/dx = 200 pas./m) at various times: (a) t = 0.1s; (b) t = 0.25s; (c) t = 0.5s; (d) t = 1s..... 95

5.11 Sketch of the Computational Space for Positive DEP (not to scale)..... 97

5.12 Contours of the dimensionless electric potential φ..... 98

LIST OF FIGURES
(Continued)

Figure **Page**

5.13 The solution of the Laplace equation. (a) Electric field **E** lines; (b) $\mathbf{E} \cdot \nabla \mathbf{E}$ (force) lines..... 99

5.14 Instantaneous snapshots of the suspension structure with the inclusion of the near-field interactions (image method) without pressure driven flow at the various times: (a) t = 1s; (b) t = 3s; (c) t = 6s; (d) t = 10s..... 100

5.15 Instantaneous snapshots of the suspension structure, including the near-field interactions (image method) in presence of a pressure driven flow (dp/dx=10 pas./m) at various time: (a) *t* = 1s; (b) *t* = 3s; (c) *t* = 6s; (d) *t* = 10s..... 101

5.16 Instantaneous snapshots of the suspension structure, including the near-field interactions (image method) in presence of a pressure gradient (dp/dx=20 pas./m) at various times: (a) *t* = 1s; (b) *t* = 3s; (c) *t* = 6s; (d) *t* = 10s..... 103

5.17 Instantaneous snapshots of the suspension structure, including the near-field interactions (image method) with the pressure driven flow (dp/dx=50 pas./m) at various times: (a) t = 1s; (b) t = 3s; (c) t = 6s; (d) t = 10s; (e) t = 15s..... 104

NOMENCLATURE

A_m, B_m	coefficient
a	particle radius
$\mathbf{C}$	capacitance matrix
$\mathbf{E}$	electric field
E_0	chacteristic electric field
F	dielectric displacement, or flux
$\mathbf{F}_\alpha$	electrostatic force on particle α
$\mathbf{F}_D$	drag force
$\mathbf{F}_b$	buoyancy force
$\mathbf{F}_i^{\mathbf{H}}$	hydrodynamic force on particle α
$\mathbf{G}^{\mathbf{E}}$	potential gradient in absence of particles, -E
$f_{//}$, $f_\perp$, f_Γ	force function
$\mathbf{g}$	the acceleration due to gravity
j	$j=\sqrt{-1}$
l_x, l_y, l_z	dimensions in x, y, z-axis direction, respectively
$\mathbf{M}$	potential matrix
Ma	Mason number
$\mathbf{n}$	surface normal
$\mathbf{P}, p$	dipole moment
$\mathbf{q}$	vector of N particle charges moment

$\mathbf{r}$	distance between particles α, β centers position $\mathbf{y}$ and $\mathbf{x}$, $r = \lvert\mathbf{x}-\mathbf{y}\rvert$, and $\nabla_y = \dfrac{\partial}{\partial(\mathbf{y}-\mathbf{x})}$
$\mathbf{S}$	vector of N particle dipoles moment
$\mathbf{T}$	Maxwell stress tensor
$\mathbf{u}_p$, $\mathbf{u}_c$	velocities of particle, fluid, respectively
V	the volume of the domain
W, ϑ	energy density
α	constant, $\varepsilon_p/\varepsilon_c$
β	constant, $(\varepsilon_p-\varepsilon_c)/(\varepsilon_p+2\varepsilon_c)$
φ	electrical potential
ϕ	particle volume fraction
$\boldsymbol{\varepsilon}$	vector of N particle electric field
ε	dielectric permittivity
ε_0	dielectric permittivity for free space
η	fluid viscosity at zero-field
η_p	apparent viscosity of the suspension
τ	shear stress
$\dot{\gamma}$	shear rate
τ_0	dynamic or Bingham yield stress
σ	conductivity of the suspension
ζ	zeta potential

ρ	density

Subscripts

c	fluid
p	particle

Superscripts

-	inside of the particle
+	outside of the particle

CHAPTER 1

INTRODUCTION

1.1 Overview

Interesting phenomena happen when polarizable particles suspended in a nonconductive medium are subjected to external AC or DC electric fields. The suspension is called electrorheological (ER) fluid. Electrorheological fluids are most commonly colloidal suspensions, and their stiffening under an electric field is reversible. Both polarizable particles and medium are dielectric materials. The dielectric constants of the suspended particles and the suspending medium are different so that neutral particles can be polarized when subjected to an external electric field.

Particles form chain structures aligned in the direction of the electric field in the case of a uniform electric field. This stacking of an electrorheological fluid is sometimes called the "Winslow effect" after its first investigator, Willis Winslow[1] in 1949. In a non-uniform electric field, the induced dipoles (charges) within the particles interact with the field to give rise to dielectrophoresis[2], electrorotation[3], or traveling wave dielectrophoresis[3,4], depending on the nature of the imposed electric field.

Nowadays, suspended particles are extensively used in applications, e.g. in modern materials, manufacturing and medical/pharmaceutical operations, including fluidized bed reactors, jet printers, active shock absorber devices, particle handling, biological assays and drug discovery. In other situations, particles can be harmful, such as in the case of particulate pollution of the environment and in industry. In both situations, there is a need to manipulate particles for concentration, transport, separation or removal.

Particular attention should be given to the recent increased utilization of AC electrokinetic methods (with either a uniform or non-uniform electric field) for a wide range of applications in biological science research and medicine. Dielectrophoretic devices have been used to manipulate, separate and identify cells and microorganisms[5,6].

Next, some basic terms used in the remaining of this thesis are defined, although for further information the interested reader is referred to Ramos et al.[7,8] for a thorough review of AC electrokinetic structures and electrostatic forces.

1.1.1 Dielectric Material[9]

A substance that is a poor conductor of electricity but an efficient supporter of electrostatic fields is called a dielectric material. In practice, many dielectric materials are solid, including porcelain (ceramic), mica, glass, plastics, and the oxides of various metals. Some liquids and gases can also serve as good dielectric materials. Dry air is an excellent dielectric material, and is used in variable capacitors and some transmission lines. Distilled water is also a fairly good dielectric material.

1.1.2 Dielectric Constant

The dielectric constant is a characteristic quantity of a given dielectric substance, sometimes called the relative permittivity. In general, the dielectric constant is a complex constant, with its real part ε' giving reflective surface properties (Fresnel reflection coefficients), and its imaginary part ε'' giving the radio absorption coefficient[10]:

$$\varepsilon = \frac{\varepsilon_e}{\varepsilon_0} = \varepsilon' - j\varepsilon'' \tag{1.1}$$

where ε_e is the electric permittivity and ε_0 is the permittivity of free space (= $8.8542e^{-12}$ F/m), $j = \sqrt{-1}$.

A perfect dielectric substance is a material that exhibits the displacement of current only, so that it stores and returns electrical energy as if it were an ideal 'battery'. The relative permittivity of a perfect dielectric substance is a scalar.

1.1.3 Dipole Moment[11]

An elementary dipole can be thought as a pair of opposite charges with magnitude q. The dipole moment is defined as the magnitude of the charge times the distance between the two charges and its direction is toward the positive charge. The dipole moment is a useful concept for atoms and molecules where the effect of charge separation is measurable. Dipole moments are much more common than isolated charges.

1.2 Background and Theory

The study of the suspension of polarizable particles in electrolyte subjected to external electric fields requires an understanding of the interactions between the suspending medium, the electric field and the particles. The effects of the drag force and particle-particle interactions are important in colloidal suspensions.

1.2.1 Hydrodynamic Force[7]

Particles in ER fluid suspensions are much larger than the molecules comprising the continuous phase so that the suspending fluid phase is generally treated as a continuum. The continuous phase is usually sufficiently viscous so that the suspended particles experience drag forces when moving in the fluid, even if there is no bulk flow. The drag

force is related to the size, shape, surface characteristics of the particle and the relative velocity of the particles compared to that of the fluid. For a smooth sphere isolated in an infinite medium and for zero Reynolds number, the drag force takes the form

$$\mathbf{F}_D = -6\pi\eta a(\mathbf{u}_p - \mathbf{u}_c) \tag{1.2}$$

where a is the radius of the particle, η is the viscosity of the fluid, $\mathbf{u}_c$, $\mathbf{u}_p$ are the velocities of the fluid and particle, respectively.

When more than one particle is present, there exist hydrodynamic interactions between the particles, and between the particles and the bounding electrodes, but these are often ignored in models of ER suspensions.

1.2.2 Brownian Force[7]

The fluid phase can also influence sub-micron particle dynamics via Brownian motion. In this case, the thermal motion of the continuous phase molecules gives rise to an erratic motion of the particles.

1.2.3 Buoyancy Force[7,12]

The buoyancy force is the force acting on a particle through gravity. For a particle with density ρ_p suspended in a medium with density ρ_c, the buoyancy force is:

$$\mathbf{F}_b = V(\rho_p - \rho_c)\mathbf{g} \tag{1.3}$$

where $\mathbf{g}$ is the acceleration due to gravity and V is the volume of the particle. This force is responsible for sedimentation. For a sub-micrometre particle, this force is usually ignored.

1.3 Electrorheological Fluids

A comprehensive review of colloidal suspensions can be found in Gast and Zukoski[13] (1989) while Jordan and Shaw[14] reviewed the dependence of the electrorheological (ER) effects on electrical and structural parameters and the existing theories of the ER mechanism. They thought that the required properties for the dispersed dielectric include high polarizability and a limited, but finite, conductivity. The latter is often achieved by adding water to the suspension. In 1996, M. Parthasarathy and D. Klingenberg[15] surveyed the mechanisms of ER fluids and models used to study suspensions and in 2002, H. Tian[16] provided the scientific community with a current review of electrorheological suspensions. In this section, a short review of electrorheological fluids and the models used to study the particles movement is performed.

"Electrorheological (ER) fluid" indicates a class of liquids, which stiffen into semi-solids when subjected to an external electric field with the strength of several kilovolts per millimeter. Typical electrorheological fluids usually contain a disperse phase and a continuous phase. The disperse phase has a volume fraction (volume occupied by the disperse phase divided by the total volume) between 0.05 and 0.50. Generally, the disperse phase consists of polarizable particles made of cornstarch, silica, or even zeolite, with a size ranging from 1 to 100 micrometers and which are approximately spherical, and non-conducting or semi-conducting. The continuous phase has a field-free viscosity in the range of 0.1~10 Pa.s and is made of a non-conducting solvent, for example, kerosene, chlorinated hydrocarbons, silica oil or corn oil. The disperse particles and the suspending fluids have different dielectric constants. Generally, the dielectric constants for the suspending fluid range from 2 to 15 and those of the

particles range from 2 to 40. The particle-to-fluid dielectric constant ratio typically varies from 2 to 10. The fluid and particles are such that the particles are close to being neutrally buoyant and sedimentation is minimized.

1.3.1 Fundamentals and Mechanisms

Electrorheological fluids are the most common colloidal suspensions. Their stiffening under electric fields is reversible, which is the fundamental difference between ER fluids and ferro-fluids[17,18]. A ferro-fluid is a suspension of permanently magnetized particles, which implies that there exist polarization forces even in absence of an external magnetic field. On the contrary, for an ER suspension, there are no polarization forces on an initially charge-free particle in absence of an imposed electric field. Brownian forces are usually negligible for ER fluids, and the fluid and particles motion is governed by electrostatic and viscous forces, the latter being related by the parameter referred to as the Mason number, *Ma*. Since the magnetic dipoles are permanent in ferro-fluids, the rheological properties scale linearly with the applied magnetic field at high field strengths. However, there is a quadratic dependence on the field strength in an ER fluid since the particle dipoles are induced by the external electric fields. There is also a torque acting on each particle in a ferro-fluid given by the cross product of its dipole and the applied field which gives rise to an anti-symmetric stress tensor as shown by Batchelor[19,20]. In an ER fluid of nearly spherical particles, the induced dipole is aligned with the local electric field, so there is no net torque on the particle. However, because the "effective torque" exerted on the deformed or strained chains of particles, there are anti-symmetric stresses in ER fluids.

The uniform field-induced fibrous particles form chains parallel to the applied field. For electric fields of the order of 1 kV/mm, the effective viscosities can increase by a factor of up to 10^5. The other rheological properties, such as yield stress, shear modulus, and so on, can also abruptly change. The ER fluid responds in milliseconds to the application of an electric field. Other remarkable properties include that these effects are reversible and happen rapidly.

After Winslow published his observations, Uejima[21] showed that the shear stress of the electrorheological fluid was fairly well modeled as a Bingham model. The shear stress is thus given by:

$$\tau(\dot{\gamma}, E) = \tau_0(E) + \eta\dot{\gamma} \quad \text{for } \tau > \tau_0 \tag{1.4a}$$

$$\dot{\gamma} = 0 \quad \text{for } \tau < \tau_0 \tag{1.4b}$$

where E is the applied electric field strength, τ is the shear stress, $\dot{\gamma}$ is the shear rate, τ_0 is the dynamic or Bingham yield stress, and η is the plastic (fluid) viscosity.

Studies often report that the apparent suspension viscosity $\tau/\dot{\gamma}$ should be distinguished from the plastic (fluid) viscosity η. Marshall et al.[22] noted that the yield stress was linear in the volume fraction range studied and Smoluchowski[23] obtained an apparent viscosity equation in the dilute suspension of the form:

$$\eta_p = \eta\left(1 + 2.5\phi\left(1 + \frac{1}{\sigma\eta a^2}\left(\frac{\zeta\varepsilon_0\varepsilon_c}{2\pi}\right)^2\right)\right) \tag{1.5}$$

where η_p indicates the apparent viscosity of the suspension, η is the viscosity of the continuous phase (pure fluid), ϕ is the particle volume fraction, σ is the conductivity of the suspension, a is the radius of the particle, ζ is the zeta potential of the particle, and ε_c

is the dielectric constant of the continuous phase. Recent works of Klingenberg[24] report that the yield stress reaches a maximum at about 35-40 percent of solids volume while Brady's group[25-27] investigated the yield stress, normal stress, etc.

1.3.2 Electrostatic Force

Particles experience both hydrodynamic and electrostatic interparticle forces when suspended in a dielectric fluid subjected to a uniform electric field. In principle, the exact electrostatic force in an electrorheological fluid can be computed from the integration of the Maxwell stress over each particle, and in which the electric field is computed by solving the many-body electrical potential problem within the system. However, this problem is challenging from a practical viewpoint for a number of particles larger than two.

ER fluids are heterogeneous, multicomponent systems consisting of particles and medium. Moreover, the particles are often of non-spherical irregular shape, and/or may be porous. This is thus an exceptionally complicated system, which makes the task of calculating the electrostatic force acting on a particle quasi-impossible. Therefore, many simplified models have been introduced for that purpose. While the idealized electrostatic polarization model was the first simple model, variations of this model were introduced later. The Maxwell-Wagner polarization model is another simple model taking account the conductivities of the particles and/or medium.

1.3.2.1 Idealized Electrostatic Polarization Model. The idealized electrostatic polarization model describes a suspension consisting of monodisperse, neutrally buoyant, hard particles suspended in a Newtonian fluid. Both phases are ideal dielectric substances.

Due to the divergence and curl-free properties of the electrostatic field, the electrical potential can be computed by solving Laplace's equation:

$$\nabla^2 \varphi = 0 \tag{1.6}$$

with the boundaries at each spherical particle/continuous phase interface satisfying the interfacial conditions:

$$\varphi^- = \varphi^+ \tag{1.7a}$$

$$-\alpha \nabla \varphi^- \cdot \mathbf{n} = -\nabla \varphi^+ \cdot \mathbf{n} \tag{1.7b}$$

and

$$\varphi \to -\mathbf{E} \cdot \mathbf{r} \text{ when } r \to \infty \tag{1.7c}$$

where $\alpha = \varepsilon_p / \varepsilon_c$ denotes the ratio of the dielectric constant of the spheres to that of the continuous phase, and $\mathbf{n}$ is the surface normal vector. The superscript "+" indicates the inside of the sphere while "-" refers to the outside.

Once the potential is solved, the local electric field can be computed by $\mathbf{E} = -\nabla \varphi$. The force acting on the particle is then determined by integrating the Maxwell stress tensor on the surface of the particle according to:

$$\mathbf{F} = \iint \mathbf{T} \cdot \mathbf{n} da \tag{1.8}$$

where the stress tensor has the components:

$$T_{ij} = \frac{1}{4\pi}\left(E_i E_i - \frac{1}{2}\delta_{ij} E^2 \right) \tag{1.9}$$

In this work, we seek a further simplification to the electrostatic problem.

For an uncharged, isolated, hard sphere suspended in a continuous medium far from the electrodes, the solution of the potential both inside and outside the sphere, in spherical coordinates, reads:

$$\varphi^{+} = -Er\cos\theta + \frac{Ea^3(\varepsilon_p - \varepsilon_c)}{(\varepsilon_p + 2\varepsilon_c)r^2}\cos\theta \tag{1.10}$$

$$\varphi^{-} = -\frac{3\varepsilon_c}{\varepsilon_p + 2\varepsilon_c}Er\cos\theta \tag{1.11}$$

Considering that the potential of a dipole has expression:

$$\varphi = \frac{p_{eff}\cos\theta}{4\pi\varepsilon_c r^2} \tag{1.12}$$

and comparing the potential outside the particle with that of the dipole, the effective dipole moment induced in a particle can be expressed as:

$$p_{eff} = 4\pi\varepsilon_c \beta a^3 E \tag{1.13}$$

Here, $\beta = \frac{\varepsilon_p - \varepsilon_c}{\varepsilon_p + 2\varepsilon_c}$ denotes the Clausius-Mossotti factor.

With the assumption that the presence of the other particles does not alter the distribution of dipoles on this particle, the force on the particle *i* at the origin can be expressed by:

$$\mathbf{F}_i^p = 12\pi\varepsilon_0\varepsilon_c(\beta E)^2 a^2\left(\frac{a}{r}\right)^4\left(\left(3\cos^2\theta_{ij} - 1\right)\mathbf{e}_r + \sin 2\theta_{ij}\mathbf{e}_\theta\right) \tag{1.14}$$

Equation (1.14) is not accurate when two particles are close to each other because of the disturbance field created by the spheres. Klingenberg[28] solves Laplace's equation for two particles suspended in a fluid by integrating the Maxwell stress tensor, and obtains the exact force acting on the particle as:

$$\mathbf{F}_i^p = 12\pi\varepsilon_0\varepsilon_c(\beta E)^2 a^2\left(\frac{a}{r}\right)^4\left(\left(2f_{//}\cos^2\theta_{ij} - f_{\perp}\sin^2\theta_{ij}\right)\mathbf{e}_r + f_{\Gamma}\sin 2\theta_{ij}\mathbf{e}_\theta\right) \tag{1.15}$$

where θ_{ij} is the angle between the sphere centerline and the applied electric field, $\mathbf{e}_r$ is the unit vector along the sphere centerline, $\mathbf{e}_\theta$ is the azimuthal unit vector, and $f_{//}$, $f_\perp$ and f_Γ are three force functions related to the dielectric constant ratio $\alpha = \varepsilon_p/\varepsilon_c$ and the length ratio *a/r*. Equation (1.15) simplifies to Equation (1.14) by simply setting $f_{//}$, $f_\perp$ and f_Γ as unity when the point-dipole assumption is adopted and the particle-to-fluid dielectric constant reaches 1.

Klingenberg et al.[29-31] performed the dynamic simulation of the ER fluids using the point-dipole model for the electrostatic forces and the stokes drag formula to model the hydrodynamic force. Anderson[32] studied analytically the electrostatic force on ideal dielectric spherical particles in an ER fluid in the infinite-α limit. Whittle[33] performed a computer simulation with a method similar to that of Klingenberg et al.[29-31] based on a dipole-dipole interaction modified at short range. Wu et al.[34-36] developed a multiple image method to compute the interparticle force in a polydisperse suspension containing particles of various sizes.

Bonnecaze and Brady developed a method to compute the electrostatic force by expanding the integral form of Laplace's equation to study electrorheological suspensions[19,37,38] and their rheological properties.[25-27]

1.3.2.2 Maxwell-Wagner Polarization Model. The Maxwell-Wagner polarization model[39-41] was derived to describe the suspension by considering the conductivities and permittivities of the particles and suspending fluid. The simplest Maxwell-Wagner polarization model considers that the conductivities and permittivities are constant, independent of the frequency. The complex dielectric constants of the particles and the fluid can be written as:

$$\varepsilon_k(\omega) = \varepsilon_k - j(\sigma_k / \varepsilon_0 \omega) \tag{1.16}$$

where $k = p, c$ and $j = \sqrt{-1}$.

By solving Laplace's equation to determine the electric field and using the point-dipole approximation, the time-average force acting on the particle at the origin, due to the presence of the other particles at (R_{ij}, θ_{ij}), is:

$$\mathbf{F}_i^p = 12\pi\varepsilon_0\varepsilon_c\beta_{eff}^2 E_{EMS}^2 a^2 \left(\frac{a}{r}\right)^4 \left(\left(2f_{//}\cos^2\theta_{ij} - f_\perp \sin^2\theta_{ij}\right)\mathbf{e}_r + f_\Gamma \sin 2\theta_{ij}\mathbf{e}_\theta\right) \tag{1.17}$$

where $E_{EMS}^2 = E^2/2$, and β_{eff} is the effective relative polarizibility satisfying:

$$\beta_{eff}^2(\omega) = \beta_d^2 \frac{\left[(\omega t_{mw})^2 + \frac{\beta_e}{\beta_d}\right]^2 + (\omega t_{mw})^2\left[1 - \frac{\beta_e}{\beta_d}\right]^2}{\left[1 + (\omega t_{mw})^2\right]^2} \tag{1.18}$$

where $\beta_d = \frac{\varepsilon_p - \varepsilon_c}{\varepsilon_p + 2\varepsilon_c}$, $\beta_e = \frac{\sigma_p - \sigma_c}{\sigma_p + 2\sigma_c}$ and $t_{mw} = \varepsilon_0 \frac{\varepsilon_p + 2\varepsilon_c}{\sigma_p + 2\sigma_c}$.

The coefficient β_{eff}, and thus the force, depends on both frequency and time. In one limit, the permittivities dominate the response:

$$\lim_{\omega t_{mw} \to \infty} \beta_{eff}^2(\omega) = \beta_d^2 \tag{1.19}$$

while in another limit, the conductivities dominate the response:

$$\lim_{\omega t_{mw} \to 0} \beta_{eff}^2(\omega) = \beta_e^2 \tag{1.20}$$

T. B. Jones et al.[42] studied the dielectric levitation using the Maxwell-Wagner relationship. Kadaksham et al.[43] investigated the effects of the dielectric constant on the aggregation of polarizable particles in electrostatic suspensions of yeast cells. Wu et. al.[44] performed a study of dielectric and conduction effects in ohmic electrorheological fluids.

The nonlinear conduction model[45,46] is also used to evaluate the electrostatic force on conducting particles where the nonlinear conduction plays a crucial role.

1.3.3 Applications of ER Fluid

Since the mechanical properties of ER fluids can be easily controlled within a wide range of behaviors (from liquids to solids), ER fluids can be used as electric and mechanical interfaces in various industrial applications. For example, in the automotive industry[47-51], the electronic control of stress transfer through such fluids has applications in devices such as active shock absorbers, engine mounts, clutches, brakes, actuators and damping systems. It can also be used in robotic arm joints and hands[52-54]. A successful area of applications of ER fluids is the domain of actuators[55]. Here, the desired forces can be generated as required. Further potential applications[55,56] are continuing to be invented and patented nowadays.

Devices employing electrorheological (ER) fluids are generally more energy-efficient than hydraulic, mechanical or electromechanical devices that accomplish the same functions. In addition, the rapid response of ER fluids to the application of an electric field within milliseconds makes ER devices attractive and for this reason ER fluids are often called "smart" fluids[57,58].

Although ER fluids hold great promise as elegant means of providing continuously variable forces for the control of mechanical vibrations, the development of industrial devices has been hampered by the following problems which still need to be resolved before commercialization can take place: (a) the yield stress is not sufficiently high; (b) the ER fluid errs once contaminated; (c) the ER effect is significantly affected

by the working temperature; (d) if the buoyancy force is not negligible, particles sedimentation needs to be overcome.

1.4 Dielectrophoresis

The term dielectrophoresis (DEP) was first used by Pohl[2] to describe the translational motion of the particles caused by the interaction of the induced dipoles of particles with the applied non-uniform electric field. The DEP force does not depend on the polarity of the electric field so that it can be found with both AC and DC fields. An AC field induces frequency-dependent dipoles on polarizable particles.

1.4.1 Theory

The interaction of the dipole and a non-uniform field gives rise to dielectrophoresis. Unlike electrophoresis, in which motion is determined by the net intrinsic electrical charge carried by the particle, dielectrophoretic motion is determined by the magnitude and polarity of the induced charges within the particle due to the applied non-uniform electric field.

Figure 1.1 shows a basic dielectrophoretic effect, in which electrodes are used to generate spatially non-uniform electric field. The positively charged body moves towards the negative electrode while the neutral body is polarized, and therefore attracted towards areas where the field is either the strongest (when the body is more polarizable than the surrounding medium) or the weakest (if the body is less polarizable).

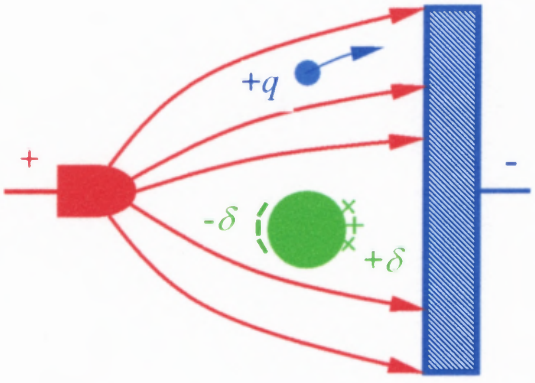

Figure 1.1 Diagram of a charged particle and a neutral particle in a non-uniform electric field. The positively charged body moves towards the negative electrode. The neutral body, on another hand, is polarized and therefore attracted towards areas where the electric field is the strongest (when the body is more polarizable than the surrounding medium) or the weakest (if the body is less polarizable).

Polarizable particles experience a DEP force when the electric field is spatially non-uniform. The DEP force does not depend on the polarity of the electric field so that it is present in both AC and DC fields. A particle experiences a DEP force even when only one particle is suspended in the domain as shown in Figure 1.1. Dielectrophoresis can be either positive or negative, depending on the dielectric constants of the particle and the medium. If ε_p is larger than ε_c, the particle which is more polarizable than the fluid is attracted towards the electric field intensity maxima and repelled from the minima (positive dielectrophoresis) while if ε_p is smaller than ε_c, the particle is less polarizable than the fluid, the particle is attracted towards the electric field intensity minima and repelled from the maxima (negative dielectrophoresis). For ideal dielectrics, the magnitude of the permittivity of the particle is constant and equal to ε_p, and that of the medium is ε_c. Obviously, for positive DEP, $\beta > 0$ and for negative DEP, $\beta < 0$. Since electric field maxima are located at the electrodes tips and the electric field minima are placed away from the electrodes, whether the particle is attracted towards or directed

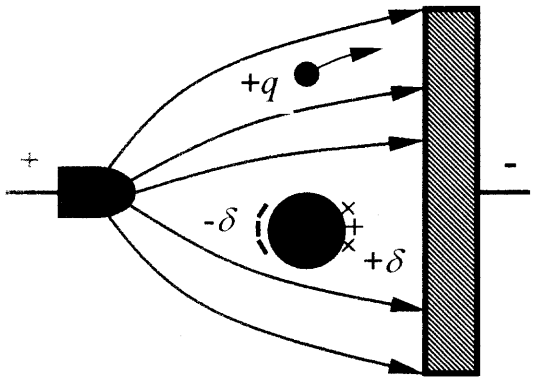

Figure 1.1 Diagram of a charged particle and a neutral particle in a non-uniform electric field. The positively charged body moves towards the negative electrode. The neutral body, on another hand, is polarized and therefore attracted towards areas where the electric field is the strongest (when the body is more polarizable than the surrounding medium) or the weakest (if the body is less polarizable).

Polarizable particles experience a DEP force when the electric field is spatially non-uniform. The DEP force does not depend on the polarity of the electric field so that it is present in both AC and DC fields. A particle experiences a DEP force even when only one particle is suspended in the domain as shown in Figure 1.1. Dielectrophoresis can be either positive or negative, depending on the dielectric constants of the particle and the medium. If ε_p is larger than ε_c, the particle which is more polarizable than the fluid is attracted towards the electric field intensity maxima and repelled from the minima (positive dielectrophoresis) while if ε_p is smaller than ε_c, the particle is less polarizable than the fluid, the particle is attracted towards the electric field intensity minima and repelled from the maxima (negative dielectrophoresis). For ideal dielectrics, the magnitude of the permittivity of the particle is constant and equal to ε_p, and that of the medium is ε_c. Obviously, for positive DEP, $\beta > 0$ and for negative DEP, $\beta < 0$. Since electric field maxima are located at the electrodes tips and the electric field minima are placed away from the electrodes, whether the particle is attracted towards or directed

away from the electrodes depends on the relative magnitude of the permittivity ε_p of the particle versus that of the medium ε_c. Negative dielectrophoresis has the advantage in practice that it allows the collection of particles in a contactless fashion, away from electrodes and boundaries.

1.4.2 Dielectrophoretic (DEP) Force

In classic dielectrophoresis[2,59], when a neutral particle is placed in a static field at equilibrium, the electrostatic DEP force is determined from the effective moment method according to the formula:

$$\mathbf{F}_{\mathrm{DEP}} = (\mathbf{P} \cdot \nabla)\mathbf{E} \tag{1.21}$$

where **P** is the effective dipole moment vector. For an isolated spherical particle with radius a suspended in a fluid with absolute dielectric permittivity $\varepsilon_0\varepsilon_c$ (ε_0 is the permittivity of free space, $\varepsilon_0 = 8.8542 * 10^{-12} F/m$), the effective dipole moment can be written as:

$$\mathbf{P} = 4\pi\varepsilon_0\varepsilon_c\beta a^3\mathbf{E} \tag{1.22}$$

Substitution in Equation (1.21) leads to the classical expression of the DEP force:

$$\mathbf{F}_{\mathrm{DEP}} = 4\pi a^3\beta\varepsilon_0\varepsilon_c\mathbf{E} \cdot \nabla\mathbf{E} \tag{1.23}$$

Perfect dielectrics are commonly used in dielectrics theory for its simplicity in models or numerical simulations. In reality, ideal or perfect dielectric materials with a nonzero in-phase dielectric constant do not exist. The real dielectrics do conduct electricity so that the dielectric constant should be replaced by a complex (absolute) dielectric constant, or permittivity, in Equation (1.1). In view of this, the time-averaged DEP force is given by:

$$\langle \mathbf{F}_{\mathrm{DEP}} \rangle = 4\pi a^3 \varepsilon_0 \varepsilon_c \,\mathrm{Re}(\beta) \cdot \nabla \bar{E}_{rms}^2 \tag{1.24}$$

where Re refers to the real part.

The study of the dielectrophoretic force acting on a non-spherical particle is challenging. There is only limited information in the literature on this topic. H. Morgan[60] investigated rod-shaped viral particles and provided the DEP force expression as:

$$\mathbf{F}(t) = \frac{2\pi abc}{3} \varepsilon_0 \varepsilon_c \,\mathrm{Re}\left(\frac{\varepsilon_p^* - \varepsilon_c^*}{\varepsilon_c^*} \right) \nabla \mathbf{E}_{EMS}^2 \tag{1.25}$$

where the major axis of the particle is parallel to the electric field.

Recently, J. Kadaksham et al.[61] performed numerical simulations solving the full hydrodynamics equations for the fluid-particle system (thus fully resolving the hydrodynamic fluid-particles and particle-particle interactions) and taking into account both the electrostatic interparticle interactions and the DEP force. In their work, the electrostatic interparticle force exerted on a particle is calculated from the summation of the interactions between this particle and all others using the point-dipole approximation. L. Dong[62] studied the DEP force by modifying the Clausius-Mossotti function with the influence of the near-field using the multiple image method. T. B. Jones[63] developed a dyadic tensor representation for multipolar moments to formulate the expression of the dielectrophoretic force.

1.4.3 Applications of Dielectrophoresis

1.4.3.1 Biotechnology DEP. The first significant demonstration of biological dielectrophoresis involved the separation of living biological cells by Pohl[2]. Since then, there has been an increasing interest in applying the technique for the selective

separation, collection and manipulation of bioparticles. Another important use of DEP in biotechnology is electrofusion, first reported by Senda et al.[64] in 1979. Later, Zimmermann and his colleagues[65-67] derived an efficient method to simulate the alignment of cells prior to electrofusion. This technology should be useful for applications such as cancer research and treatment. Washizu et al.[68-71] have investigated the DEP control and manipulation of cells and other biological particles, focusing upon the development of practical technologies for the automated processing of cells and other biological particles such as DNA. In basic cell studies, one can investigate the cell structure by using DEP measurements to develop models based on their dielectric properties. This task is usually posed to the investigator as an inverse problem, where the cell structure must be inferred from its measured DEP spectra. The dielectric properties of sub-micrometre particles have also been measured and characterized[76] using a non-uniform electric field. At the submicron scale, DEP has been used successfully for the manipulation of a variety of sub-micrometre particles, such as DNA, viruses and latex spheres[72-75]. Green et al.[77-80] used it to separate DNA molecules and proteins, cancer cells from blood and different bacteria. Orientation and positioning of DNA molecules and other biological macromolecules with microfabricated electrodes have also been reported[81]. Recent trends in lab-on-a-chip devices show a growing use of dielectrophoresis (DEP) to manipulate biological objects such as cells and organic molecules[82-85]. All these applications are based on differences in particle and fluid conductivities and/or permittivities, which could control the DEP force. Bringing the advances of microelectronic miniaturization into biological and clinical analyses, combinatorial chemistry and high throughput screening require new tools.

1.4.3.2 Mineralogical DEP. In conventional mineral industrial systems, DEP was first used to separate ores and minerals[86,87]. Conventional electrostatic methods, which rely upon differences in the electrical charging tendencies of various constituents of crushed ores and minerals, have been used in dry separation processes for many years. Wet separation processes[86], which use variable frequency, non-uniform AC electric fields, offer an alternative in certain commercially important mineral recovery operations.

DEP is also used to manipulate colloidal crystallization[88,89]. By using strong electric fields at low frequency, colloidal particles can be ordered into three-dimensional crystals rapidly and reversibly.

1.4.3.3 Microactuators. Many kinds of electrodes with different geometries have been used for DEP research and applications. Recent advances in microfabrication techniques have stimulated a set of new DEP structures that differ dramatically from the axi-symmetric electrodes. For example, a MEMS fabricated planar, salient electrode was used to create an azimuthally periodic electric field by Washizu et al.[90] The polynomial-designed planar arrays of electrodes produce a traveling electric field wave that can transport cells in an assembly line fashion. The castellated-designed electrode structures were fabricated on glass and on silicon substrates, and can be used for both characterization and separation.

1.5 Objectives and Outline of This Thesis

1.5.1 Objectives

The primary objective of this research is to compare the capture efficiency of particles using different electrode designs. In recent years, the manipulation of cells and microorganisms using nonuniform electric fields has shown great promise. Getting the best results in separating and sorting cells, virus and particles in a short time is one key issue in modern biotechnology. When the particles size, shape and surface characteristics and the properties of the suspending fluid are known, the applied spatially non-uniform electric fields generated with various electrode geometries will give rise to different capture efficiencies.

While it is not easy to obtain sub-micrometer particles of the same size and shape, the suspending fluid should also be clean and have specific viscosity and density, and thus fully controlled experiments can be a challenge. If the capture efficiency of particles can be studied numerically under different electric fields, numerical results should serve as useful and cheap guides for the design of efficient devices.

In modern numerical simulations, several microscopic models were employed to relate forces, parameters and other features at the microscopic level to the suspension macroscopic properties. Most of the models fall into three categories: description of the macrostructure and property evaluations; equilibrium or near-equilibrium statistical mechanics; and particle-level simulation[14]. In the latter category, many researchers have developed simulation techniques similar to molecular dynamics methods. The basic idea is to consider the equation of motion of each particle, deduce the suspension structure

taking into account all individual particles, and then evaluate the bulk properties of interest. Within this framework, the particle' equation of motion reads:

$$\mathbf{m} \cdot \frac{d\mathbf{U}}{dt} = \mathbf{F}^{\mathbf{P}} + \mathbf{F}^{\mathbf{H}} \tag{1.26}$$

where $\mathbf{m}$ is the generalized mass/moment of the particle, $\mathbf{F}^{\mathbf{P}}$ is the generalized force/torque vector on the particle, which includes all nonhydrodynamic forces and torques, and $\mathbf{F}^{\mathbf{H}}$ represents the hydrodynamic forces and torques. The present research focuses on calculating the non-hydrodynamic, electrostatic forces and torques.

Bonnecaze et al.[37-38] first presented an energy method by expanding the integral Laplace equation in the case of a uniform electric field. When an ER fluid is subjected to a non-uniform electric field, the electrostatic forces, including both the interaction between the induced dipole of a particle and the imposed electric field, and the various interactions between the induced dipoles of the different particles, need to be considered. This thesis extends the energy method to calculate the electrostatic forces where ER fluids are subjected to non-uniform electric fields. The near-field interaction is added by using the multiple image method to compute the induced dipoles in near touching particles. Our simulation technique can account for both far- and near-field effects of electrostatic interactions with or without pressure-driven flow.

1.5.2 Outline

This thesis uses a Molecular-like dynamics method to numerically study electrorheological suspensions subjected to uniform and non-uniform electric fields. The hydrodynamic force is represented by the Stokes viscous drag, while the electrostatic force is computed from differentiating the electrostatic density of the suspension with

respect to the particles position to include both the interactions between particles and electric field, and the interactions between particles. The near-field effects are included by considering the interactions between the various pairs of particles using the multiple image method. The capturing efficiencies are computed with and without the addition of near-field effects, and with and without fluid flow pressure gradient.

The first Chapter gives a brief review on the hydrodynamics background, the fundamental theory and mechanisms of electrorheological fluids and dielectrophoresis, and different models used by former researchers to compute electrostatic forces when the suspensions are subjected to uniform or non-uniform electric fields.

In the second Chapter, the physical model, governing equations and numerical methods used in this thesis are presented.

The third Chapter focuses on the methods used to compute the electrostatic forces. Electrostatic forces are determined in both a uniform electric field and a non-uniform electric field for a two particles system, and then for a multiparticle suspension subjected to a nonuniform electric field.

In Chapter 4, numerical results are presented for a two particles suspension using different methods to calculate the electrostatic forces, while numerical results are presented for a multiparticle suspension with or without the presence of a flow pressure gradient in Chapter 5.

Finally, Chapter 6 summarizes the results of this thesis and presents recommendations based on this research for future work.

CHAPTER 2

PHYSICAL MODEL AND GOVERNING EQUATIONS

2.1 Physical Model

When a dielectric neutral particle suspended in a perfect dielectric liquid is subjected to an external electric field, the particle becomes polarized with dipoles (positive and negative charges). The response to the application of the electric field takes place within milliseconds so that the induced dipoles appear rapidly as the field is switched on but also disappear fast once the field is removed.

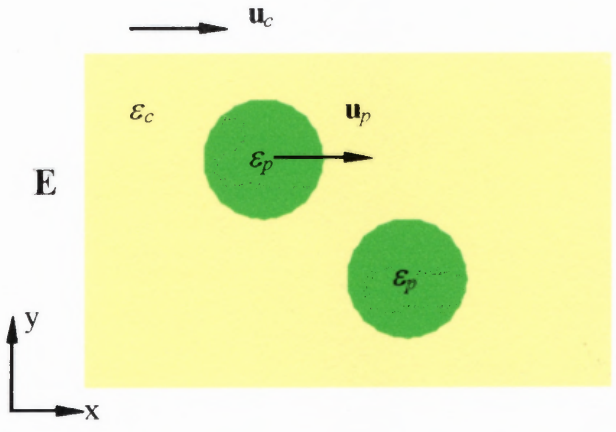

Figure 2.1 Sketch of the diagram of two polarizable particles suspended in a fluid and subjected to an electric field.

Before a physical model is considered, the following assumptions are made: the suspended particles are monodisperse, neutrally buoyant, hard, dielectric spheres with a real dielectric constant ε_p and radius a; the fluid is incompressible and Newtonian with a real dielectric constant ε_c and viscosity η. Both phases (fluid and particles) are assumed

to be charge-free and have zero conductivity. The pressure-driven flow may be applied by imposing a pressure gradient in the x direction.

The schematic shown in figure 2.1 is a typical computational cell with dimensions l_x, l_y, l_z in the x, y, z directions, containing polarizable particles and medium.

Hereafter, the governing equations are presented in this Chapter for the particles and the fluid, including the electrostatic forces induced by the nonuniform electric field due to the mismatch of the dielectric constants of the particles and the fluid.

2.2 Governing Equations

2.2.1 Electric Field

The system consisting of the insulating dielectric particles and incompressible fluid is subjected to an electric field. The corresponding electrical potential satisfies Laplace's equation everywhere because of the divergence and curl-free properties of the electrostatic field, that is,

$$\nabla^2 \varphi = 0 \tag{2.1}$$

subjected to the boundary conditions:

$$\varphi = \varphi_0 \qquad \text{on electrodes} \tag{2.1a}$$

$$\frac{\partial \varphi}{\partial \mathbf{n}} = 0 \qquad \text{on other edges} \tag{2.1b}$$

The electric field can be then be deduced from $\mathbf{E} = -\nabla \varphi$.

The potential equations are made dimensionless by using the following characteristic length and strength of the electric field: the length l_y in the y direction and

the strength of the electric field $E = 10^{+6}$. It follows that the characteristic potential is E_0 times l_y.

2.2.2 Fluid Flow

In this section, the governing equations for the incompressible, Newtonian fluid flow are stated where the temperature gradient due to the presence of the electric field is ignored.

Let the density, viscosity and velocity of the fluid be ρ_c, η, and $\mathbf{u}_c$, respectively. The fluid motion is described by the Navier-Stokes equations.

The continuity equation is given by:

$$\nabla \cdot \mathbf{u}_c = 0 \tag{2.2}$$

while the momentum equation reads:

$$\rho_c \frac{d\mathbf{u}_c}{dt} = -\nabla p + \eta \nabla^2 \mathbf{u}_c \tag{2.3}$$

The boundary conditions are such that:

$$\mathbf{u}_c = \mathrm{U_L} \quad \text{on the walls} \tag{2.4a}$$

and

$$\frac{\partial \mathbf{u}_c}{\partial \mathbf{n}} = 0 \text{ on the boundary edges} \tag{2.4b}$$

The governing equations are nondimensionalized using the following characteristic velocity, length and time scale: the characteristic velocity U, characteristic length in the y direction l_y, and time scale $t_s = \frac{a}{U}$, respectively. The Reynolds number then becomes: $\mathrm{Re} = \frac{UL\rho}{\eta}$.

2.2.3 Particle Motion

A molecular-like dynamics method used to describe the motion of the particles is described in this section. Since the particles are considered neutrally buoyant (the density of the particles is equal to that of the fluid), the gravity is neglected, and thus, the motion of a single particle α is governed by:

$$m \frac{d\mathbf{u}_p}{dt} = \mathbf{F}_\alpha^H + \mathbf{F}_\alpha^P \tag{2.5}$$

where $\mathbf{u}_p$ is the velocity of the particle denoted by the subscript α, $\mathbf{F}_\alpha^H$ is the hydrodynamic force, and $\mathbf{F}_\alpha^P$ is the electrostatic force, respectively. In this work, hydrodynamic interactions between particles, as well as between particles and the bounding electrodes, are ignored and the hydrodynamic force on a spherical particle is taken as the Stokes' drag force (Equation (1.2)).

Under the assumption that the acceleration of the particles is negligible, the left hand side of Equation (2.5) is also neglected, and therefore, the equation of motion becomes:

$$\mathbf{F}_\alpha^H + \mathbf{F}_\alpha^P = \mathbf{0} \tag{2.6}$$

Substituting the Stokes drag force in Equation (2.6) for a spherical particle, the previous equation becomes:

$$-6\pi a\eta(\mathbf{u}_p - \mathbf{u}_f) + \mathbf{F}_\alpha^P = \mathbf{0} \tag{2.7}$$

Thus,

$$\frac{d\mathbf{x}}{dt} = \mathbf{u}_p = \mathbf{u}_f + \frac{1}{6\pi a\eta}\mathbf{F}_\alpha^P \tag{2.8}$$

Non-dimensionalizing this equation and integrating it over a time step Δt, the evolution equation for the change in particle location **x** can be written as:

$$\Delta \mathbf{x} = \mathbf{u}_p \cdot \Delta t = (\mathbf{u}_f + Ma^{-1} \frac{1}{6\pi a\eta} \mathbf{F}_\alpha^P) \cdot \Delta t \tag{2.9}$$

In this derivation, the following characteristic length, time, and force scales have been used to nondimensionalize Equation (2.9): the particle radius a, the inverse shear rate $\dot{\gamma}^{-1}$, the hydrodynamic force $6\pi\eta a^2\dot{\gamma}$, and the electrostatic force $12\pi\varepsilon_0\varepsilon_c a^2(\beta E)^2$. Here, $Ma = \eta\dot{\gamma}/2\varepsilon_0\varepsilon_c(\beta E)^2$ (E being the characteristic magnitude of the electric field) is defined as the dimensionless coefficient, the Mason number, which represents the relative importance of the viscous forces to the electrostatic forces.

2.2.4 Repulsive Force

In this paper, all particles are assumed to be solid spheres. To prevent particle overlapping (which is obviously not allowed in physical space), a near field repulsive force is included, which is described as a function of the position vector of the particles (see Figure 2.2).

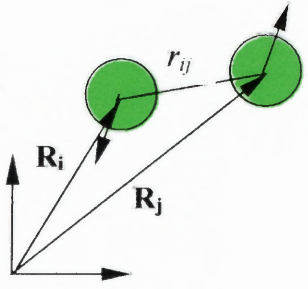

Figure 2.2 Schematic of the imposed near field repulsive force between two particles.

The force is defined as:

$$\mathbf{F}_{rep} = \begin{cases} \mathbf{0} & r_{ij} \geq 2a + \delta \\ b(\mathbf{R}_i - \mathbf{R}_j) & r_{ij} < 2a + \delta \end{cases} \tag{2.10}$$

where b is a coefficient depending on the distance between the two particles r_{ij}, and δ is an infinitely small gap used in the simulations. The repulsive force is added to Equation (3.8) at each time step to prevent the particles from overlapping in space.

2.3 Numerical Method

In this section, the numerical method used for solving the governing equations of motion is described in detail. Specifically, the suspension of particles is numerically simulated following three steps:

1. Calculate the electric fields in absence of particles.
2. Calculate the flow field in case a pressure gradient is imposed.
3. Calculate both the hydrodynamic force and the electrostatic force, and deduce the instantaneous positions of N particles at time t according to the electric field computed in step (1) and the flow field computed in step (2).

2.3.1 Electric Field

The electric field is calculated after solving for the electrical potential from equation (2.1) with the appropriate boundary conditions. The finite element method is used here to solve the Poisson's equation. Note that if f = 0, Poisson's equation reduces to Laplace's equation.

In this study, the medium is assumed to be homogeneous. It also supposed that the electrodes and channel walls are long in the z direction, and therefore the problem can be solved in two dimensions (2D).

Within the framework of the finite element method[91], the following shape functions are considered:

$$S = \{u : u \in H', u = g\} \quad \text{on } \Gamma_g \tag{2.11}$$

$$V = \{v : v \in H', v = 0\} \quad \text{on } \Gamma_h \tag{2.12}$$

together with the integrated form of Poisson's equation

$$\iint_{\Omega} v(\nabla^2 u - f)dxdy = 0 \tag{2.13}$$

which, in 2D, can be rewritten in weak form as:

$$\oint_{\Gamma_g + \Gamma_h} v\frac{\partial u}{\partial n}ds - \iint_{\Omega} \nabla u \cdot \nabla v dxdy = \iint_{\Omega} fv dxdy \tag{2.14}$$

The electric field and its gradient are then obtained by using six-node triangle elements[92]. Two-dimensional Lagrangian shape functions can be generated using the products of one-dimensional shape functions.

The electrodes are inserted within the wall boundaries and assumed to be energized at constant potential values.

2.3.2 Flow Field

The fluid is assumed to be an incompressible Newtonian liquid with constant density ρ_c and viscosity η, and, as previously mentioned, the problem is considered to be two-dimensional. The 2D governing equations are solved using the SIMPLER algorithm developed by Patankar[93, 94]. This algorithm has been successfully implemented to solve many problems of Newtonian fluid flow and heat transfer in both laminar and turbulent regimes. In certain cases, the flow is driven by a pressure gradient in the x direction.

Using the computed electric field, the electrostatic force on every individual particle is then determined by using the method proposed in the next chapter. This force, combined with the hydrodynamic force derived from Stokesian dynamics, allows one to simulate dynamically the motions of particles in suspension.

CHAPTER 3

ELECTROSTATIC FORCE

Polarizable particles suspended in a dielectric fluid experience both a hydrodynamic force and an electrostatic force. In this section, the electrostatic force acting on the particles is determined in the cases of only two particles and a relatively high number of particles. The electrostatic force can be computed by differentiating the energy density of the suspension with respect to the particle position.

If the imposed electric field is uniform, the electrostatic force exerted on a particle of the ER suspension is mainly the electrostatic particle-particle interaction force. In the case of a nonuniform electric field, in addition to the particle-particle interaction force, a polarizable particle also experiences a dielectrophoretic force. The exact electrostatic force acting on a particle can be calculated by solving the many-body potential problem and integrating the Maxwell stresses over the particles. However, this is a difficult task if there are more than two particles suspended, even in the case where the applied electric field is uniform. Bonnecaze et al.[37] developed an alternative energy method to calculate the grand capacitance matrix for a uniform electric field from which the force acting on a particle can be calculated.

In this work, the energy method is extended to the case of nonuniform fields with the addition of the near-field effects by calculating the electrostatic force on each pair of particles. In the case of a uniform electric field, one can use the two following methods to calculate the energy density: (a) directly solve Laplace's equation to obtain the electrical potential of the two particles system, and then compute the induced dipole moment of the

particles; (b) use the multiple image method to derive the induced dipole moment of the particles. In the case of a non-uniform electric field, however, it is extremely difficult to obtain a general solution by solving directly Laplace's equation subjected to various boundary conditions. Nevertheless, the induced dipole moment could be calculated from the image method and the electrostatic force within a multiparticles suspension could be computed by expanding the integral form of Laplace's equation[37-38], with or without the addition of the near-field influences.

3.1 Exact Electrostatic Force for two Particles in a Uniform Field

For two dielectric spherical particles suspended in a dielectric medium, there is creation of induced dipoles within the particles if the dielectric constants of the medium and the particle are different. The direction and magnitude of the dipole moment in a particle can be determined approximately by computing the electric field around the particle.

Due to the properties of the electrostatic field, with zero-curl and zero-divergence, the electrostatic potential satisfies Laplace's equation everywhere. By solving the latter equation, the electric field, which contains the contribution of the imposed electric field, as well as that generated by the induced dipole, is determined. The inter-particle force can then be determined by differentiating the integral of the energy density with respect to the particle position.

3.1.1 Electrical Potential of the Particles

Two equal-sized spherical particles with a dielectric constant ε_p and a radius a suspended in a fluid of dielectric constant ε_c and subjected to a uniform electric field **E** are considered. For convenience, the latter field is chosen along the z direction, that is $\mathbf{E} = E\mathbf{z}$.

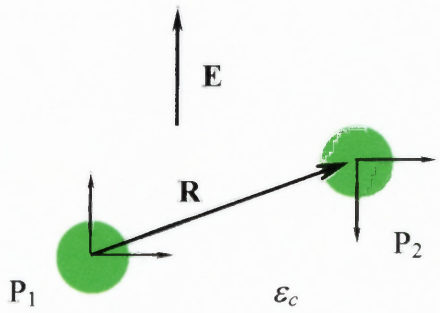

Figure 3.1 Schematic of two dielectric particles suspended in a dielectric fluid. Two systems of spherical coordinates are considered: A right-hand one whose origin coincides with the center of Particle 1, and a left-hand one whose origin coincides with the center of Particle 2.

The electrostatic potential is governed by Laplace's equation:

$$\nabla^2 \varphi = 0 \tag{3.1}$$

with appropriate boundary conditions (i) on the particle surface:

$$\varphi^- = \varphi^+ \tag{3.1a}$$

$$-\alpha \nabla \varphi^- \cdot \mathbf{n} = -\nabla \varphi^+ \cdot \mathbf{n}, \tag{3.1b}$$

and (ii) at infinity:

$$\varphi \to -\mathbf{E} \cdot \mathbf{r} \text{ when } r \to \infty \tag{3.1c}$$

where $\alpha = \varepsilon_p / \varepsilon_c$ is the ratio of the dielectric constant of the particles to that of the continuous phase.

Two (twin) systems of spherical coordinates[95,96], whose origins coincide with the centers of the particles, are used to solve the two-particles problem. Particle 1 (resp. Particle 2) is chosen to possess a right-hand (resp. left-hand) spherical coordinates system.

Let E_0 and E_1 be the two components of **E**, which are parallel and perpendicular, respectively, to the line joining the centers of the particles, and R the distance separating the particles centers. The general solution of the electrostatic potential can be written as a multipole expansion about the origin of each coordinate system:

$$\psi_j^- = -\mathbf{E}\cdot\mathbf{r} + \sum_{m=0}^{1}\sum_{n=m}^{\infty} E_m d_{mn}^j (r_j/a)^n P_n^m(\eta_j)\cos m\phi \qquad \text{for } r < a \tag{3.2a}$$

$$\psi^+ = -\mathbf{E}\cdot\mathbf{r} + \sum_{m=0}^{1}\sum_{n=m}^{\infty} E_m [g_{mn}^j (a/r_j)^{n+1} P_n^m(\eta_j) + g_{mn}^{3-j}(a/r_{3-j})^{n+1} P_n^m(\eta_{3-j})]\cos m\phi \tag{3.2b}$$

$$\text{for } r > a$$

where the index j = 1 and 2 refer to Particles 1 and 2, the superscripts - and + indicate the potentials inside and outside the particles, and $P_n^m(\cos\theta_j)$ denote the Legendre polynomials. By applying the boundary condition (3.1a), one can write the following equation for the coefficients:

$$\sum_{\rho=m}^{\infty} d_{m\rho}^j P_\rho^m(\eta_j) = \sum_{n=m}^{\infty}[g_{mn}^j P_n^m(\eta_j) + g_{mn}^{3-j}\sum_{s=m}^{\infty}\binom{n+s}{s+m}(a/R)^{n+s+1} P_s^m(\eta_{3-j})] \tag{3.4}$$

Substitution of the identity

$$\left(\frac{a}{r_i}\right)^{n+1} P_n^m(\cos\theta) = \left(\frac{a}{R}\right)^{n+1}\sum_{s=m}^{\infty}\binom{n+s}{n+m}\left(\frac{r_{3-i}}{R}\right)^s P_s^m\left(\cos\theta_{3-i}\right) \tag{3.5}$$

in equation (3.4) then leads to a first relation between the coefficients d_{mn} and g_{mn} as follows

$$d_{mn}^{j} = g_{mn}^{j} + \sum_{s=m}^{\infty} \binom{n+s}{n+m} g_{mn}^{3-j} (a/R)^{n+s+1} \tag{3.6}$$

By applying the second boundary condition (3.1b), one obtains a second equation connecting the coefficients d_{mn} and g_{mn}:

$$\alpha d_{mn}^{j} + [(n+1)/n] g_{mn}^{j} - \sum_{s=m}^{\infty} \binom{n+s}{n+m} g_{mn}^{3-j} (a/R)^{n+s+1} = a(\alpha - 1)(-1)^{(j-1)(m-1)} \delta_{1n} \tag{3.7}$$

Combining the above two equations (3.6) and (3.7) in a manner which cancels out d_{mn}, the coefficients g_{mn}^{1} and g_{mn}^{2} satisfy:

$$g_{mn}^{j} / \beta_n + \sum_{s=m}^{\infty} \binom{n+s}{n+m} g_{ms}^{3-j} (a/R)^{n+s+1} = a(-1)^{(j-1)(m-1)} \delta_{1n} \tag{3.8}$$

where $\beta_n = [n(\alpha - 1)]/[n(\alpha + 1) + 1]$, with the particular case $\beta_1 = \beta$ when $n = 1$.

Since the particles are spheres of equal sizes, in the twin coordinates systems, the symmetry gives:

$$a g_{mn} = g_{mn}^{(1)} = (-1)^{m-1} g_{mn}^{(2)} \tag{3.9a}$$

and

$$a d_{mn} = d_{mn}^{(1)} = (-1)^{m-1} d_{mn}^{(2)} \tag{3.9b}$$

Substituting equation (3.9a) into equation (3.8), the coefficients g_{mn} are found to satisfy

$$(-1)^{m-1} g_{mn} / \beta_n + \sum_{s=1}^{\infty} \binom{n+s}{n+m} g_{ms} (a/R)^{n+s+1} = \delta_{1n} \tag{3.10}$$

To Solve Equation (3.10), one expresses the solutions as power series of a/R in the forms

$$g_{0n} = \beta_n \left(\frac{a}{R}\right)^{n-1} \sum_{r=0}^{\infty} b_{nr} \left(\frac{a}{R}\right)^{r} \tag{3.11a}$$

and

$$g_{1n} = \beta_n \left(\frac{a}{R}\right)^{n-1} \sum_{r=0}^{\infty} c_{nr} \left(\frac{a}{R}\right)^{r} \tag{3.11b}$$

and solve for the coefficients b_{nr} and c_{nr} of the series. The set of coefficients d_{mn} can be determined in a similar fashion.

After substituting the coefficients g_{mn} and d_{mn} into equations (3.2a) and (3.2b), one can deduce the electric potentials inside and outside the particles in their respective system of coordinates.

3.1.2 Electrostatic Force on the Particle

For any two particles suspended in a fluid, the dipole moment induced in a particle due to the presence of another particle can be calculated (see Jeffrey[95]) by using:

$$\mathbf{P} = (\varepsilon_p - \varepsilon_c) \int_V \nabla \varphi dV \tag{3.12}$$

where the dielectric constants of the particles and the fluid are ε_p and ε_c, respectively. By introducing the potential of Section 3.1.1, the dipole moment of particle 1 reads:

$$\mathbf{P(R)} = 4\pi a^3 \beta_1 \varepsilon_0 \varepsilon_c \left\{ \mathbf{E} - \sum_{l=3}^{\infty} \left(\frac{a}{R}\right)^{l} \left(A_l \mathbf{E} - B_l \frac{\mathbf{E}\cdot\mathbf{R}}{R^2} \mathbf{R} \right) \right\} \tag{3.13}$$

where $\mathbf{R}$ is the vector connecting the center of Particle 1 to the center of Particle 2, and A_l and B_l are known coefficients, the first few being

$$A_3 = \beta_1 \quad A_4 = A_5 = 0 \quad A_6 = -\beta_1^2 \quad A_7 = 0 \quad A_8 = -3\beta_1\beta_2 \quad A_9 = \beta_1^3 \quad A_{10} = -6\beta_1\beta_3$$
$$B_3 = 3\beta_1 \quad B_4 = B_5 = 0 \quad B_6 = 3\beta_1^2 \quad B_7 = 0 \quad B_8 = 6\beta_1\beta_2 \quad B_9 = 9\beta_1^3 \quad B_{10} = 10\beta_1\beta_3$$

Equation (3.13) can be rewritten as:

$$\mathbf{P(R)} = 4\pi a^3 \beta_1 \varepsilon_0 \varepsilon_c \mathbf{E} - 4\pi a^3 \beta_1 \varepsilon_0 \varepsilon_c \sum_{l=3}^{\infty} \left(\frac{a}{R}\right)^{l} \left(A_l \mathbf{E} - B_l \frac{\mathbf{E}\cdot\mathbf{R}}{R^2} \mathbf{R} \right) \tag{3.13a}$$

The first term in Equation (3.13a) is the dipole moment induced by the applied electric field, while the second term can be considered as the induced dipole moment due to the presence of the second particle.

From classical electrodynamics[97], the electrostatic force exerted on the particle can then be determined by differentiating the energy density with respect to the particle's position:

$$\mathbf{F} = -\frac{\partial \vartheta}{\partial \mathbf{R}} = -\frac{\partial(\mathbf{P}\cdot\mathbf{E})}{\partial \mathbf{R}} \tag{3.15}$$

The expression of the force on Particle 1 because of the presence of Particle 2 reads:

$$\mathbf{F}_1^2 = c\sum_{l=3}^{\infty}\frac{a^l}{R^{l+2}}\left[lA_l\mathbf{R}_{12}(\mathbf{E}\cdot\mathbf{E}) + 2B_l\mathbf{E}(\mathbf{R}_{12}\cdot\mathbf{E}) - (l+2)B_l\frac{(\mathbf{R}_{12}\cdot\mathbf{E})(\mathbf{E}\cdot\mathbf{R}_{12})\mathbf{R}_{12}}{R^2}\right] \tag{3.16}$$

The electrostatic force can also be determined by integrating the Maxwell stress tensor over the particle surface using Equation (1.9) and deducing the electric field $\mathbf{E}$ from $\mathbf{E} = -\nabla\varphi$. This alternative method leads to Equation (3.16) as well.

For a two particles suspension subjected to a non-uniform field, the electrical potential near the particles cannot be simply solved by using the uniform boundary conditions. Therefore, the above method for deriving the expression for the dipole moment cannot be directly extended to the non-uniform case. For practical purposes, it is assumed that the induced dipole moment in Particle 1 due to the presence of Particle 2 can be represented in a similar manner whether the electric field is uniform or not, that is the electrostatic energy of Particle 1 can be computed from the product of the dipole moment and the electric field taken at the center of the particle.

If the electric fields at the center of two particles are $\mathbf{E}_1$ and $\mathbf{E}_2$, respectively, then the inter-particle electrostatic force acting on Particle 1 reads:

$$\mathbf{F}_1^2 = -\frac{\partial(\mathbf{P}_1^2 \cdot \mathbf{E}^1)}{\partial \mathbf{x}_1} \tag{3.17}$$

where $\mathbf{P}_1^2$ is the induced dipole moment on Particle 1 due to the presence of the electric field $\mathbf{E}_2$ at the center of Particle 2. Equation (3.17) then takes the expression:

$$\mathbf{F}_1^2 = c\sum_{l=3}^{\infty} \frac{a^l}{R^{l+2}} \left[lA_l \mathbf{R}_{12} (\mathbf{E}_2 \cdot \mathbf{E}_1) + B_l \mathbf{E}_2 (\mathbf{R}_{12} \cdot \mathbf{E}_1) + B_l (\mathbf{E}_2 \cdot \mathbf{R}_{12}) \mathbf{E}_1 - (l+2) B_l \frac{(\mathbf{R}_{12} \cdot \mathbf{E}_1)(\mathbf{E}_2 \cdot \mathbf{R}_{12}) \mathbf{R}_{12}}{R^2} \right] \tag{3.18}$$

where c is the coefficient equal to $c = 4\pi a^3 \beta \varepsilon_0 \varepsilon_c$. $\mathbf{R}_{12}$ is the vector along the direction connecting the center of Particle 1 to that of Particle 2, and R is the distance between the two particles centers. Notice that this approximation ignores the influence of the difference in electric fields at the center of Particle 2.

It is interesting to notice that when $l = 3$, the particle-particle force takes the same expression as that given in reference[61]:

$$\mathbf{F}_1 = \frac{1}{4\pi\varepsilon_0\varepsilon_c} \frac{3}{r^5} \left(\mathbf{r}_{ij} (\mathbf{p}_i \cdot \mathbf{p}_j) + (\mathbf{p}_i \cdot \mathbf{r}_{ij}) \mathbf{p}_j + (\mathbf{r}_{ij} \cdot \mathbf{p}_j) \mathbf{p}_i - \frac{5}{r^2} \mathbf{r}_{ij} (\mathbf{p}_i \cdot \mathbf{r}_{ij}) (\mathbf{r}_{ij} \cdot \mathbf{p}_j) \right) \tag{3.19}$$

in a uniform electric field, where $\mathbf{p}_l = 4\pi a^3 \varepsilon_0 \varepsilon_c \beta \mathbf{E}_l$ ($l = i$ or j).

3.2 Two Particles Multiple Image Method

In classical electrodynamics, the method of images is commonly used to represent the geometry of the domain by means of a small number of suitably placed charges of appropriate magnitudes.

In this section, the multiple image method is used to calculate the induced dipole moment in a spherical particle due to the other particles.

3.2.1 Image Method for a Uniform Electric Field

First, the induced dipole of a conducting spherical particle with radius a when a point dipole with moment p is placed near this particle is considered. It is well known that the electric field vanishes inside the conducting sphere while the electric potential outside the sphere can be found by using the image method. Let the distance from the point dipole to the center of the particle be r. The image dipole p' can be computed by the fact that the electrical potential inside the sphere is zero. The location of the image dipole is inside the conductor at a distance r' from the center, where $r' = a^2 / r$.

When the orientation of the dipole is perpendicular to the line between the dipole and the sphere center, the dipole moment p' is given by:

$$p' = -p\left(\frac{a}{r}\right)^3 \tag{3.20a}$$

while in the case where the dipole is parallel to the line, the image dipole moment is given by:

$$p' = 2p\left(\frac{a}{r}\right)^3 \tag{3.20b}$$

Two conducting spheres (radii a and b) placed in a medium with dielectric constant ε_c subjected to a uniform electric field $\mathbf{E_0} = E_0\mathbf{z}$ are now considered. The two spheres are electrically neutral and are located at a distance r from center to center. The two particles are denoted by the indices a and b. The applied electric field induces charges in the surface of each sphere which contribute to the dipole in each sphere such that the dipole moments are $p_{a0} = \varepsilon_c E_0 a^3$ and $p_{b0} = \varepsilon_c E_0 b^3$, respectively. The dipole moment p_{a0} induces an image dipole p_{b1} inside the sphere b, p_{b0} induces an image dipole

p_{a1} inside the sphere a, while p_{b1} induces another image dipole inside the sphere a, etc. (as shown in fig. 1). Consequently, multiple images are formed, making the total image dipole moment in the sphere a the summation of the infinite series p_{a0}, p_{a1}, p_{a2}, p_{a3}, p_{a4}, p_{a5}, ... and the total image dipole inside the sphere b the summation of p_{b0}, p_{b1}, p_{b2}, p_{b3}, p_{b4}, p_{b5}, ...

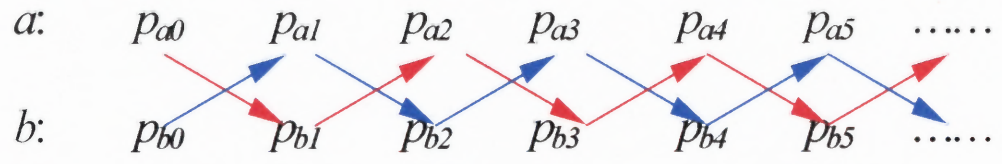

Figure 3.2 Illustration of the interaction between Particle a and Particle b through multiple images of the dipole moments.

If the two particles are ideal dielectric spheres with the same dielectric constant ε_p, the similar infinite series of image dipoles can also be determined using the image method. With the applied electric field $\mathbf{E_0} = E_0\mathbf{z}$, the magnitudes of the induced dipole moment inside the spheres are given by:

$$p_{a0} = 4\pi\beta\varepsilon_c E_0 a^3 \tag{3.21a}$$

and

$$p_{b0} = 4\pi\beta\varepsilon_c E_0 b^3 \tag{3.21b}$$

where $\beta = \dfrac{\varepsilon_p - \varepsilon_c}{\varepsilon_p + 2\varepsilon_c}$. The direction of the moment is the same as that of the electric field.

Similarly, for a point dipole placed near a dielectric particle a, the dipole moment for transverse and longitudinal field can be given by:

$$p'_T = (-\beta)p\left(\frac{a}{r}\right)^3 \tag{3.22a}$$

and

$$p'_L = (2\beta)p\left(\frac{a}{r}\right)^3 \tag{3.22b}$$

In a uniform electric field, if the two particles have the same size with radius a, the image dipoles p_{a1}, p_{a2}, p_{a3}, p_{a4}, p_{a5}, ... take the expressions (for simplicity, only the transverse dipole component is given here):

$$p'_{aT1} = (-\beta)p_{a0}\left(\frac{a}{r_0}\right)^3 = -\beta p_{a0}\left[\frac{\sinh\alpha}{\sinh 2\alpha}\right]^3 \tag{3.23a}$$

$$p'_{aT2} = (-\beta)p_{b1}\left(\frac{a}{r_1}\right)^3 = (-\beta)^2 p_{a0}\left(\frac{ar}{r^2-a^2}\right)^3\left(\frac{a}{r}\right)^3 = (-\beta)^2 p_{a0}\left[\frac{\sinh\alpha}{\sinh 3\alpha}\right]^3 \tag{3.23b}$$

$$p'_{aT3} = (-\beta)p_{a1}\left(\frac{a}{r_2}\right)^3 = \cdots = (-\beta)3p_{a0}\left[\frac{\sinh\alpha}{\sinh 4\alpha}\right]^3 \tag{3.23b}$$

$\vdots$

and so on, where r_1 is the distance from the image dipole of Sphere b to the center of Sphere a given by $r_1 = r - \frac{a^2}{r}$. Similarly, the expressions of the subsequent image dipole moments induced in sphere a can be calculated.

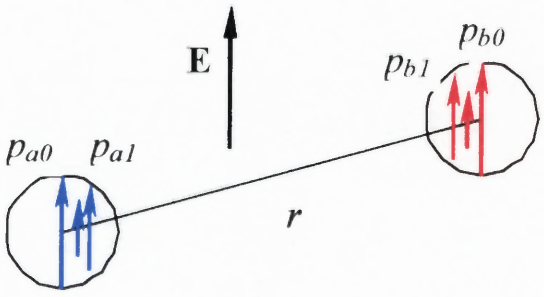

Figure 3.3 Two equal-sized dielectric spheres in a uniform electric field.

Hence, the total dipole moment of Sphere *a* can be computed from:

$$p_{aT} = p_{a0}\sum_{n=0}^{\infty}(-\beta)^n\left[\frac{\sinh\alpha}{\sinh(n+1)\alpha}\right]^3 \tag{3.24a}$$

and

$$p_{aL} = p_{a0}\sum_{n=0}^{\infty}(2\beta)^n\left[\frac{\sinh\alpha}{\sinh(n+1)\alpha}\right]^3 \tag{3.24b}$$

where the parameter α satisfies $\cosh\alpha = \frac{r}{2a}$. Because the two particles have the same size *a*, the image dipole of Sphere *b* have similar expressions in a uniform electric field.

Using θ_{ij} as the angle between the sphere centerline and the applied electric field **E**, the dipole moment induced in Particle *a* due to the presence of another particle *b* can be written as:

$$\mathbf{P} = p_{a0}\sin\theta_{ij}\sum_{n=0}^{\infty}(2\beta)^n\left[\frac{\sinh\alpha}{\sinh(n+1)\alpha}\right]^3\mathbf{e}_r + p_{a0}\cos\theta_{ij}\sum_{n=0}^{\infty}(-\beta)^n\left[\frac{\sinh\alpha}{\sinh(n+1)\alpha}\right]^3\mathbf{e}_\theta \tag{3.25}$$

From classical electrodynamics, the electrostatic energy density *W* of the suspension is computed by

$$W = \frac{1}{2V}\int_V \mathbf{P}\cdot\mathbf{E}d\mathbf{r} = \frac{1}{2}\sum_{n=1}^{\infty}\mathbf{P}_i\cdot\mathbf{E}_i \tag{3.26}$$

The force exerted on a particle α due to the presence of a particle β can be calculated by differentiating the energy with respect to the particle position as:

$$\mathbf{F}_\alpha^\beta = -\frac{\partial W}{\partial \mathbf{r}} \tag{3.27}$$

where $\mathbf{r}$ is defined as $\mathbf{x}_\beta - \mathbf{x}_\alpha$.

Therefore, in a uniform electric field, the electrostatic energy reads:

$$W = p_{aT}E\sin^2\theta + p_{aL}E\cos^2\theta \tag{3.28}$$

The force on the Particle a is expressed as:

$$\mathbf{F}_1^2 = F_r\mathbf{e}_r + F_\theta\mathbf{e}_\theta \tag{3.29}$$

where

$$F_r = -\frac{\partial W}{\partial r} = E(\frac{\partial p_{aT}}{\partial r}\sin^2\theta + \frac{\partial p_{aL}}{\partial r}\cos^2\theta) \tag{3.29a}$$

and

$$F_\theta = -\frac{1}{r}\frac{\partial W}{\partial \theta} = \frac{1}{r}E(p_{aT} - p_{aL})\sin 2\theta \tag{3.29b}$$

where p_{aT} and p_{aL} satisfy Equations (3.24a) and (3.24b).

Equation (3.29) can be compared with Klingenberg's exact force formula:

$$\mathbf{F}^\alpha = 12\pi\varepsilon_0\varepsilon_c(\beta E)^2 a^2\left(\frac{a}{r}\right)^4\left(\left(2f_{//}\cos^2\theta_{ij} - f_\perp\sin^2\theta_{ij}\right)\mathbf{e}_r + f_\Gamma\sin 2\theta_{ij}\mathbf{e}_\theta\right) \tag{3.30}$$

One can now introduce the following force coefficients

$$f_\Gamma = \frac{1}{r}(p_{aT} - p_{aL})E\Big/F_0 \tag{3.31a}$$

$$f_{\perp} = -\frac{\partial p_{aT}}{\partial r} E \Big/ F_0 \tag{3.31b}$$

$$f_{//} = \frac{\partial p_{aL}}{\partial r} E \Big/ 2F_0 \tag{3.31c}$$

where $F_0 = 12\pi\varepsilon_0\varepsilon_c a^3 \beta^2 E^2$.

3.2.2 Dipole Moment in Particles in the case of a Non-uniform Field

In the case where the applied electric field is non-uniform, the field induced dipole moments in two equal-sized particles 1 and 2 with radii a are:

$$\mathbf{p}_{10} = 4\pi\beta\varepsilon_0\varepsilon_c \mathbf{E}_1 a^3 \tag{3.32a}$$

and

$$\mathbf{p}_{20} = 4\pi\beta\varepsilon_0\varepsilon_c \mathbf{E}_2 a^3 \tag{3.32b}$$

where $\mathbf{E}_1$ and $\mathbf{E}_2$ are the electric fields at the center of each particle, respectively.

When there are more than one particle suspended in the medium, there is a need to take into account the interactions between the particles, especially when two particles are close. Considering a pair of nearly touching particles, with a center-to-center separation r, one can write the total image dipole moment of Particle a in even and odd terms:

$$p_{1T} = p_{10}\sum_{n=0}^{\infty}(-\beta)^{2n}\left[\frac{\sinh\alpha}{\sinh(2n+1)\alpha}\right]^3 + p_{20}\sum_{n=0}^{\infty}(-\beta)^{2n+1}\left[\frac{\sinh\alpha}{\sinh 2(n+1)\alpha}\right]^3 \tag{3.33a}$$

and

$$p_{1L} = p_{10}\sum_{n=0}^{\infty}(2\beta)^{2n}\left[\frac{\sinh\alpha}{\sinh(2n+1)\alpha}\right]^3 + p_{20}\sum_{n=0}^{\infty}(2\beta)^{2n+1}\left[\frac{\sinh\alpha}{\sinh 2(n+1)\alpha}\right]^3 \tag{3.33b}$$

using a method similar to that used in the case of a uniform electric field.

Similarly, the total image dipole moment of Particle *b* is given by:

$$p_{2T} = p_{20}\sum_{n=0}^{\infty}(-\beta)^{2n}\left[\frac{\sinh\alpha}{\sinh(2n+1)\alpha}\right]^3 + p_{10}\sum_{n=0}^{\infty}(-\beta)^{2n+1}\left[\frac{\sinh\alpha}{\sinh 2(n+1)\alpha}\right]^3 \tag{3.34a}$$

and

$$p_{2L} = p_{20}\sum_{n=0}^{\infty}(2\beta)^{2n}\left[\frac{\sinh\alpha}{\sinh(2n+1)\alpha}\right]^3 + p_{10}\sum_{n=0}^{\infty}(2\beta)^{2n+1}\left[\frac{\sinh\alpha}{\sinh 2(n+1)\alpha}\right]^3 \tag{3.34b}$$

In a non-uniform electric field, the electrostatic energy of Particle *a* can be written as:

$$W = \frac{1}{2}\mathbf{p}_1\cdot\mathbf{E}_1 = 2\pi\beta\varepsilon_1 a^3\left[\alpha_1 E_1^2 + \alpha_2 E_1 E_2\right] \tag{3.35}$$

Including the first three terms of the dipole moment, the coefficients α_1 and α_2 take the expression:

$$\alpha_1 = 1+\left[(2\beta)^2\left(\frac{\sinh\alpha}{\sinh 3\alpha}\right)^3\cos^2\theta_1 + (-\beta)^2\left(\frac{\sinh\alpha}{\sinh 3\alpha}\right)^3\sin^2\theta_1\right] \tag{3.35a}$$

$$\alpha_2 = 2\beta\left(\frac{a}{r}\right)^3\cos\theta_1\cos\theta_2 + (-\beta)\left(\frac{a}{r}\right)^3\sin\theta_1\sin\theta_2 \tag{3.35b}$$

where $\cos\theta_i = \dfrac{\mathbf{E}_i\cdot\mathbf{r}}{|\mathbf{E}_i||\mathbf{r}|}$, i = 1 or 2.

By differentiating the electrostatic energy with respect to the particle position, one obtains the electrostatic force acting on Particle 1:

$$\mathbf{F}_1^2 = 2\pi\beta\varepsilon_1 a^3\left\{\frac{6\beta a^3}{r^5}\left[(\mathbf{E}_1\cdot\mathbf{r})\mathbf{E}_2 + (\mathbf{E}_2\cdot\mathbf{r})\mathbf{E}_1 + (\mathbf{E}_2\cdot\mathbf{E}_1)\mathbf{r} - 5\frac{(\mathbf{E}_1\cdot\mathbf{r})(\mathbf{E}_2\cdot\mathbf{r})\mathbf{r}}{r^2}\right]\right\}$$

$$+2\pi\beta\varepsilon_1 a^3\left\{2\left(1+\frac{\beta^2}{(r_1^2-1)^3}\right)\mathbf{E}_1\cdot\nabla\mathbf{E}_1\right.$$

$$-\frac{6\beta^2}{a^2(r_1^2-1)^4}\mathbf{E}_1^2\mathbf{r}-3\beta^2\frac{8r_1^2-2}{r^4(r_1^2-1)^4}(\mathbf{E}_1\cdot\mathbf{r})^2\mathbf{r}$$

$$+6\beta^2\frac{1}{r^2(r_1^2-1)^3}(\mathbf{E}_1\cdot\mathbf{r})(\mathbf{r}\cdot\nabla\mathbf{E}_1)+6\beta^2\frac{1}{r^2(r_1^2-1)^3}(\mathbf{E}_1\cdot\mathbf{r})\mathbf{E}_1$$

$$+6\beta a^3\frac{(\mathbf{E}_1\cdot\mathbf{r})(\mathbf{r}\cdot\nabla\mathbf{E}_2)+(\mathbf{E}_2\cdot\mathbf{r})(\mathbf{r}\cdot\nabla\mathbf{E}_1)}{r^5}-2\beta a^3\frac{\mathbf{E}_1\cdot\nabla\mathbf{E}_2+\mathbf{E}_2\cdot\nabla\mathbf{E}_1}{r^3}\Bigg\} \tag{3.36}$$

where $r_1=\frac{r}{a}$.

The force formula $\mathbf{F}_1^2$ is based on the first three terms of the dipole moment. Notice that the traditional DEP force and the dipole-dipole interaction force used in reference[61] are recovered here as the first two terms, and that the electric field $\mathbf{E}_2$ taken at the center of Particle 2, together with its gradient $\nabla\mathbf{E}_2$, enter in the expression of $\mathbf{F}_1^2$ and therefore affect the force acting on Particle 1.

3.3 Multi-Particles Electrostatic Force

When more than two particles suspended in a dielectric fluid are subjected to a spatially non-uniform electric field, the electrostatic force acting on a given particle consists of two parts: (a) the interaction between the induced dipole of the particle with the non-uniform electric field; (b) the interaction between the induced dipole of the particle and dipoles of the other particles. In principle, the exact electrostatic forces acting on a particle can be calculated theoretically from the solution of the many-body potential problem and the integration of the Maxwell stresses over each particle in the domain. For practical purposes, however, this is a huge task if there are more than two particles in the suspension, even in the case of a uniform electric field.

In this section, a general method to compute the electrostatic force by expanding the integral form of Laplace's equation is presented. This method was first developed by Bonnecaze et al.[37,38] to determine the grand capacitance matrix, the properties of the ER fluid, and the electrostatic force on a particle within a suspension subjected to a uniform electric field. In this section, the integral form of Laplace's equation was expanded in terms of a Taylor series to obtain the electrostatic force in the case of a non-uniform electric field.

3.3.1 Taylor Expansion

For N particles suspended in a fluid, the electric potential and the gradient of the potential at the center of the particle can be expanded using a Taylor series when truncated at the dipole level[37,38]:

$$\varphi(\mathbf{R}_\alpha)-\varphi^{\mathrm{E}}(\mathbf{R}_\alpha)=\frac{q_\alpha}{4\pi\varepsilon_0\varepsilon_c a}[1+h(\rho)]+\frac{1}{4\pi\varepsilon_0\varepsilon_c}\sum_{\substack{\beta\\ \beta\neq\alpha}}(q_\beta\frac{1}{r}+\mathbf{S}_\beta\cdot\nabla\frac{1}{r}) \tag{3.37}$$

$$\nabla\varphi(\mathbf{x})-\mathbf{G}^E=-\frac{1}{4\pi\varepsilon_0\varepsilon_c}\sum_{\alpha}(q_\alpha\nabla_y\frac{1}{r}+\mathbf{S}_\alpha\cdot\nabla_y\nabla_y\frac{1}{r}) \tag{3.38}$$

For spherical particles, O'Brien[98] used the Faxén-type law of dipoles and derived the formula:

$$\nabla\varphi_\alpha(\mathbf{R}_\alpha)=-\frac{\mathbf{S}_\alpha}{4\pi\varepsilon_0\varepsilon_c\beta a^3} \tag{3.39}$$

Thus, the potential gradient at the center of the particle can also be approximately in terms of the N particle charges and dipoles as follows:

$$-\mathbf{G}^E=\frac{\mathbf{S}_\alpha}{4\pi\varepsilon_0\varepsilon_c a^3\beta}-\frac{1}{4\pi\varepsilon_0\varepsilon_c}\sum_{\substack{\beta\\ \beta\neq\alpha}}(q_\beta\nabla\frac{1}{r}+\mathbf{S}_\beta\cdot\nabla\nabla\frac{1}{r}) \tag{3.40}$$

Combining equations (3.37) and (3.40), one can derive the following expression:

$$\begin{Bmatrix} \mathbf{\Phi} \\ -\mathbf{G}^E \end{Bmatrix} = \begin{pmatrix} \mathbf{M}_{\varphi q} & \mathbf{M}_{\varphi S} \\ \mathbf{M}_{Eq} & \mathbf{M}_{ES} \end{pmatrix} \begin{Bmatrix} \mathbf{q} \\ \mathbf{S} \end{Bmatrix} \tag{3.41}$$

where $\mathbf{\Phi}$ is the vector obtained by subtracting the external potential from the particle potential evaluated at the particles centers, $\varphi(\mathbf{R}_\alpha) - \varphi^{\mathbf{E}}(\mathbf{R}_\alpha)$, and $\mathbf{q}$ and $\mathbf{S}$ are the vectors of the N particle charges and dipoles, respectively.

Let $\boldsymbol{\varepsilon} = -\mathbf{G}^{\mathbf{E}}$ be the electric field in absence of the particles. Equation (3.41) can then be rewritten as:

$$\begin{Bmatrix} \mathbf{\Phi} \\ \boldsymbol{\varepsilon} \end{Bmatrix} = \begin{pmatrix} \mathbf{M}_{\varphi q} & \mathbf{M}_{\varphi S} \\ \mathbf{M}_{Eq} & \mathbf{M}_{ES} \end{pmatrix} \begin{Bmatrix} \mathbf{q} \\ \mathbf{S} \end{Bmatrix} = \mathbf{M} \cdot \begin{Bmatrix} \mathbf{q} \\ \mathbf{S} \end{Bmatrix} \tag{3.42}$$

where the matrix $\mathbf{M}$ is referred to as the grand potential matrix[37]. It is composed of sub-matrices which couple the variables appearing as subscripts; for example, $\mathbf{M}_{\varphi q}$ is the matrix coupling the potentials and the charges, etc. The grand potential matrix, together with its sub-matrices, can be computed according to the expansion of Laplace's equation; for example, $\mathbf{M}_{ES}$ is the $3N$ X $3N$ submatrix such as:

$$\mathbf{M}_{ES} = \frac{1}{4\pi\varepsilon_0\varepsilon_c\beta a^3} \cdot \mathbf{I} - \frac{1}{4\pi\varepsilon_0\varepsilon_c} \sum_{\substack{\beta \\ \beta \neq \alpha}} \nabla_y \nabla_y \frac{1}{r} \tag{3.43}$$

3.3.2 Electrostatic Force

Since Laplace's equation, subjected to the appropriate boundary conditions, is linear together with the external electric field, the N particle charges, the dipole moments and potentials, one can write:

$$\begin{pmatrix} \mathbf{q} \\ \mathbf{S} \end{pmatrix} = \begin{pmatrix} \mathbf{C}_{q\varphi} & \mathbf{C}_{qE} \\ \mathbf{C}_{S\varphi} & \mathbf{C}_{SE} \end{pmatrix} \begin{pmatrix} \mathbf{\Phi} \\ \boldsymbol{\varepsilon} \end{pmatrix} = \mathbf{C} \cdot \begin{pmatrix} \mathbf{\Phi} \\ \boldsymbol{\varepsilon} \end{pmatrix} \tag{3.44}$$

where $\mathbf{q}$ and $\mathbf{\Phi}$ are the N-dimensional vectors containing the particle charges and potentials, $\mathbf{C}$ is the grand capacitance matrix with its sub-matrices relating the variables appearing in their subscripts; for example, $\mathbf{C}_{q\Phi}$. relates the particle charges to their potentials.

In classic electrodynamics[97], it is known that the energy of charged particles in the absence of an electric field is one-half the sum of the product of the particle charges and their local potentials. Thus, for charge-free particles in an electric field, the electrostatic energy density is given by:

$$\vartheta = \frac{1}{2V_c} \sum_{\alpha} \mathbf{S}^{\alpha} \cdot \mathbf{E} = -\frac{1}{2V_c} \mathbf{S} \cdot \boldsymbol{\varepsilon} \tag{3.45}$$

where ϑ is the energy density for a system of N particles in a volume V_c. $\mathbf{S}^{\alpha}$ is the induced dipole moment of Particle α, and $\mathbf{E}$ is the local electric field taken at the center of this particle.

For charge-free particles ($\mathbf{q} = \mathbf{0}$), the dipole moment can be derived from Equation (3.44) as:

$$\mathbf{S}_E = \hat{\mathbf{C}}(\mathbf{x}) \cdot \boldsymbol{\varepsilon} \tag{3.46}$$

where

$$\hat{\mathbf{C}}(\mathbf{x}) = \mathbf{C}_{S\phi} \cdot \mathbf{C}_{q\phi}^{-1} \cdot \mathbf{C}_{qE} - \mathbf{C}_{SE} \tag{3.47}$$

Substituting Equations (3.46) and (3.47) into Equation (3.45), the electrostatic energy density becomes

$$\vartheta = -\frac{1}{2V}\boldsymbol{\varepsilon}\cdot\hat{\mathbf{C}}(\mathbf{x})\cdot\boldsymbol{\varepsilon} \tag{3.48}$$

From classical electrodynamics, the force on Particle α is computed from the differentiation of the energy density with respect to the particle position, i.e.

$$\mathbf{F}^{\alpha} = -\frac{\partial\vartheta}{\partial\mathbf{x}_{\alpha}} \tag{3.49}$$

In the case of a non-uniform electric field, the potential gradient is spatially related to the position $\mathbf{x}$. Taking into account the fact that $\hat{\mathbf{C}}(\mathbf{x})$ is a symmetric matrix, the electrostatic force can be expressed as

$$\mathbf{F}^{\alpha} = \frac{1}{2}(\boldsymbol{\varepsilon}(\mathbf{x})\cdot\frac{\partial\hat{\mathbf{C}}(\mathbf{x})}{\partial\mathbf{x}_{\alpha}}\cdot\boldsymbol{\varepsilon}(\mathbf{x}) + 2\frac{\partial\boldsymbol{\varepsilon}(\mathbf{x})}{\partial\mathbf{x}_{\alpha}}\cdot\hat{\mathbf{C}}(\mathbf{x})\cdot\boldsymbol{\varepsilon}(\mathbf{x})) \tag{3.50}$$

Notice that in the case of a uniform electric field[18], the electric field strength is constant everywhere, the gradient of the electric field becomes zero, and the electrostatic force in Equation (3.50) simplifies to:

$$\mathbf{F}^{\alpha} = \frac{1}{2}\boldsymbol{\varepsilon}\cdot\frac{\partial\hat{\mathbf{C}}(\mathbf{x})}{\partial\mathbf{x}_{\alpha}}\cdot\boldsymbol{\varepsilon} \tag{3.51}$$

It follows that Equation (3.50) can be used to determine the electrostatic force in both uniform and nonuniform electric fields. Furthermore, it is interesting to point out that the grand capacitance matrix $\mathbf{C}$ and all its submatrices include both the long-ranged many-body interactions as well as the lubrication-like near field interactions, and so does the electrostatic force.

3.3.3 Electrostatic Force with Near-field Effects

Unfortunately, an exact computation of the capacitance matrix **C** and its sub-matrices is not possible due to the presence of infinite terms. Notice that the capacitance matrix **C** can be determined theoretically by inverting the grand potential matrix **M**. In practice, **M** is truncated at dipole levels and therefore its inversion does not coincide with the real capacitance matrix. The matrix **C** can be approximately computed from the potential matrix **M**[37] by means of the relation

$$\mathbf{C} \approx \mathbf{M}^{-1} + \mathbf{C}_{2b} - \mathbf{C}_{2b}^{\infty} \tag{3.52}$$

which includes both near- and far-fields, as well as multi-particles interactions. **M,** the potential matrix, can be calculated easily by expanding the integral form of Laplace's equation of both the potential and its gradient as expressed in Equation (3.41).

In the case of an nonuniform electric field, the computation of the exact two-body capacitance matrix, $\mathbf{C}_{2b}$, unlike that corresponding to a uniform electric field, cannot be calculated by solving directly Laplace's equation, because of the difficulty of obtaining analytically the general solution of Laplace's equation with different boundary conditions. Hence, the multiple image method[34,97] is now introduced to compute the induced dipole moment of a pair of particles when the latter are nearly touching. It is worth pointing out that the image method also uses the integral equation approach to calculate the electrostatic energy, and then the force is computed by differentiating the energy with respect to spatial coordinates.

The far-field two-body capacitance matrix, C_{2b}^{∞}, is determined through the same method as that used to calculate the invert of **M**, that is by neglecting the presence of

other particles, except for the *i*th and *j*th particles located in the computational cell. The force is computed by using the equation:

$$\mathbf{F}_j^{i\infty} = \frac{1}{2}\boldsymbol{\varepsilon}\cdot\frac{\partial \mathbf{C}_{2b}^{\infty}}{\partial \mathbf{x}_\alpha}\cdot\boldsymbol{\varepsilon} + \frac{\partial \boldsymbol{\varepsilon}}{\partial \mathbf{x}_\alpha}\cdot\mathbf{C}_{2b}^{\infty}\cdot\boldsymbol{\varepsilon} \tag{3.53}$$

The exact two body interaction force $\mathbf{F}_j^i$ is computed from the image method, as expressed in Equation (3.36) in the case of a nonuniform electric field and Equation (3.18) or (3.29) in the case of a uniform electric field.

Therefore, the general electrostatic force with the addition of near-field effects can be expressed as:

$$\mathbf{F}_P^i = \frac{1}{2}\boldsymbol{\varepsilon}\cdot\frac{\partial \hat{\mathbf{C}}(\mathbf{x})}{\partial \mathbf{x}_\alpha}\cdot\boldsymbol{\varepsilon} + \frac{\partial \boldsymbol{\varepsilon}}{\partial \mathbf{x}_\alpha}\cdot\hat{\mathbf{C}}(\mathbf{x})\cdot\boldsymbol{\varepsilon} + \sum_{\substack{j=1\\ j\neq i}}^{N}(\mathbf{F}_j^i - \mathbf{F}_j^{i\infty}) \tag{3.54}$$

3.3.4 Electrostatic Force without Near-field Effects

In the case of a dilute suspension in which particles do not concentrate in particular areas, near-field interactions can be neglected in the capacitance matrix and the dipole moments take the expression:

$$\mathbf{S} \approx -\mathbf{C}_{\mathbf{SE}}\cdot\boldsymbol{\varepsilon} = -\mathbf{M}_{\mathbf{ES}}^{-1}\cdot\boldsymbol{\varepsilon} \tag{3.55}$$

Substituting Equation (3.55) into Equation (3.50), the force expression can be rewritten as:

$$\mathbf{F}^{\alpha} = \frac{1}{2}\boldsymbol{\varepsilon}(\mathbf{x})\cdot\frac{\partial \mathbf{M}_{\mathbf{ES}}^{-1}(\mathbf{x})}{\partial \mathbf{x}_\alpha}\cdot\boldsymbol{\varepsilon}(\mathbf{x}) + \frac{\partial \boldsymbol{\varepsilon}(\mathbf{x})}{\partial \mathbf{x}_\alpha}\cdot\mathbf{M}_{\mathbf{ES}}^{-1}(\mathbf{x})\cdot\boldsymbol{\varepsilon}(\mathbf{x}) \tag{3.56}$$

Using tensor properties, the first term in the right hand side of Equation (3.56) reads:

$$\frac{1}{2}\boldsymbol{\varepsilon}(\mathbf{x})\cdot\mathbf{M}_{\mathbf{ES}}^{-1}(\mathbf{x})\cdot\frac{\partial \mathbf{M}_{\mathbf{ES}}(\mathbf{x})}{\partial \mathbf{x}_\alpha}\cdot\mathbf{M}_{\mathbf{ES}}^{-1}(\mathbf{x})\cdot\boldsymbol{\varepsilon}(\mathbf{x}) \tag{3.57}$$

Because the sub-matrix $\mathbf{M}_{ES}$ is symmetric, Equation (3.57) can be written by using Equation (3.55) as:

$$\frac{1}{2}\mathbf{S}\cdot\frac{\partial\mathbf{M}_{ES}(\mathbf{x})}{\partial\mathbf{x}_\alpha}\cdot\mathbf{S} \tag{3.58}$$

Using the expression (3.43) of $\mathbf{M}_{ES}$ in Equation (3.58), the first term of Equation (3.50) becomes:

$$\frac{1}{2}\cdot\frac{1}{4\pi\varepsilon_0\varepsilon_c}\mathbf{S}^\alpha\cdot((\sum_{\substack{\beta\\ \beta\neq\alpha}}\nabla_y\nabla_y\nabla_y\frac{1}{r})\cdot\mathbf{S}^\beta) \tag{3.59}$$

If the effects of other particles' dipoles are also neglected, Equation (3.43) is further simplified to:

$$\mathbf{M}_{ES}=\frac{1}{4\pi\varepsilon_0\varepsilon_c\beta a^3}\cdot\mathbf{I} \tag{3.60}$$

By taking into account Equation (3.60), one can derive the following expression for the second term on the right-hand side of Equation (3.50):

$$\frac{\partial\boldsymbol{\varepsilon}(\mathbf{x})}{\partial\mathbf{x}_\alpha}\cdot\mathbf{M}_{ES}^{-1}(\mathbf{x})\cdot\boldsymbol{\varepsilon}(\mathbf{x})=4\pi\varepsilon_0\varepsilon_c\beta a^3\boldsymbol{\varepsilon}(\mathbf{x})\cdot\nabla\boldsymbol{\varepsilon}(\mathbf{x}) \tag{3.61}$$

which is simply the classical point-dipole approximation of the dielectrophoretic force acting on an isolated spherical particle α and used by many investigators.

Combining Equations (3.59) and (3.61), it is clear that the electrostatic force derived with the energy method is the same as that of others[61] if both the near-field interactions and the many body interactions are neglected.

When the suspension is subjected to a uniform electric field, the electrostatic force is determined by:

$$\mathbf{F}^{\alpha} = \frac{1}{2} \cdot \frac{1}{4\pi\varepsilon_0\varepsilon_c} \mathbf{S}^{\alpha} \cdot ((\sum_{\substack{\beta \\ \beta \neq \alpha}} \nabla_y \nabla_y \nabla_y \frac{1}{r}) \cdot \mathbf{S}^{\beta}) \tag{3.62}$$

In fact, from Taylor's expansion, the force acting on a particle with some charge distribution can be approximately evaluated by:

$$\mathbf{F}^{\alpha} = q_{\alpha}\mathbf{E}(\mathbf{x}) + \frac{1}{2}\mathbf{S}^{\alpha} \cdot \nabla\mathbf{E}(\mathbf{x}) + \cdots \tag{3.63}$$

where **E**(x) is the value of the local electric field at the center of the particle α. For N charge-free particles, the local gradient of the electric field at the center of the particle α is approximately given by:

$$\nabla\mathbf{E}(\mathbf{x}) = \frac{1}{4\pi\varepsilon_0\varepsilon_c} \sum_{\substack{\beta \\ \beta \neq \alpha}} \nabla_y \nabla_y \nabla_y \frac{1}{r} \cdot \mathbf{S}^{\beta} \tag{3.64}$$

Combining Equations (3.63) and (3.64), and considering that the particles are charge-free, the electrostatic force on the particle α due to the presence of other particles is:

$$\mathbf{F}^{\alpha} = \frac{1}{2} \cdot \frac{1}{4\pi\varepsilon_0\varepsilon_c} \mathbf{S}^{\alpha} \cdot \sum_{\substack{\beta \\ \beta \neq \alpha}} \nabla_y \nabla_y \nabla_y \frac{1}{r} \cdot \mathbf{S}^{\beta} + \cdots \tag{3.65}$$

that is exactly the same expression as Equation (3.62).

The electrostatic force without the addition of near-field effects, is obtained by combining Equations (3.59) and (3.61) as:

$$\mathbf{F}_P = \frac{1}{8\pi\varepsilon_0\varepsilon_c} \mathbf{S}_E^i \cdot \sum_{\substack{j=1 \\ j \neq i}}^{N} \nabla\nabla\nabla \frac{1}{r} \cdot \mathbf{S}_E^j + 4\pi\varepsilon_0\varepsilon_c\beta a^3 \boldsymbol{\varepsilon} \cdot \nabla\boldsymbol{\varepsilon} \tag{3.66}$$

Using Equation (3.66) in Equation (2.9), the particle location **x** can be computed from:

$$\mathbf{x}_n = \mathbf{x}_{n-1} + \left(\mathbf{u}_c + \frac{1}{6\pi a\eta} \left(\frac{1}{8\pi\varepsilon_0\varepsilon_c} \mathbf{S}_E^i \cdot \sum_{\substack{j=1 \\ j\neq i}}^{N} \nabla\nabla\nabla \frac{1}{r} \cdot \mathbf{S}_E^j + 4\pi\varepsilon_0\varepsilon_c \beta a^3 \boldsymbol{\varepsilon} \cdot \nabla\boldsymbol{\varepsilon} \right) \right) \cdot \Delta t \tag{3.67}$$

The latter equation can be nondimensionalized by using the characteristic particles radius a, time $t_s = \frac{a}{U}$, velocity U taken on the centerline of the channel for a pressure driven flow between 2D parallel plates, and electrostatic force $12\pi\varepsilon_0\varepsilon_c(\beta E)^2 a^2$. The Mason number, Ma, or ratio of the viscous drag force to the electrostatic forces, is such that $Ma = \eta U / 2\varepsilon_0\varepsilon_c(\beta E)^2 a$.

CHAPTER 4

TWO PARTICLES PROBLEM

In this chapter, the suspension properties of two particles are studied. When particles are suspended in a dielectric fluid and subjected to an electric field, as described in the previous chapter, the particles experience both a hydrodynamic and an electrostatic force. The hydrodynamic force is approximated by Stokes' drag, while the electrostatic force is computed using either the energy method (Equation (3.16)) or the image method (Equation (3.29)) in the case of a uniform electric field. This electrostatic force accounts for both the near- and far-field interactions. As discussed earlier, the electrostatic force computed from the image method can also be used to calculate the force acting on particles in the case of a non-uniform electric field.

4.1 Two Particles in a Uniform Field

In this section, suspensions consisting of two particles suspended in a liquid are studied in the case of a uniform electric field. IM represents the results obtained with the image method (from Equation (3.29)), DD those obtained with the point-dipole approximation, and NF, FF those computed from the energy method with and without near-field effects, respectively (Equations (3.54) and (3.66)).

4.1.1 Convergence of the Multiple Image Method

The analytical multiple image method gives different results depending on how many terms are retained in the multiple image expressions and various models are recovered with the particular truncations considered. If only one term is retained, i.e., $n = 1$, the

method reduces to the point-dipole model, and the total dipole of a given particle is solely due to the applied field. If two terms are retained, i.e., $n = 2$, the dipole-induced-dipole model is recovered; if more than two terms are retained, the method corresponds to the multiple-induced-dipole method, i.e., $n = 3$ to ∞, but in the latter case the force diverges as r/a$\rightarrow$2, i.e. when two particles are touching.

The multiple image method can then be used to compare the various models. Table 4.1 lists the force obtained from the multiple image method with different truncations when two particles are placed initially along the z direction, such that the line joining their centers is parallel to the electric field. Computations were carried out when the particles are at a distance $r = 2.2a$ and $r = 3a$ of each other and for two different particle-to-fluid dielectric constant ratios $\alpha = 2.0$ and $\alpha = 10.0$. The force is non-dimensionalized by $12\pi\varepsilon_0\varepsilon_c\beta^2E^2a^2$. Table 4.1 shows that the method converges as the number of terms is increased, and the convergence is faster for the lowest dielectric constant ratio. Indeed, for $\alpha = 2.0$ the value of the force is observed to remain constant with eight terms or more, even when the two particles are very close (r/a = 2.0), while convergence requires fifteen terms for $\alpha = 10.0$.

Table 4.1 Convergence of the Multiple Image Method

n	$\varepsilon_p / \varepsilon_c = 2.0$		$\varepsilon_p / \varepsilon_c = 10.0$	
	r/a=2.2	r/a=3.0	r/a=2.2	r/a=3.0
3	.109721	.026220	.183055	.029664
4	.110484	.026223	.203662	.029731
6	.110639	.026223	.219773	.029739
8	.110641	.026223	.222032	.029739
9	.110641	.026223	.222740	.029739
15	.110641	.026223	.222744	.029739
20	.110641	.026223	.222744	.029739
40	.110641	.026223	.222744	.029739
60	.110641	.026223	.222744	.029739
80	.110641	.026223	.222744	.029739
100	.110641	.026223	.222744	.029739

Note: Value of the electrostatic force for various truncations of the series (n refers to the number of terms considered), for two particle-to-fluid dielectric constant ratios and two values of the distance between the particles.

4.1.2 Comparison of the Force Computed with Different Methods

Unfortunately, there are only limited results in the literature for the many-body electrostatic interaction force obtained with various methods. The available data for two identical spheres suspended in a fluid subjected to a uniform electric field are the exact results of Klingenberg et al.[24] (presented in Gast and Zukoski[13]) obtained by calculating the electrostatic force by integrating the Maxwell stress tensor on the particle surface for two particle-to-fluid dielectric constant ratios $\alpha = 2.0$ and $\alpha = 10.0$. The conclusion was that the energy method with near field effects led to results very close to the exact data of Klingenberg for these two dielectric constant ratios.

Table 4.2 compares the results of the force functions from calculations performed in this thesis, in the case of two particles with two different particle-to-fluid dielectric constant ratios ($\alpha = 2.0$ and $\alpha = 10.0$) and two different distances between the particles. Here, the various techniques described above have been used, specifically the energy method with (NF) and without (FF) the near-field interactions and the image method (IM) with fifteen terms retained in the series. In addition, results are compared with Klingenberg's exact data, as reported in reference[13]. The letter "K" refers to Klingenberg's data. For convenience, the electric field was assumed to be along the z direction. The computational space is a closed box with dimensions 1.6mm, 0.4mm, and 1.6mm in the x, y, and z directions, respectively. The test fluid dielectric constant is 7.3, and the particle-to-fluid dielectric constant ratios are chosen to be 2.0 and 10.0 to easily compare the force.

Table 4.2 shows that the electrostatic force computed from the energy density formulation with the inclusion of the near-field interactions (Equation (3.16)) is in excellent agreement with the exact two particle interaction data of reference[18], for both particle-to-fluid dielectric constant ratios, even when the two particles are nearly touching. However, if the near-field effects are neglected, the results do not agree as much and the discrepancy increases as (i) the particles get closer to each other and (ii) the particle-to-fluid dielectric constants ratio increases. For example, when the distance ratio r/a is 2.2, the error is 25% for $\alpha = 2.0$, but for $\alpha = 10.0$, the error is as large as 70%. In addition, it was found that whether or not the near-field interactions were included, the energy method gave results closer to exact values than the point-dipole method. Notice that when the applied electric field is uniform and the point dipole approximation is used,

the force functions are unity for all particle separations and for any particle-to-fluid dielectric constant ratio.

Table 4.2 Comparison of the Force Functions for a Two-particle Suspension in a Uniform Electric Field

	$f_{//}$				$f_{\perp}$				f_{Γ}			
r/a	K	FF	NF	IM	K	FF	NF	DD	K	FF	NF	IM
						α=10.0						
2.0	5.20	1.51	5.20	5.36	.62	.84	.62	.58	1.46	1.12	1.46	1.55
2.2	2.09	1.35	2.09	2.20	.72	.87	.72	.72	1.20	1.08	1.19	1.25
2.5	1.45	1.22	1.45	1.50	.83	.91	.83	.83	1.10	1.05	1.09	1.11
3.0	1.18	1.12	1.18	1.20	.92	.95	.92	.92	1.04	1.03	1.03	1.04
						α=2.0						
2.0	1.50	1.14	1.50	1.56	.82	.94	.82	0.83	1.08	1.04	1.08	1.10
2.2	1.27	1.10	1.26	1.29	.88	.95	.88	0.89	1.05	1.03	1.05	1.06
2.5	1.11	1.07	1.13	1.12	.94	.97	.93	0.94	1.03	1.02	1.03	1.03
3.0	1.09	1.04	1.06	1.06	.97	.98	.97	0.97	1.01	1.01	1.01	1.01

Note: K represents Klingenberg's data from Gast et al. (1989); NF and FF represent results computed from the energy method with or without near-field interactions, and IM refers to the image method.

The next calculation compares the electrostatic forces acting on Particle 1 for different β values. Two particles are placed in a fluid subjected to an electric field. The centerline joining the centers of the particles is parallel to the electric field. The force was calculated with four different methods: the image method, the dipole-induced-dipole method, and the energy method with and without near-field effects. Figure 4.1 shows the dimensionless electrostatic force (nondimensionalized with $12\pi\varepsilon_0\varepsilon_c\beta^2E^2a^2$) versus β when the initial distance between two particles is (a) three radii and (b) six radii. The results demonstrate that for a given distance between the two particles, the dimensionless force calculated from the dipole-dipole interaction method is independent of β due to the nondimensionalization. It significantly differs from Klingenberg's exact force value, which monotonically increases with β. While both the image method and the energy method recover the increase, the image method gives results the closest to the exact

values. The energy method with the inclusion of both near-field and far-field interactions was found to lead to the next accurate results while the discrepancy between the exact value and the force computed from the energy method with only far field effects was quite large, particularly when the particles were the closest and at the largest β values.

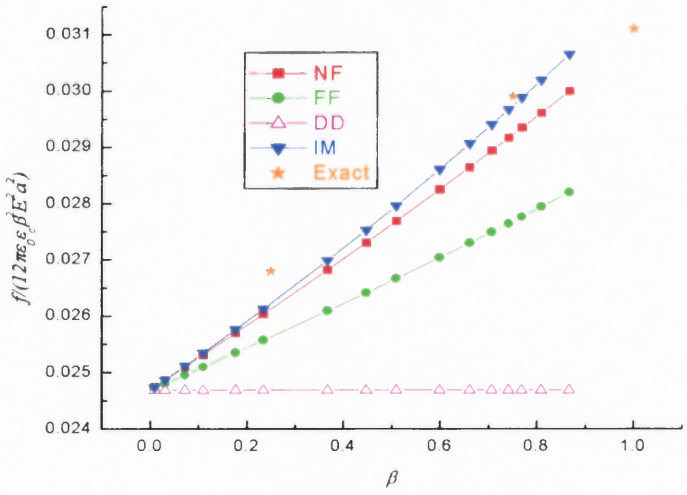

(a)

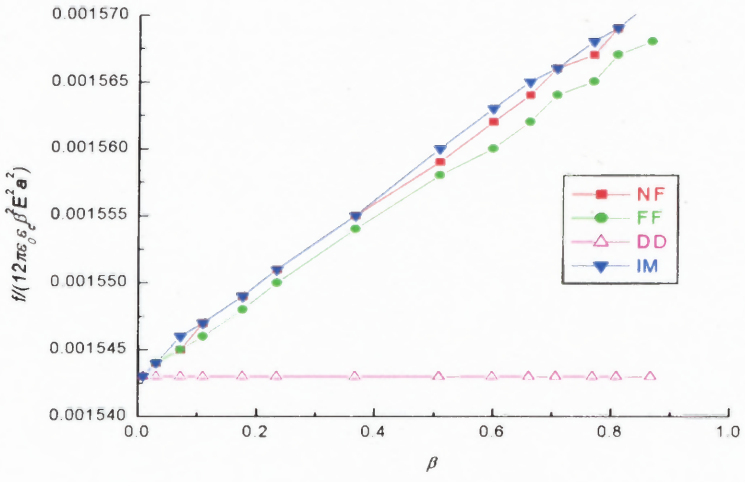

(b)

Figure 4.1 Force versus the particle-to-fluid dielectric constant ratio β when the distance between the two particles is (a) $r = 3a$; (b) $r = 6a$.

4.1.3 Comparison of Particles Trajectories

The particles trajectories obtained with the various methods were plotted for comparison. Initially, the two particles are placed at the locations (0.6, 0.6, 0.2) and (1.0, 1.0, 0.2), with the line joining their centers neither parallel nor perpendicular to the imposed electric field. The particles are expected to get attracted to each other and align with the electric field.

Figure 4.2(a) displays the particle trajectories using the energy method (with or without near-field effects) and the image method. The x-y plot in Figure 4.2(a) shows that approximately the same results are obtained with the image method and the energy method with and without the inclusion of the near-field effects. However, the point-dipole assumption leads to different results.

Likewise, the time traces of Particle 1's coordinates (x- and y-coordinates versus time) in Figures 4.2(b) and (c) show that the energy method with near-field interactions and the image method give similar results, while the dipole-induced-dipole leads to a discrepancy due to the fact that the particle takes a longer time in this case to reach their final position where they touch each other, than in the other models. Recall that the dipole-induced-dipole computes the dipole of a particle only from its interaction with the external electric field, which leads to an inaccuracy in the force computed, particularly as the two particles get close to each other.

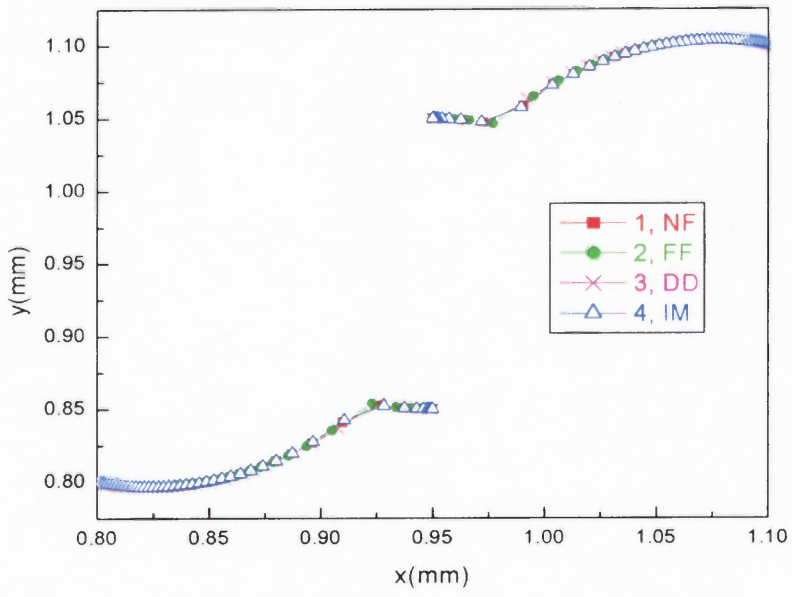

(a)

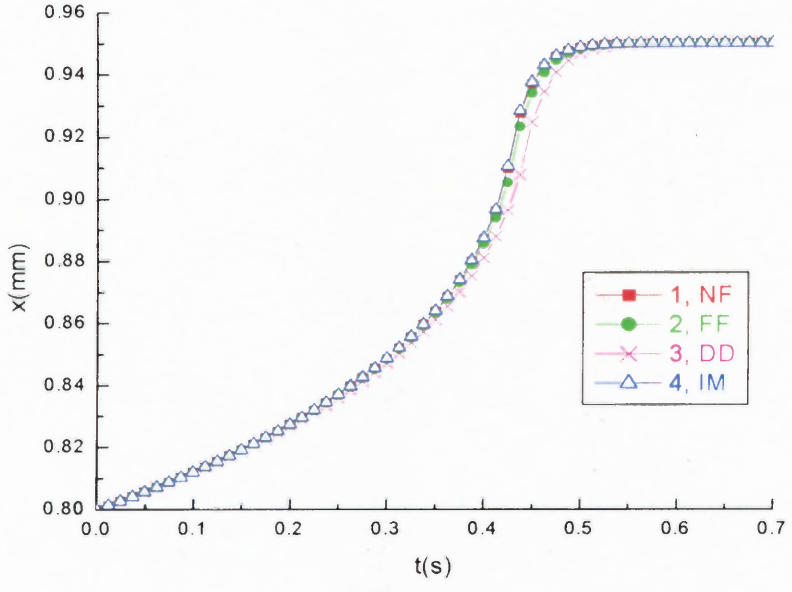

(b)

Figure 4.2 (a) Trajectory of Particle 1 in a two-particle motion computed with four methods. The *x*-coordinate of Particle 1 as a function of time, computed with four different methods. (■ NF refers to the energy method with the inclusion of the near-field effects; • FF refers to the energy method in which the near-field effects have been neglected; × DD refers to the dipole-induced-dipole method; Δ IM refers to the image method where fifteen terms have been retained.)

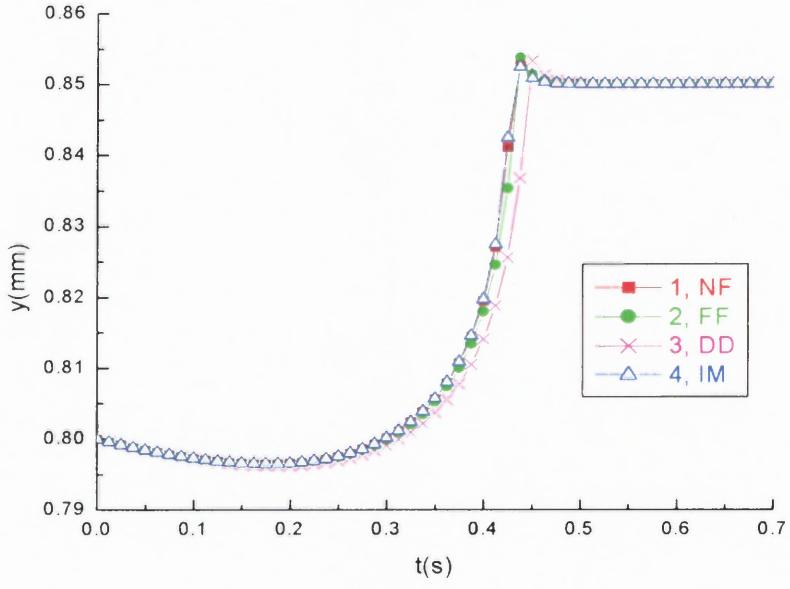

(c)

Figure 4.2 (continued) (c) The *y*-coordinate of Particle 1 as a function of time, computed with the four different methods. (■ NF refers to the energy method with the inclusion of the near-field effects; • FF refers to the energy method in which the near-field effects have been neglected; × DD refers to the dipole-induced-dipole method; Δ IM refers to the image method where fifteen terms have been retained.)

4.1.4 Attraction, Repulsion, and Alignment

In this section, we compute the trajectories of particles in the case of attraction, repulsion, rotation and alignment of the two particles with different initial positions related to the applied uniform electric field. The electrostatic force is computed from the image method, as expressed in Equation (3.29).

The electric field is generated by two parallel plates placed in two x-z planes at a distance l_y of each other. The electric field is then in the y direction. The computational domain has dimensions 1.6mm, 1.6mm, and 0.4mm in the x, y, and z directions, respectively. The dielectric constant is 7.3 for the fluid and 14.6 for the particles.

The first example displays the case of particle attraction (see Figure 4.3(a)) between two particles initially positioned at (0.8, 0.5, 0.2) and (0.8, 1.1, 0.2). When the line joining the centers of the two particles is parallel to the applied electric field, the particles attract each other because the net attraction force is along the centerline. The attraction force acting on the particles pulls the particles toward each other, and as the particles get closer to each other, the force increases. This implies that the particles move toward one another at a faster and faster rate until they touch.

The second example studied here is the case of particle repulsion (see Figure 4.3(b)) between two particles initially positioned at (0.65, 0.8, 0.2) and (0.95, 0.8, 0.2). When the line joining the centers of the two particles is perpendicular to the applied electric field, the particles repel each other and move away from each other. As the distance between the particles increases, the repulsion force decreases, thus slowing down the particles motion gradually during the repelling process.

When two particles whose line joining their centers is initially neither parallel nor perpendicular to the electric field, as shown in Figure 4.2(c), the particles experience both attraction and repulsion forces which cause the pair to rotate and eventually align with the electric field. This phenomenon is at the origin of the formation of chain structures, which align themselves along the direction of the electric field. The simulation showed that the attraction, repulsion and/or alignment of the particles depend(s) on their positions as well as on the polarizability of the particles (the amplitude and sign of the factor β).

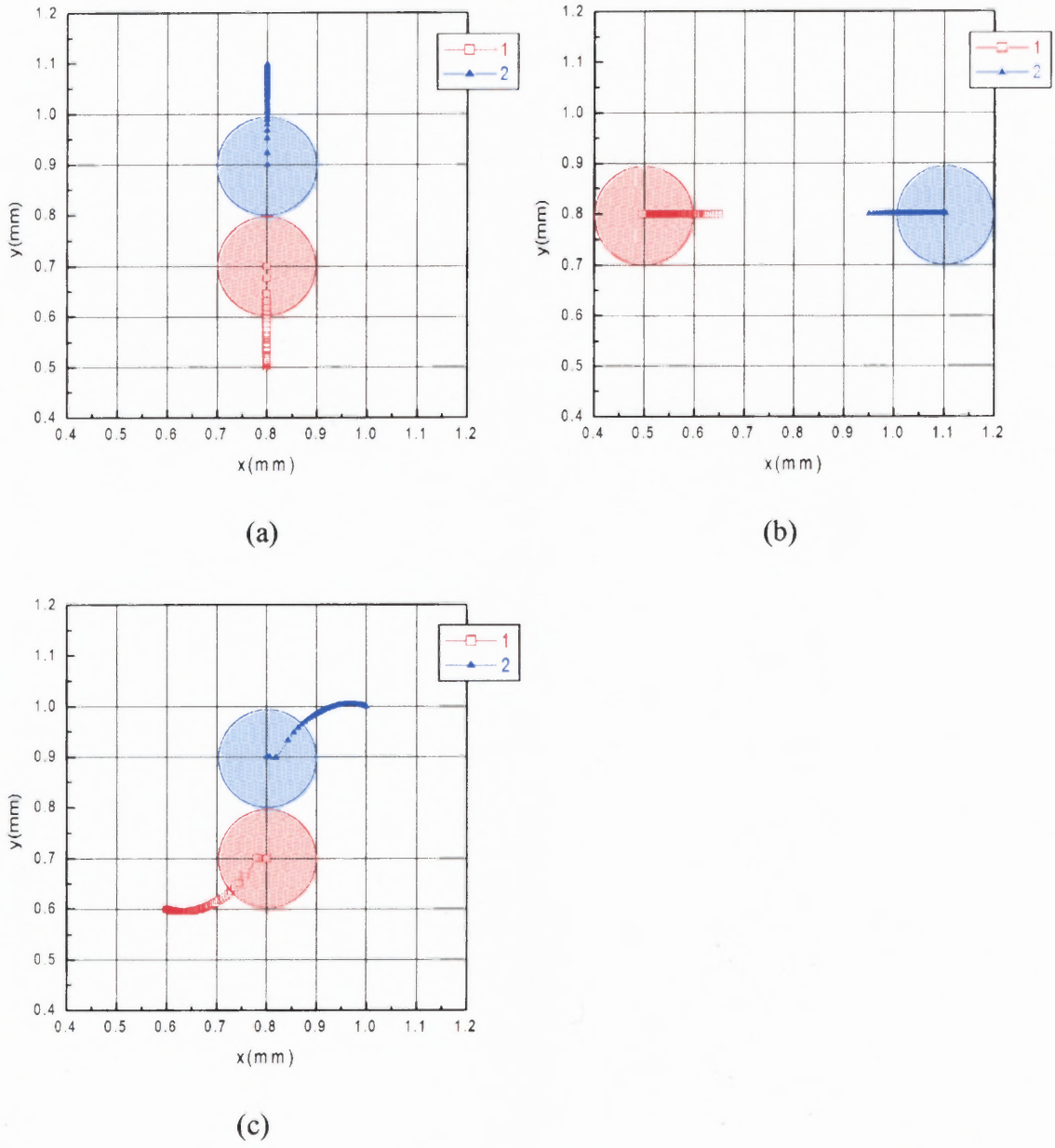

Figure 4.3 Electrostatic interactions between two particles, denoted by 1 (□) and 2 (▲), suspended in a uniform electric field: (a) two particles attract each other when the line joining their centers is parallel to the electric field; (b) two particles repulse each other when the line joining their centers is perpendicular to the electric field; (c) two particles rotate and align with the applied electric field when the line joining their centers is neither parallel nor perpendicular to the electric field.

4.1.5 Discussion

When two particles dispersed in a dielectric fluid are subjected to a uniform electric field, the electrostatic force acting on a particle can be computed from four methods: (a) the dipole-induced-dipole method with the point-dipole approximation; (b) the image method; (c) the energy method with both far-field and near-field effects; and (d) the energy method without the near-field effects. As expected, the dipole-induced-dipole method leads to the least accurate results because the point-dipole approximation assumed that the dipole induced within the particle comes from the external electric field only, and fully ignores the influence of the presence of the other particles. The energy method where the near-field effects are neglected gives better results than the dipole-induced-dipole method because it considers the influence of the other particles although it neglects the near-field interactions. The energy method to which the near-field interactions have been added leads to better results because it takes into account the influence of both the near-field and far-field interactions between the particles. Finally, the image method generates accurate results as it considers not only the influence of the other particles but also the near-field interactions in a fashion similar to the energy method in which the near-field interactions have been added. Furthermore, it can also be easily extended to calculate the electrostatic force in a non-uniform electric field.

4.2 Two Particles Suspension with Non-Uniform Electric Field

In this section the suspension with only two particles is studied when the electric field spatially non-uniform. The electrostatic force acting on a particle is computed using (i) the energy method with and without the addition of the near-field effects (Equation (3.66), (ii) the image method (with more than three terms included (Equation (3.36)), and (iii) the point-dipole approximation.

The nonuniform electric field is generated by electrodes in x-z planes located at a distance of l_{ym} of each other. The top electrode ($y = l_{ym}$) is energized at the voltage V_m while the bottom electrode ($y = 0$) is grounded. It is further assumed that the electrodes length of the electrodes in the z direction is much larger than those in the x and y directions, and therefore the electric field can be considered to satisfy a 2D problem in the x-y plane.

Both positive and negative dielectrophoretic motions are studied with different computational cells and electrodes arrangements. For positive dielectrophoresis, we consider the nonuniform electric field generated by electrodes placed outside the fluid domain and its walls, as shown in Figure 4.4. The fluid box has the dimensions l_x, l_y, l_z taken as 1.6mm, 1.6mm and 0.8mm along the x, y and z direction, respectively, while l_{ym} is chosen to be 2.4mm. However, negative dielectrophoresis is generated by electrodes placed within the walls of the fluid domain, as shown in Figure 4.10. In both cases, the density of the particles is 1010 kg/m^3, while that of the fluid is 1000 kg/m^3.

4.2.1 Positive DEP ($\beta > 0$)

In this section, the properties of the two particles suspension were studied under positive dielectrophoresis ($\beta > 0$). Both particles have the same sizes with 0.2mm in diameter. The dielectric constant is 7.3 for the fluids, and 23.3 for the particles (and thus $\alpha = 3.19$ and $\beta = 0.422$). The viscosity of the fluid is assumed to be 0.1 Pa.s and there is no initial flow in the domain.

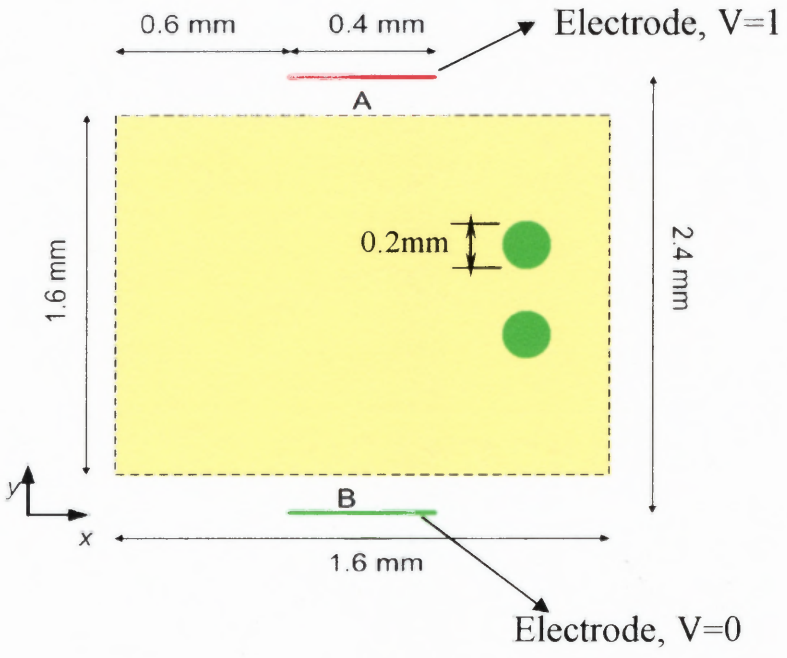

(a)

Figure 4.4 Sketch of the domain, showing the electrodes in the *x-y* plane outside the fluid box for positive dielectrophoresis ($\beta > 0$). A, B indicate the electrodes, A being the energized electrode, B being the grounded electrode.

The typical computational space used is showed in Figure 4.4 with the selected dimensions. Notice that in this case, we have assumed that the electrodes are outside the fluid channel and therefore the particles do not get very close to the electrodes. Specifically, the electrodes are placed at a 0.4mm distance from the top and bottom edges

of the fluid cell. The top electrode is energized at an electric potential whose dimensionless value is 1, while the bottom electrode is grounded, and therefore its potential is 0. The 2D Laplace equation is solved to obtain the electrical potential φ, and the electric field is deduced from the equation $\mathbf{E} = -\nabla\varphi$. Figure 4.5(a) displays the electric field, and Figure 4.5(b) shows the quantity $\mathbf{E}\cdot\nabla\mathbf{E}$ relevant to the dielectrophoretic force.

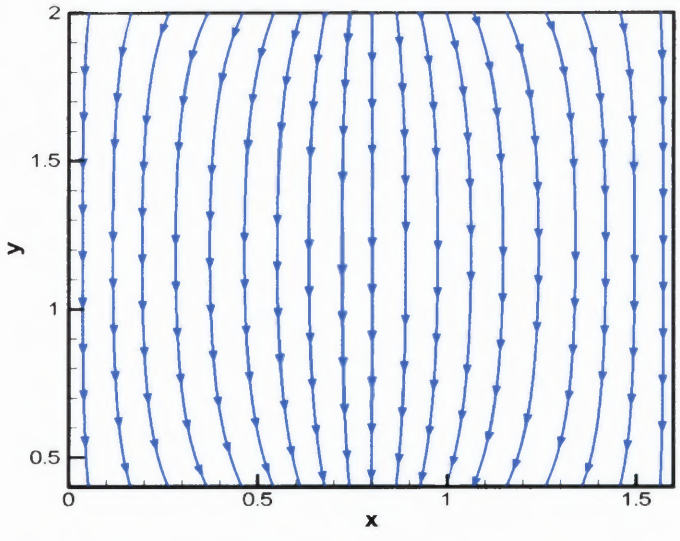

(a)

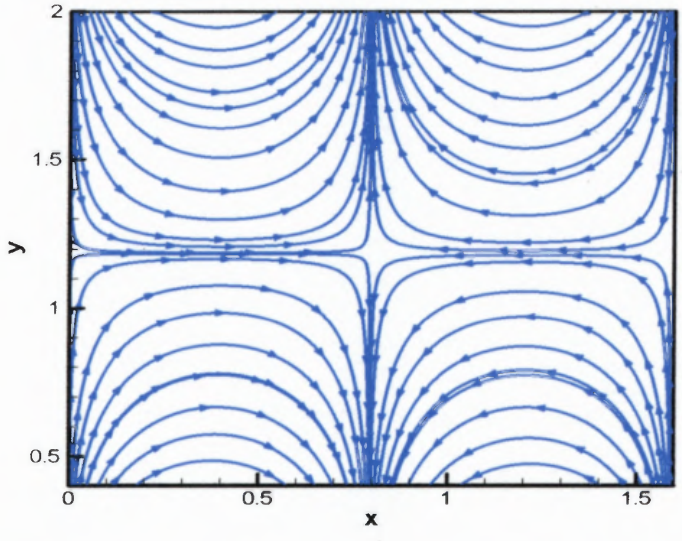

(b)

Figure 4.5 Solution of the Laplace equation. (a) Electric field **E** lines; (b) Force $(\mathbf{E}\cdot\nabla\mathbf{E})$ lines.

4.2.1.1 Convergence of the Results with Time Step Refinement. In this section, the convergence of the results with time step refinement is verified by studying the case of two particles. The initial positions of the particles are (1.3, 0.8, 0.4) and (1.3, 1.6, 0.4). For several different time steps, the y coordinate of the first particle is plotted in Figure 4.6 as a function of time by using the image method which includes the near-field effects to compute the electrostatic force. The plots show that the results for four different time steps almost overlap, thus demonstrating the convergence of the results with time step refinement.

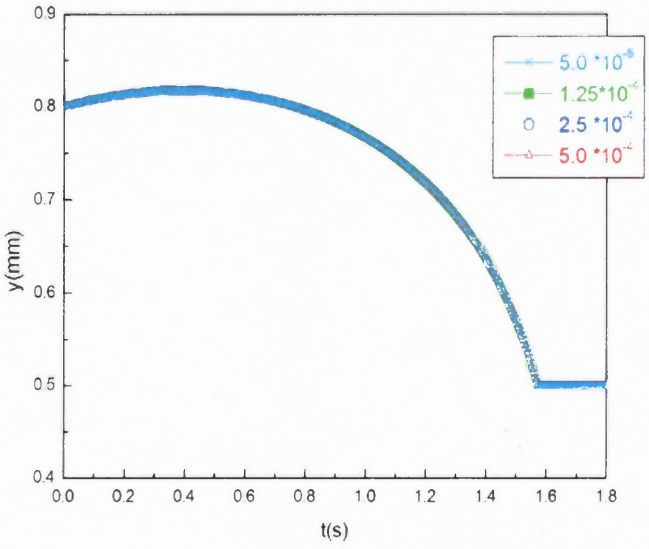

Figure 4.6 The y-coordinate of the first particle as a function of time, computed using four different time steps: (a) ▲ $5.0*10^{-5}$; (b) ■ $1.25*10^{-4}$; (c) ○ $2.5*10^{-4}$; (d) Δ $5.0*10^{-4}$.

4.2.1.2 Electrostatic Force Comparison. The electrostatic force acting on the particles includes two interactions: the interaction between the various particles, and the interaction between every individual particle and the imposed electric field. As mentioned in Chapter 3, the electrostatic force on a particle subjected to a non-uniform electric field can be determined by five different methods.

Table 4.3 lists the three components of the force acting on the first particle, considered at various distances of one another, and for two different dielectric constant ratios $\alpha = \varepsilon_p/\varepsilon_c$ (2.0 and 10.0). These components are computed by means of five different methods: (a) NF represents the results from the energy method with the inclusion of the near-field effects (Equation (3.17)); (b) FF refers to the results from the energy method taking into account the far-field effects only; (c) DD indicates the results from the dipole-induced-dipole method, where the electrostatic force is determined from the particle-particle interaction using Equation (3.19) to which the DEP force (1.23) is added; (d) IM indicates the results from the image method with the first fifteen terms; (e) DEP denote the results from the traditional DEP force only.

The two particles are placed symmetrically such that $y = 1/2\ l_y$ at the locations (1.3, y_1, 0.4) and (1.3, y_2, 0.4) and the distance between the two particles is varied by changing y_1 and y_2. The electrostatic forces are nondimensionalized with the factor $12\pi\varepsilon_0\varepsilon_c(\beta E)^2 a^2$.

The results show that the DEP method is the least accurate, as it was expected, since it considers the interaction between the particle and the electric field only, ignoring all interactions between the particles. When the particles are almost touching, the error is approximately 97% even for small values of the dielectric constant ratio $\varepsilon_p/\varepsilon_c = 2.0$. The dipole-induced-dipole approach remedies this deficiency by including both the particle-particle interactions and the interaction between the particle and the non-uniform electric field. However, it ignores both the near-field effects of the particle-particle interactions and the dipole moment induced by the dipoles of the other particles. When the particles are very close (2.2 sphere radii), the error is about 19% for the

ratio $\varepsilon_p/\varepsilon_c = 2.0$ and 50% for the ratio $\varepsilon_p/\varepsilon_c = 10.0$. The energy method, even without the inclusion of the near-field effects, leads to reasonable results (errors are 11% and 33% for the two ratios, respectively) if the suspension is dilute, i.e. the distance separating particles is large. The image method accounts for both the particle-particle and particle-field interactions, including the near-field effects. The error obtained with the image method is less then 10% for $\varepsilon_p/\varepsilon_c = 2.0$ and 16% for $\varepsilon_p/\varepsilon_c = 10.0$.

When particles are placed at a distance of four sphere radii apart, the error is less than 3% with the image method, in contrast with 58% with the DEP force only. However, for a distance of eight sphere radii apart between the particles, all methods are in good agreement, the error being less than only 5% for a ratio $\varepsilon_p/\varepsilon_c = 2.0$ and 9% for $\varepsilon_p/\varepsilon_c = 10.0$ with the DEP force only. The other methods give even smaller errors.

Table 4.3 Comparison of the Two-particle Force Components in a Non-uniform Electric Field

r/a	F_x					F_y				
	FF	NF	IM	DD	DEP	FF	NF	IM	DD	DEP
					$\varepsilon_p/\varepsilon_c = 2.0$					
2.0	-0.14317	-0.14322	-0.15339	-0.13446	-0.13352	1.16942	1.53577	1.37788	1.02892	0.02067
2.2	-0.14382	-0.14384	-0.15118	-0.13728	-0.13663	0.78196	0.88803	0.82860	0.71122	0.02286
2.5	-0.14504	-0.14504	-0.15001	-0.14061	-0.14021	0.46740	0.49294	0.47134	0.43871	0.02621
3.0	-0.14672	-0.14672	-0.14982	-0.14427	-0.14427	0.23904	0.24302	0.23712	0.23060	0.03194
4.0	-0.16671	-0.16671	-0.16832	-0.16570	-0.16563	0.10831	0.10856	0.10756	0.10689	0.04427
6.0	-0.21489	-0.21489	-0.21609	-0.21507	-0.21507	0.08646	0.08646	0.08576	0.08572	0.07350
8.0	-0.30508	-0.30508	-0.30661	-0.30602	-0.30601	0.11584	0.11584	0.11521	0.11520	0.11141
					$\varepsilon_p/\varepsilon_c = 10.0$					
2.0	-0.05574	-0.05606	-0.07083	-0.04544	-0.04451	1.53588	5.16124	2.39296	1.01514	0.00689
2.2	-0.05364	-0.05371	-0.06273	-0.04620	-0.04554	0.94155	1.44506	1.20787	0.69598	0.00762
2.5	-0.05204	-0.05206	-0.05742	-0.04714	-0.04674	0.51450	0.60648	0.55139	0.42124	0.00874
3.0	-0.05082	-0.05082	-0.05386	-0.04809	-0.04809	0.23410	0.24647	0.23238	0.20930	0.01065
4.0	-0.05650	-0.05650	-0.05794	-0.05528	-0.05521	0.08081	0.08153	0.07949	0.07738	0.01476
6.0	-0.07196	-0.07196	-0.07271	-0.07169	-0.07169	0.03725	0.03726	0.03682	0.03673	0.02450
8.0	-0.10189	-0.10189	-0.10260	-0.10201	-0.10200	0.04124	0.04124	0.04094	0.04093	0.03714

Note: NF and FF represent the results obtained with the energy method with and without the near-field interactions, IM refers to those obtained with the image method, DEP denotes the DEP force only, and DD the sum of the DEP and the dipole-dipole interaction force term.

4.2.1.3 Particle Trajectories Comparison. Figure 4.7 compares the trajectories of the two particles computed by means of the energy method with those obtained when the electrostatic force is taken as the DEP force only. The initial positions of the particles are (1.3, 1.05, 0.4) and (1.3, 1.35, 0.4). The total electrostatic force increases with increasing particle-to-fluid dielectric constant ratio α.

As recalled in Chapter 3, particles attract each other because of the presence of particle-particle interactions. This phenomenon is well reproduced by the image method if the latter includes near-field effects. In a nonuniform electric field and in the case of positive dielectrophoresis, particles are attracted toward each other quickly and then move toward the boundary together. When the electrostatic force is modeled by the DEP force only, the trajectories show that the particles move separately to the electrodes without being attracted to each other. Figure 4.7(a) allows the comparison of the two trajectories in the x-y plane. A close observation of the particles' trajectories in Figure 4.7(b) reveals that the two particles are approximately in contact at x = 1.29mm, when the image method is used to compute the electrostatic force. Figure 4.9(a) presents the trajectories obtained with the three methods: the image method with both far-fiels and near-field effects, the energy method with the far-field effects only, and the point-dipole assumption (DD), with a closer view as the particles nearly touch each other displayed in Figure 4.9(b). As expected, the results show that the trajectories differ only when the particles are close to each other.

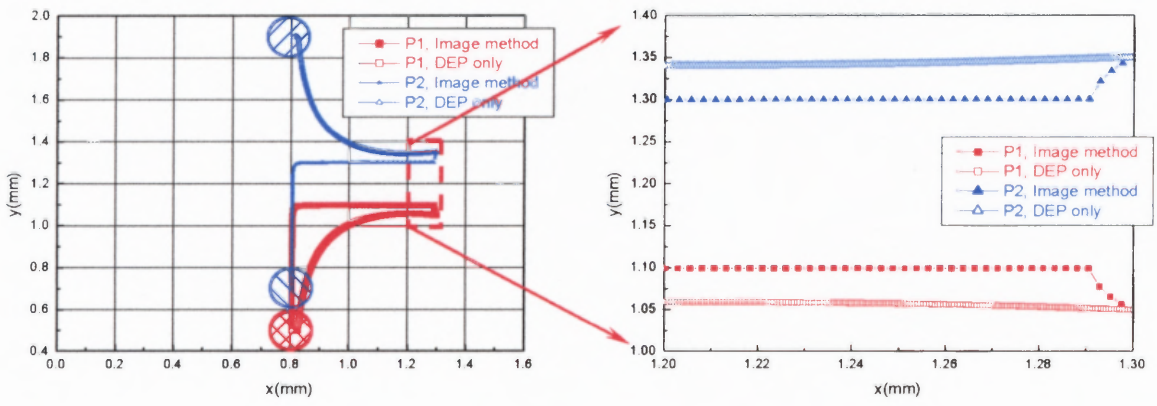

(a) (b)

Figure 4.7 Comparison of the trajectories of two particles in the case of positive dielectrophoresis obtained with the image method and the DEP force only. (a) Full view of the trajectories; (b) close view of the two particles as the latter are close to each other, near $x = 1.28$mm.

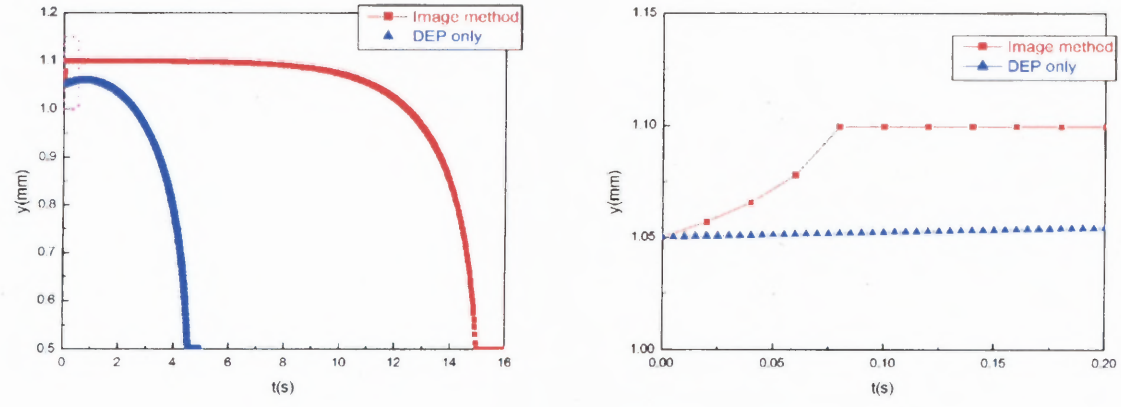

(a) (b)

Figure 4.8 Comparison of the first particle's y coordinate as a function of time in the case of positive dielectrophoresis computed with the image method and the DEP force only. (a) Full view; (b) close view as the particles get close to each other.

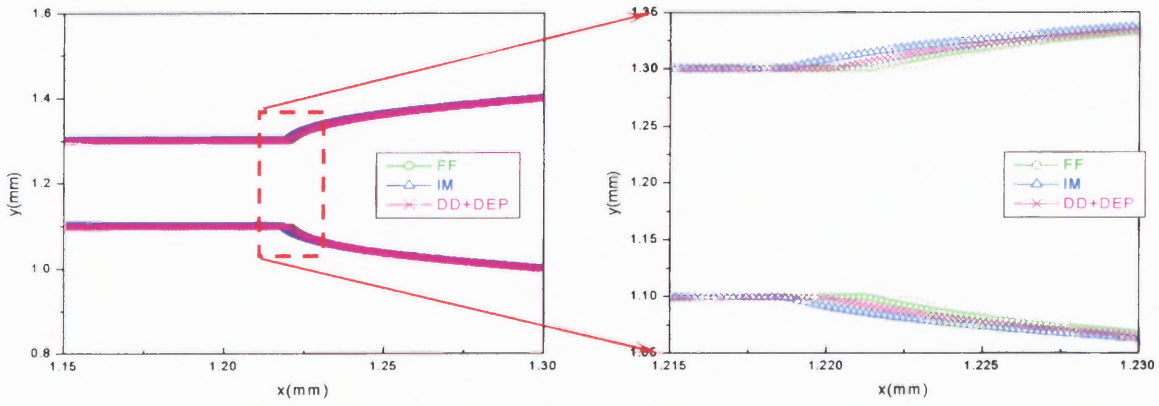

(a) (b)

Figure 4.9 Comparison of the trajectories of the two particles in the case of positive dielectrophoresis computed with the image method, the energy method without near-field interaction, and the point-dipole method. (a) General view of the trajectories; (b) closer view as the particles get close to each other, near $x = 1.22$mm.

The evolution of the first particle's y coordinate with time t is also shown (see Figure 4.8). If the electrostatic force is reduced to the DEP force only, the particles are collected at the boundaries at time t = 4.4s. However the results from the energy method, which takes full account of the particle-particle interactions, show that the collection of particles takes about 15.0s. This means that a much longer time is needed in this example to collect or separate particles when the interaction between the particles is accounted for. A closer view of the y-t plot, provided in Figure 4.8(b), indicates that the particles move first toward each other quickly and then toward the boundary as a pair, when the electrostatic force is computed from the image method.

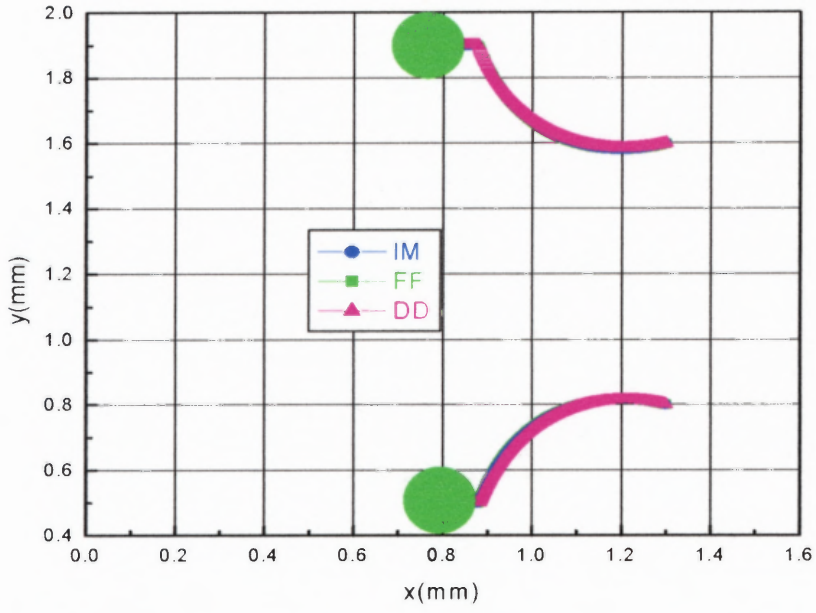

Figure 4.10 Comparison of the trajectory of the two particles in the *x-y* plane, computed with various methods.

Figure 4.10 shows the trajectories of the two particles between the locations (1.3, 0.8, 0.4) (initial position) and (1.3, 1.6, 0.4). Other parameters are kept identical. The trajectories are computed by using three methods: the energy electrostatic density method without the near-field effects, the method based on the DEP force to which dipole-dipole interactions have been added, and the multiple image method. All results are in good agreement. This is due to the fact that when the positions of the particles are far away from each other, the particle-particle interaction force is weaker than the particle-field interaction force and a rough estimate of the particle-particle interactions is sufficient.

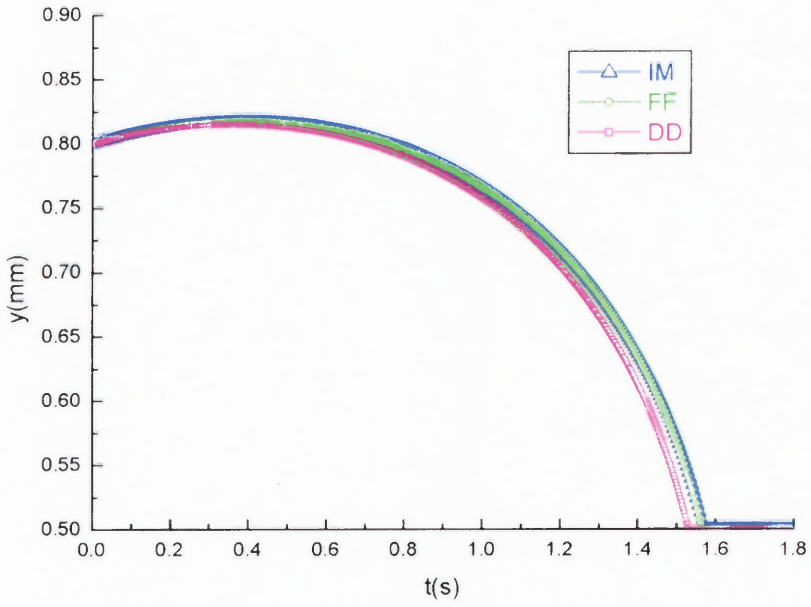

Figure 4.11 Comparison of the y coordinate of the first particle as it evolves in time, computed with various methods.

In Figure 4.11, the image method is compared with the energy method without near-field interactions and with the dipole-induced-dipole and DEP method. The image method results are computed from the dipole moments in which the first three terms were retained. From these results, we conclude that the image method, with only the first three terms in the series, is sufficient to accurately simulate the particle trajectories.

4.2.2 Discussion

Two particles suspensions subjected to a nonuniform electric field have been studied in this section. The electrostatic force was calculated using different methods. In most cases, the latter include the DEP force only, the energy method with the addition of near-field interactions, the energy method without the near-field interactions and the image method.

The results showed that the DEP only force is not enough to simulate the movement of the particles because that the DEP force is the interaction between the field and the induced dipole in a particle, but neglecting the interaction between the particles. This method also ignores the near-field effects. The dipole-induced-dipole approach is better because it considers both the interactions between the particles and between the field and the field, but it still neglecting the influence of the near-field. The energy method with the addition of the near-field interaction considers both the interaction between the particles and between the field and the field, it also consider the influence of the near-field, but the near-field interaction is computed from the approximation the uniform field. Image method is great to take count of the interaction between the particles, and it is the near-field suitable if appropriate terms are included.

4.3 Conclusions

Suspensions of polarizable particles in dielectric fluids when subjected to an applied electric field were studied numerically using molecular-dynamics-like methods. The total electrostatic force was computed from the electrostatic energy density of the suspension. Since the capacitance matrix can include both far- and near-field interactions, the electrostatic force, computed from the calculation of the capacitance matrix, can also take into account both interactions. Furthermore, the energy density method is suitable when the electric field is either uniform or non-uniform.

For a uniform electric field, the electrostatic force originates in the particle-particle interactions due to the particles' induced dipole interactions. However, for a non-uniform electric field, the electrostatic force includes two parts: the interaction between

the induced dipole and the non-uniform field, and the interaction between the particles. Both parts can take into account not only the far-field but also the near-field interactions. Simulations could predict the time-evolution of the motions of particles as function of the particle-to-fluid dielectric constant ratio, α, and distance between the particles, r/a.

The formation of particle chaining was observed as a uniform electric field was applied. However, in the case of a non-uniform electric field, particles gathered either in the high electric field or low electric field regions, depending on their polarizability. With an appropriate electric field strength, the particles moved towards electrodes if they were more polarizable than the fluid, and they moved away from the electrodes if they were less polarizable than the fluid.

CHAPTER 5

MULTI-PARTICLES PROBLEM

In this section, numerical simulations of multi-particle suspensions subjected to a nonuniform electric field are performed and discussed. Multi-particle suspensions are common in real life. How to manipulate particles dispersed in a fluid has been an interesting and challenging problem in recent years not only for numerous traditional applications but also for the advancement of novel technologies. The particles motion is simulated using a molecular dynamics like method where the hydrodynamic force on a particle is represented by the Stokes drag, and the electrostatic force is computed from the methods presented in Chapter 3. In particular, the near-field effect present in the interaction force between two particles is included by using the multiple image method.

5.1 Negative DEP

In this section, several simulations were performed in a computational domain of dimensions 2.4mm by 1.6mm by 0.8mm in the x, y and z directions. A typical computational cell used in this study is shown in Figure 5.1. The electrodes are represented by four edges within the walls of the domain.

The initial particle distribution is displayed in Figure 5.2. A total of 40 particles were placed in two layers with 20 particles in each layer, with an even distribution along the y direction, but in the x direction, particles are much closer to the edge $x = 0$. The fluid viscosity of the fluid is set to be $\eta = 0.1$ Pa.s. The particles are 0.2mm in diameter. The density of particles is 1010 kg/m^3 while that of the fluid is 1000 kg/m^3. The dielectric

constant of particles and fluid are 9.32 and 23.3, respectively. This gives the coefficient α = 0.5, and factor β = - 0.25.

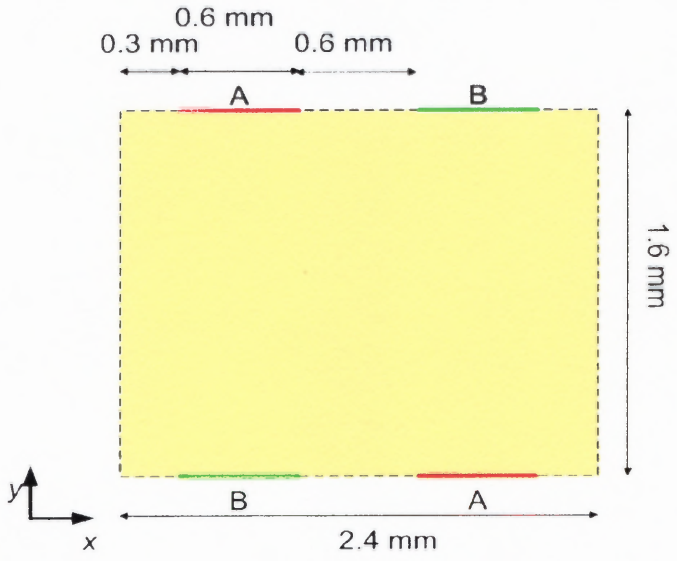

Figure 5.1 Sketch of the domain considered for the manipulation of particles by means of dielectrophoresis, where the location of electrodes (green and red) along the walls and various dimensions are specified.

The fluid flow is driven by the pressure difference between the inlet (left) and outlet (right). Since the electrodes are within the walls, they do not enter the fluid mechanics problem and the fluid can be considered moving between two parallel plates. It follows that the fluid velocity profile in the x direction is expressed as:

$$u_x = -\frac{1}{2\mu}\frac{dp}{dx}\left(y^2 - l_y y\right) \tag{5.1}$$

where l_y is the height in the y direction. This fluid velocity was also verified using the commercial software FLUENT. On the top and bottom walls, the no-slip boundary condition (velocity component u_x = 0 and $du_y/dy = 0$) was used.

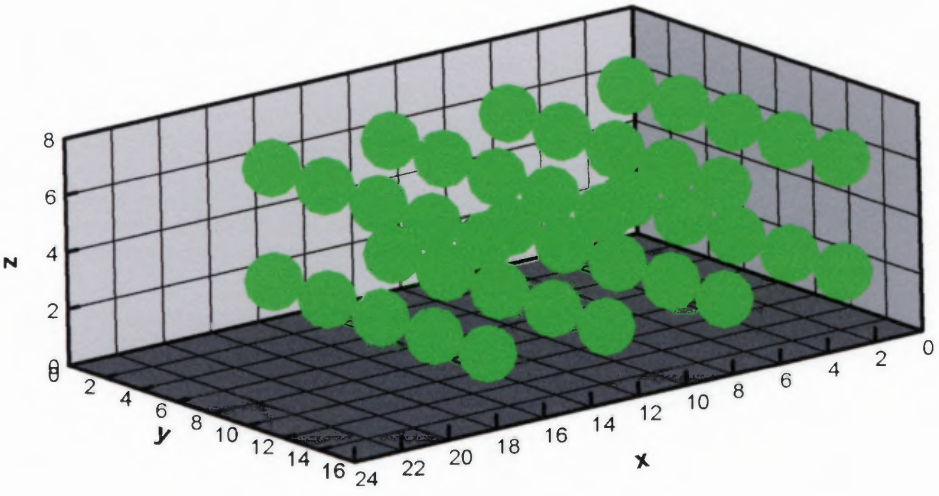

Figure 5.2 Particle array in 3-D view consisting of two layers with 20 particles in each layer.

5.1.1 Electric Field

The boundary conditions for the potential are as follows. On the electrodes, the potential was set to $\varphi = 0$ or 1 in dimensionless units, on the left-hand side and right-hand side of each electrode the condition $\partial\varphi / \partial n = 0$ was imposed, as well as at the inlet and outlet. The length of each electrode is 0.6mm.

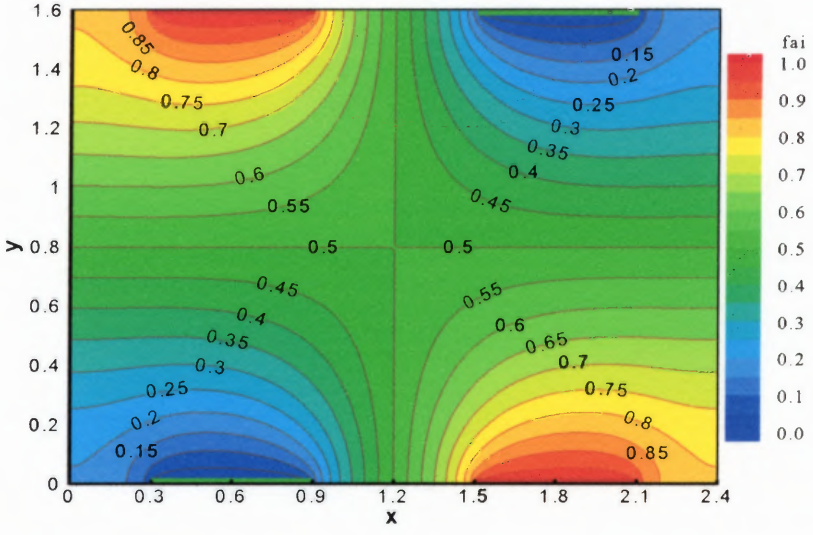

Figure 5.3 Contours of the (dimensionless) electric potential φ.

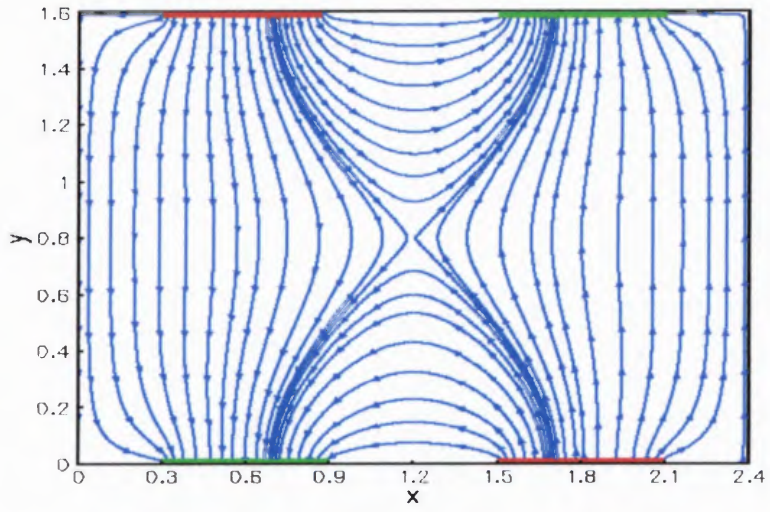

(a)

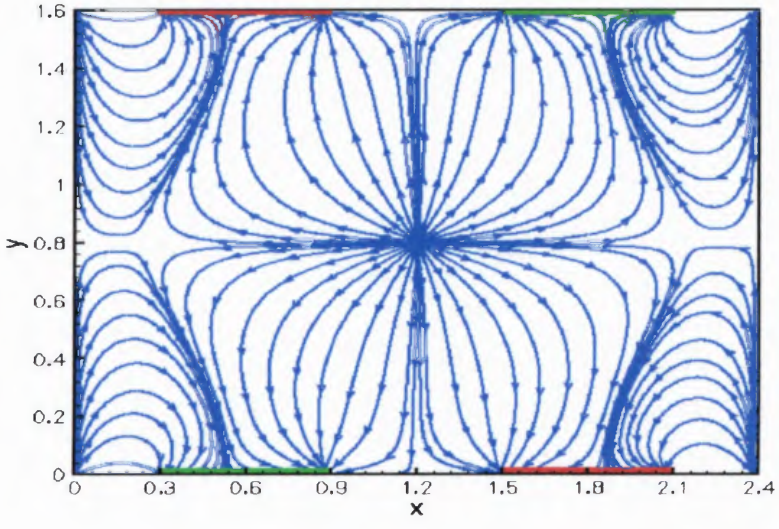

(b)

Figure 5.4 Solution of Laplace's equation. (a) Electric field (**E**) lines; (b) Electric force ($\mathbf{E}\cdot\nabla\mathbf{E}$) lines.

The electrical potential is shown in Figure 5.3. The staggered electrodes produce an electric field for which the point located in the center of the domain is a point of symmetry, its (dimensionless) potential being 0.5. The electric field **E** lines and force $\mathbf{E}\cdot\nabla\mathbf{E}$ lines are shown in Figures 5.4 (a) and (b). Local minima for the electric field

magnitude are located at the center (1.2, 0.8, z) of the cell, as well as in the four corners of the domain, while maxima are located at the tips of the electrodes. The center of the cell is a saddle point for the electric field lines. All planes in the z direction have the same electric $\mathbf{E}$ and force $\mathbf{E} \cdot \nabla \mathbf{E}$ distributions.

5.1.2 Negative DEP with dp/dx=0

In this section, the instantaneous motions of particles with negative dielectrophoresis were studied. The time step was kept at $\Delta t = 2.5*10^{-4}$. The suspension was subjected to the nonuniform electric field generated by the electrodes arranged in a staggered fashion and shown in Figure 5.1. Under negative DEP, particles should go toward the center of the domain where the electric field is minimal.

The transient motion of two particles with no initial flow is first studied. Two particles are initially placed at a distance of $r = 3a$ apart at the locations (1.9, 0.65, 0.4) and (1.9, 0.95, 0.4). As mentioned in Chapter 2, the electrostatic force plays a crucial role in driving the motion of particles in ER fluids. Most publications so far reporting numerical simulations of dielectrophoretic phenomena have accounted for the DEP force as the only electrostatic force, although reference[24] added the particle-particle interaction force. Recall that the electrostatic force computed from the energy density considers both interactions: the interaction between particles and the interaction between the particles and the nonuniform electric field.

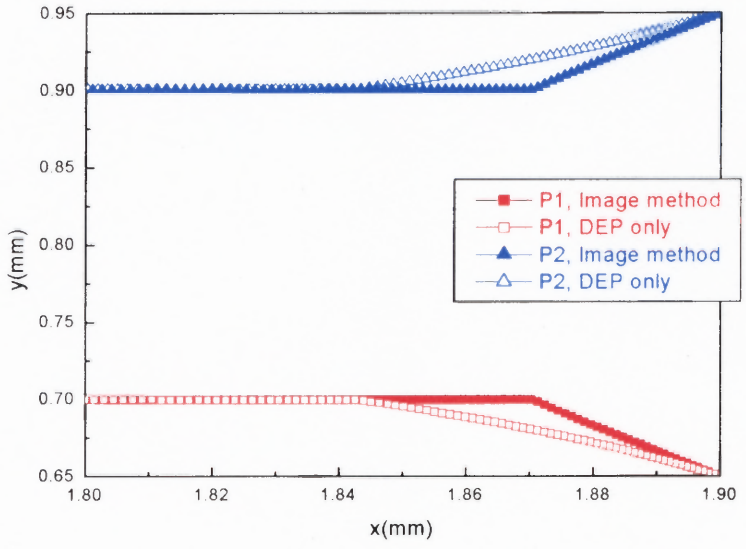

(a)

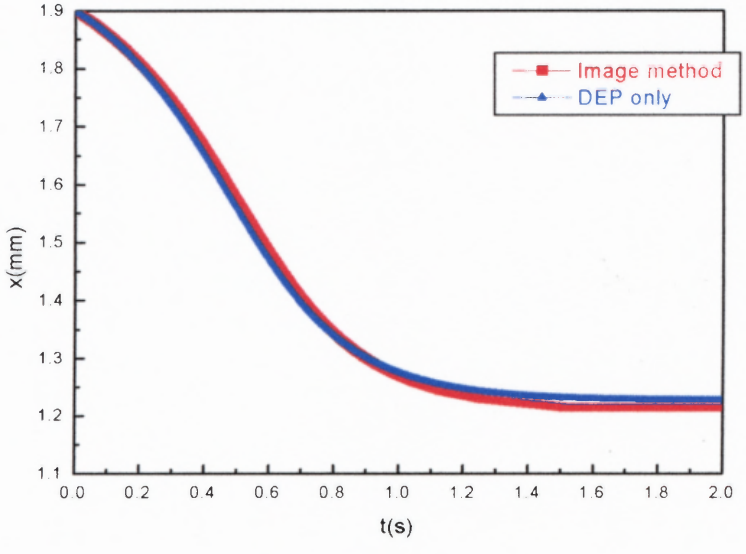

(b)

Figure 5.5 Trajectory of Particle 1 in a nonuniform electric field. (a) *x-y* plot; (b) *x-t* plot.

The results are compared with those obtained by assuming that the electrostatic force is the DEP force only or the sum of the DEP force and particle-particle interactions. Figure 5.5(a) shows the trajectories of the two particles computed with the image method and the DEP force method. The calculation based on the image method shows that the particles move first towards each other first under the particle-particle interactions, and then together towards the low electric field region where they get collected. However, when the electrostatic force is assumed to be merely the DEP force only, the two particles move towards the low electric field region separately, approximately along the force lines of Figure 5.4(b) but in the opposite direction to the arrows, due to the negative sign of β (negative dielectrophoresis). Figure 5.5(b) displays the time variation of the x coordinate of the first particle. The results showed that the particles get collected in the region of low electric field strength, and that the time of collection is approximately the same in both computations, even the initial positions of the two particles are close.

The next simulation was performed in the domain sketched in Figure 5.1 for multiparticle suspensions, with the initial fluid and particles velocities assumed to be zero. The particles are less polarizable than the surrounding fluid with β = -0.25. Imposing dp/dz = 0, that is no pressure difference between the inlet and outlet of the fluid domain, there is no bulk fluid flow. The particles are subjected to the drag force, to which a repulsive force, keeping the particles from overlapping, has been added. The simulation was performed with and without the inclusion of the near-field electrostatic interactions. In a non-uniform electric field, the electrostatic force acting on a particle includes both the interaction between the particles and the interaction between the particle and the non-uniform field. Recalling the analysis presented in the previous

section, the inter-particle interaction force depends on the electric field at the centers of particles, while the interaction force between the particle and the field depends on the electric field $\mathbf{E}$ and its gradient $\nabla\mathbf{E}$. For negative dielectrophoresis, the particles move toward the low electric field regions.

Figure 5.6 shows the initial instantaneous snapshots of the suspension computed by means of the image method in which the near-field interactions were included. Figure 5.6(a)-(e) show the configuration of the suspension at different times from 0 to 2 seconds. At time t = 0.1s, the particles close to the upper and lower left corners move quickly to the local minimum of the electric field, while the particles near $y = 1/2h$ in the first column (from the left) move to the left edge as well as regroup because of the particle-particle interactions. The particles in the third column (from the left) hardly move in the x direction, and aggregate quickly in the y direction. At time t = 0.25 s, all particles in the three right columns are collected in the middle of the domain. As the particles move close to each other, the interparticle electrostatic force plays a crucial role, driving the particles even closer to each other at a faster rate. Then, all three columns of particles aggregate and reach a stable position (where nearly all particles are collected) at about time t = 0.5 s. Note that all particles located at about $y = 1/2h$ move mostly along the x direction first, but after getting close to the plane x = 0, they move toward the corner where they remain after time t = 5s.

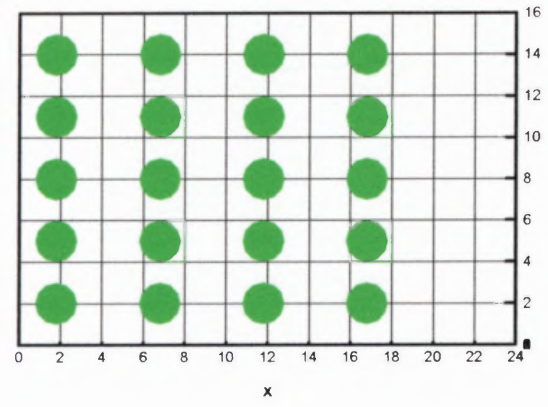

(a)

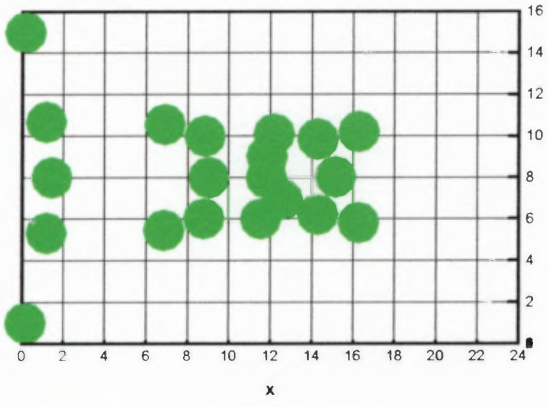

(b)

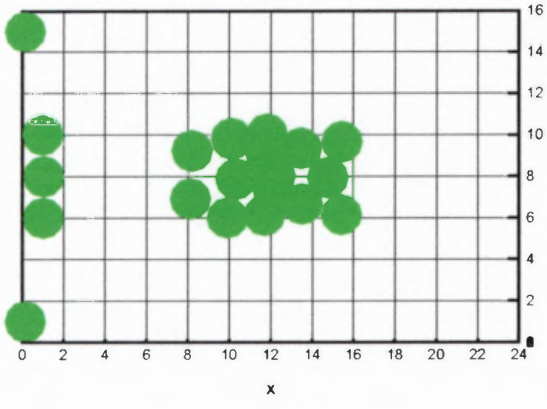

(c)

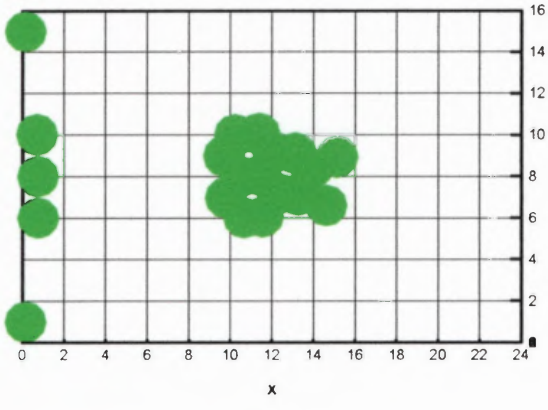

(d)

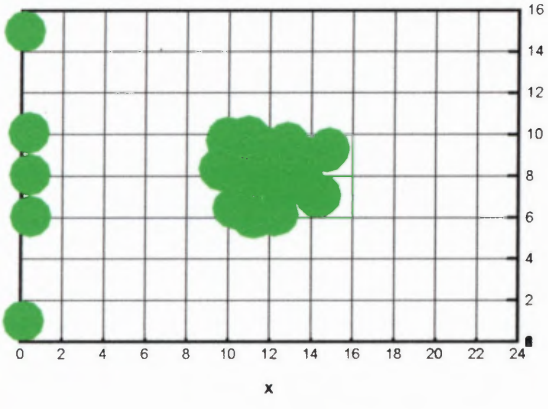

(e)

Figure 5.6 Instantaneous snapshots of the suspension computed by using the image method including the near-field interactions at the various times: (a) t = 0s; (b) t = 0.1s; (c) t = 0.25s; (d) t = 1s; (e) t = 2s. There is no pressure driven flow in this simulation.

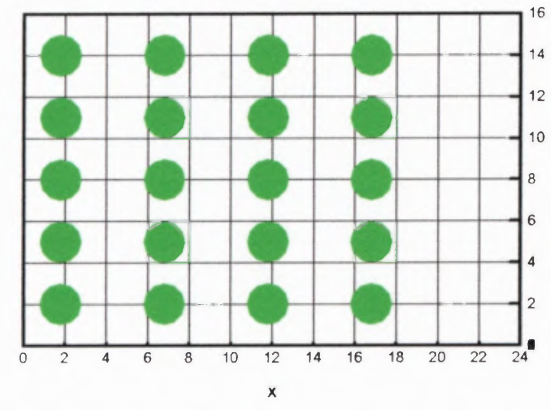

(a)

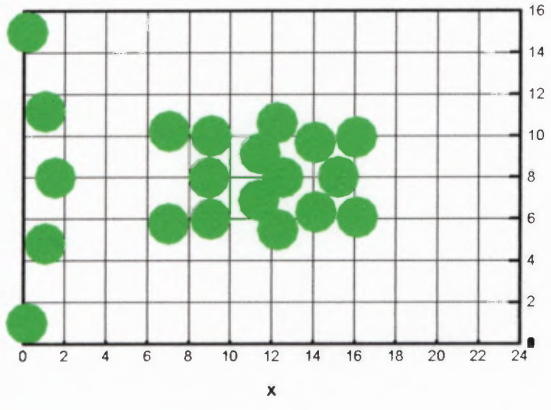

(b)

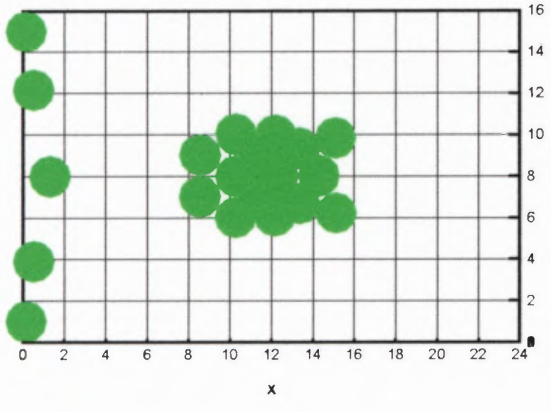

(c)

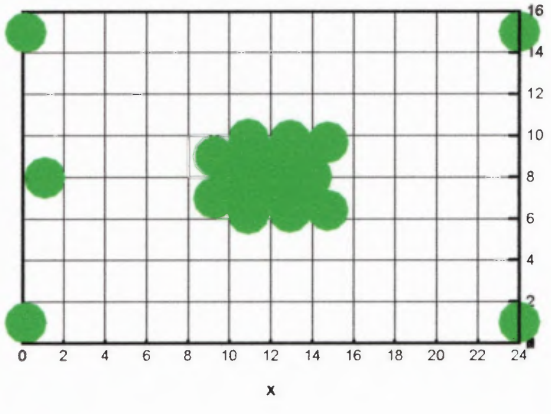

(d)

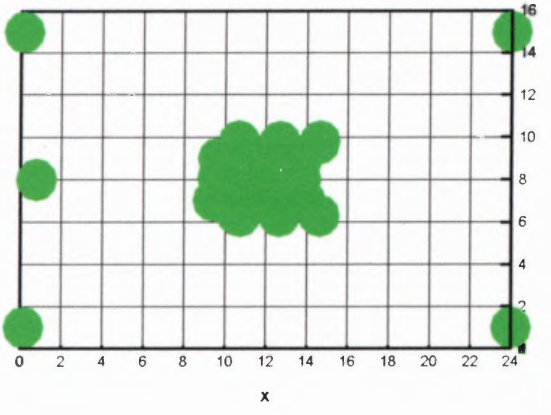

(e)

Figure 5.7 Instantaneous snapshots of the suspension computed by using the image method excluding the near-field interaction at the various times: (a) t = 0s; (b) t = 0.1s; (c) t = 0.25s; (d) t = 1s; (e) t = 2s. There is no pressure driven flow in this simulation.

Results of computations excluding the near-field effects are presented in Figure 5.7 at various times. At time t = 0.1s, similarly to what happened when near-field interactions were included, the particles in the upper and lower left corners move quickly to the local minimum of the electric field. However, the two particles near $y = 1/2\ l_y$ move to the corners separately, instead of moving close to the centerline $y = 1/2l_y$. At about t = 0.5s, the two particles reach the corners and then move to the next cell. The particle near $y = 1/2h$ move in the $-x$ direction while the particles in the second and third columns move to the center and then two bending chains pointing toward $x = 1/2l_x$ at t =0.1 s. At later times, the particles continue to aggregate and the collection ends at about at t = 0.5 s. A comparison of these transient snapshots of the suspension structures with and without the inclusion of the near-field interactions has been provided, showing that the near-field interactions do affect the motion of particles.

5.1.3 Negative DEP with dp/dx≠0

In this section, the effects of the fluid flow, combined with the effects of the near-field interactions, were studied in the case of β = -0.25. When the pressure gradient is non-zero, the fluid velocity cannot be neglected because the pressure difference between the inlet and outlet causes the fluid to move. The instantaneous particles distribution depends on the magnitude of the pressure gradient applied: if the pressure gradient is small, the bulk fluid velocity is small, and the particle motion will be nearly along the electrostatic force lines; on the other hand, if the pressure gradient is large, then the particle motion will have a non-negligible component along the fluid flow streamlines.

Figure 5.8 shows the results where the applied pressure gradient is 10 pascal/m (1 dyne/cm^3). The pressure gradient drives the fluid flow along the x direction. The particles

are placed initially in the same manner as in the previous computation. The instantaneous snapshots show that after the simulation is started, due to the weak pressure driven flow, the motion of the particles is similar to that in the previous section without any pressure gradient.

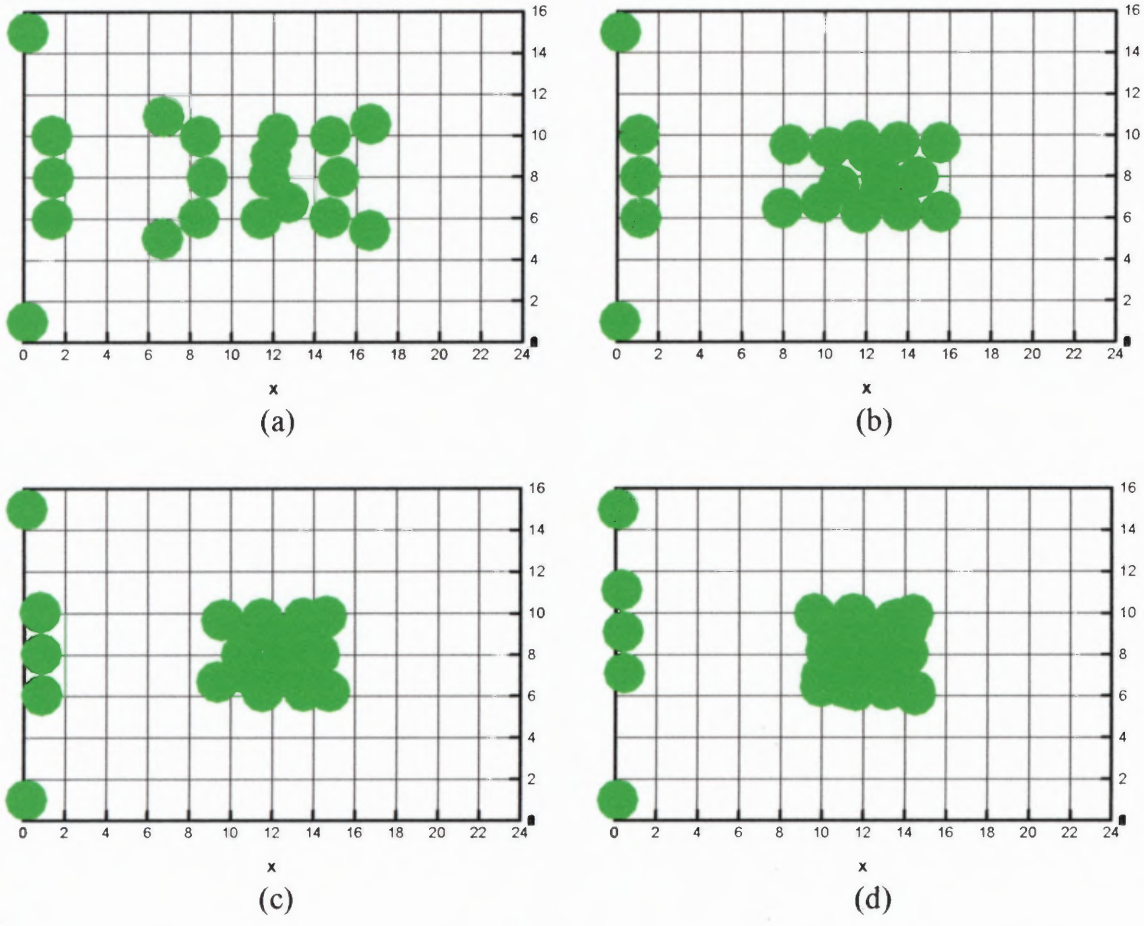

Figure 5.8 Instantaneous snapshots of the suspension structure with the inclusion of near-field interactions (image method) with pressure driven flow (dp/dx = 10 pas./m), at various times: (a) t = 0.1s; (b) t = 0.25s; (c) t = 0.5s; (d) t = 1s.

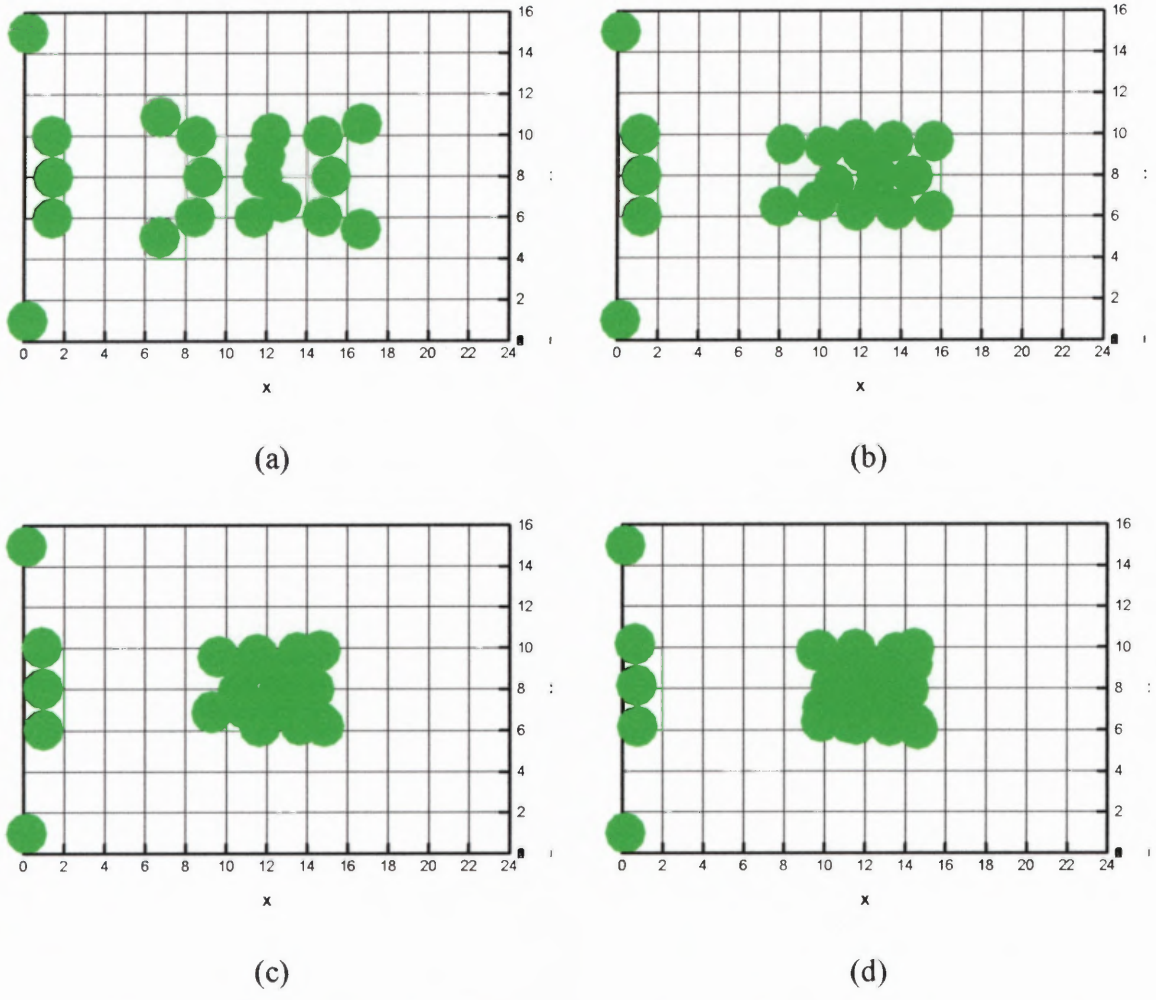

Figure 5.9 Instantaneous snapshots of the suspension structure with the inclusion of near-field interactions (image method) with pressure driven flow (dp/dx = 20 pas./m) at various times: (a) t = 0.1s; (b) t = 0.25s; (c) t = 0.5s; (d) t = 1s.

With the increase of the pressure gradient, the fluid flow velocity increases as well. Figure 5.9 shows the results when the imposed pressure gradient is 20 pascal/m (2 dyne/cm^3). At about time 0.1s, the particles on the left corners move toward the nearest corner, but the particles in the right three columns move to the center of the domain, as shown in previous simulations. The particles configurations in Figures 5.9(c) and (d) show the particles at time t = 0.5s and 1s. Particles in the right three columns continue to

aggregate at the center of the domain, but the three particles in the left column continue to move toward the left corner. Finally, at about 4s, all particles are collected.

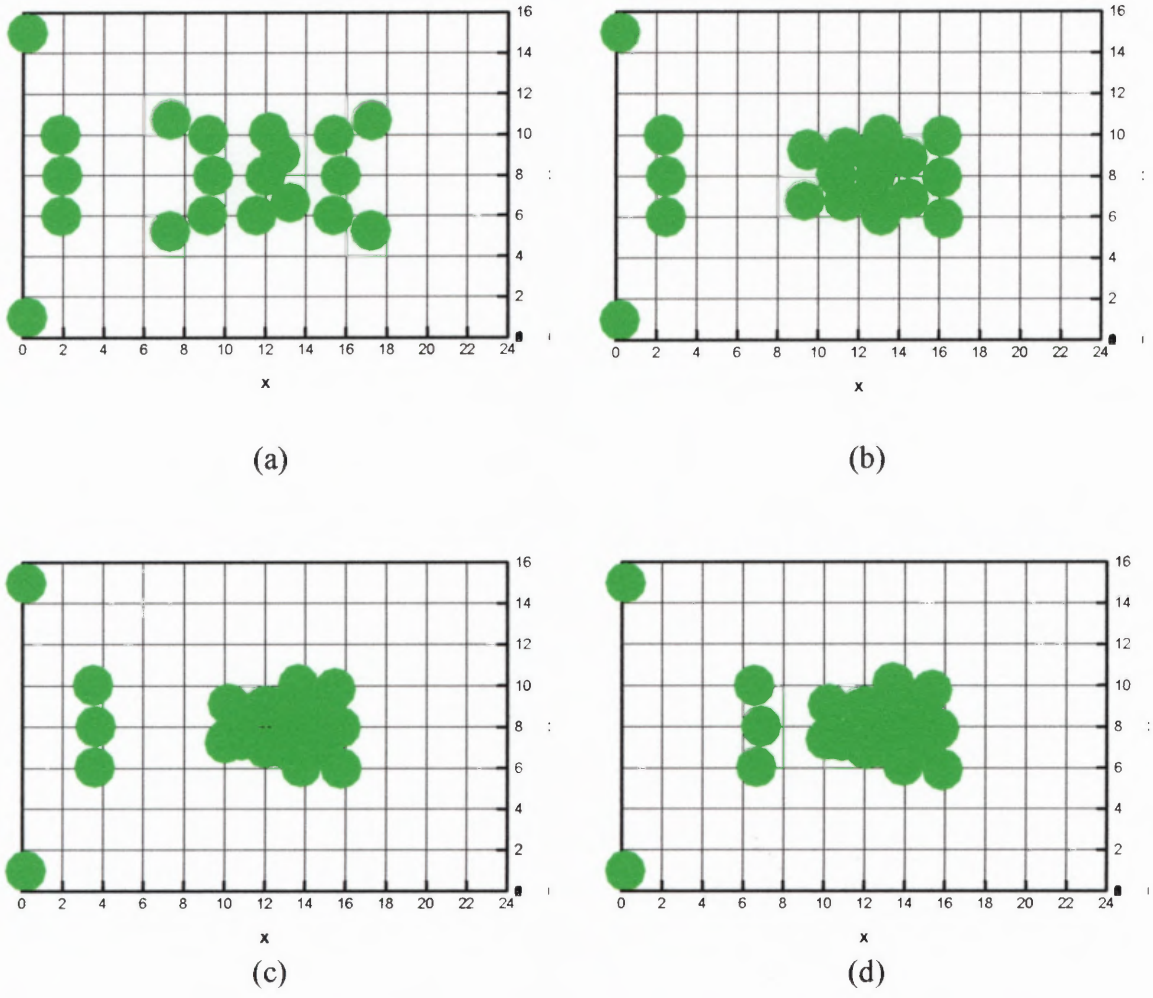

Figure 5.10 Instantaneous snapshots of the suspension structure with the inclusion of the near-field interactions (image method) with pressure driven flow (dp/dx = 200 pas./m) at various times: (a) t = 0.1s; (b) t = 0.25s; (c) t = 0.5s; (d) t = 1s.

When the pressure gradient is increased to 200 pascal/m (20 dyne/cm^3), the bulk fluid flow velocity is large. The particles located at the end of the left column move to toward the corners of the fluid domain, but all other particles move toward the center of

the cell. At about 1s, all particles are collected there, except for the particles in the corners.

5.1.4 Discussion

In this work, a colloidal suspension subjected to a non-uniform electric field has been simulated numerically the using the integral equation approach. The particles experience both a hydrodynamic interaction and an electrostatic force. The electrostatic force, including both dielectrophoretic interactions and particle-particle interactions with the inclusion of the near-field interactions, were introduced by using the multiple image method to compute the induced dipoles. Due to the fact that the capacitance matrix contains the contribution of the multi-body interactions, the derived force contains it too. In the case of negative dielectrophoresis, all particles get collected in the neighborhood of the local electric field minimum point.

5.2 Positive DEP

In this section, numerical simulations were performed in a computational space with dimensions 2.4mm by 1.6mm by 0.8mm in the x, y and z directions. Figure 5.11 shows the typical computational cell used in this section with its dimensions and the electrodes are located at y = 0mm and y = 2.4mm. The complete boundary conditions for the potential are as follows: on the electrode $\varphi = 0$ or 1 in dimensionless units, on the left-hand and right-hand edges $\partial\varphi / \partial n = 0$, and on the other edges between electrodes $\partial\varphi / \partial n = 0$. The length of each electrode is 0.6mm. The computational fluid domain is the same as that used in the negative DEP case while the electrodes are placed within the

walls, at a certain distance from the boundaries of the fluid domain, so that electrostatic interactions between particles and walls can be neglected.

5.2.1 Electric Field

The electrical potential and electric field lines are shown in Figure 5.12(a) and (b), while the $\mathbf{E} \cdot \nabla \mathbf{E}$ lines are displayed in Figure 5.13.

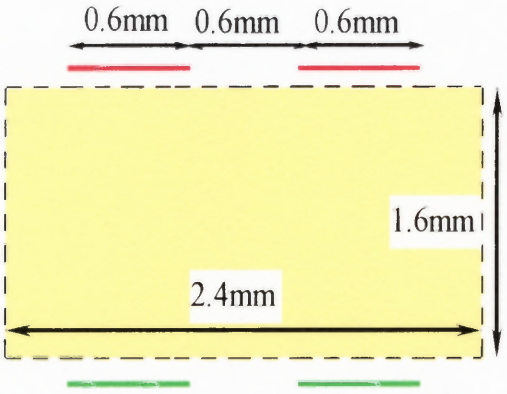

Figure 5.11 Sketch of the Computational Space for Positive DEP (not to scale).

The initial particle distribution can be observed in Figure 5.2: a total of 40 particles were placed in two layers with 20 particles in each layer along the *z* direction. In each layer in the *x*-*y* plane, 20 particles were placed in four columns along the *y* direction, with five particles in each column. Starting from the edge of the computational space, particles were evenly arranged at a distance of 0.5mm separating each particle from the next one (distance from particle center to particle center). The third column from the $x = 0$ edge is slightly lower than the middle line in the *x* direction. The fluid viscosity of the fluid is set to be constant, equal to $\eta = 0.1$ Pa.s and the particles are 0.2mm in diameter. The density of the particles is 1010 kg/m^3 and that of the fluid 1000 kg/m^3. The dielectric

constants of the particles and fluid are 26.6 and 13.3, respectively, giving a particle-to-fluid dielectric ratio $\alpha = 2.0$ and a factor $\beta = 0.25$.

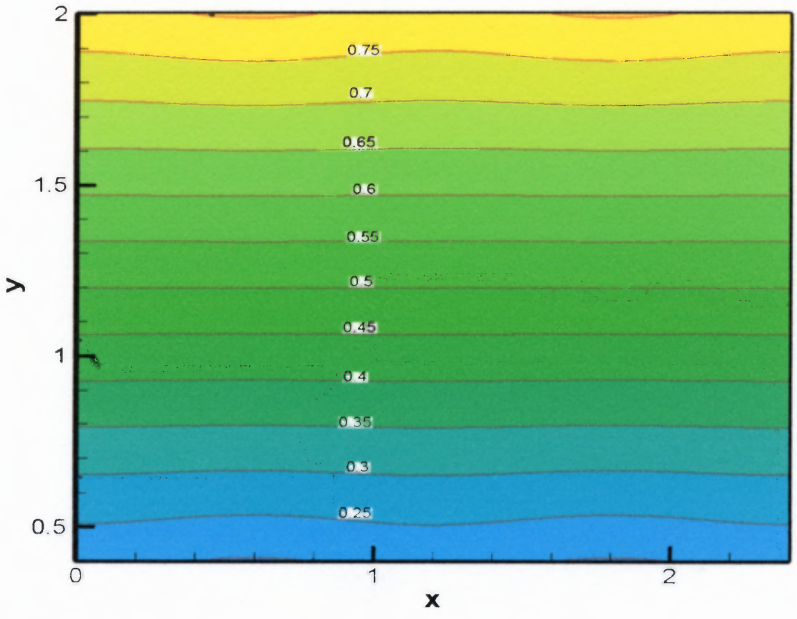

Figure 5.12 Contours of the dimensionless electric potential φ.

5.2.2 Positive DEP with dp/dx=0

The first simulation in this section was performed in the computational space shown in Figure 5.11 with time step $\Delta t = 5*10^{-4}$. Without pressure gradient, there is no bulk fluid flow.

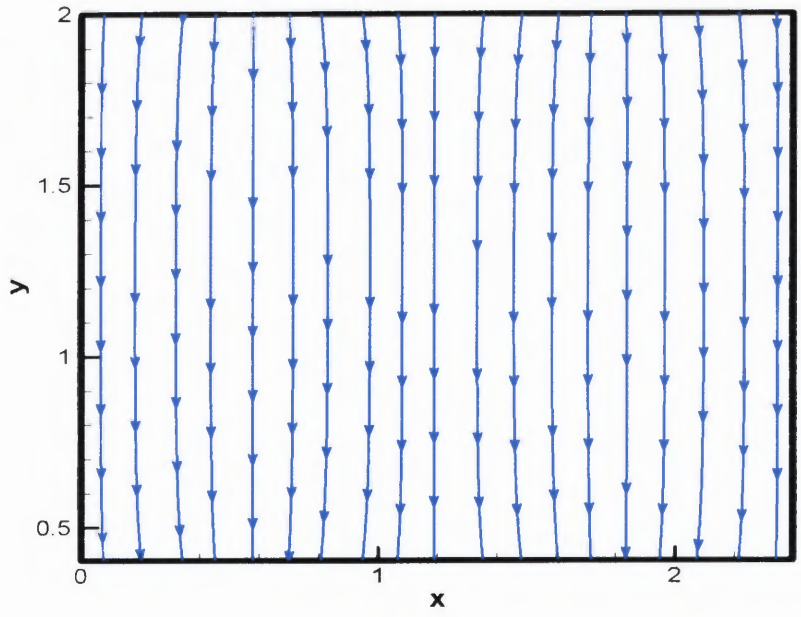

(a)

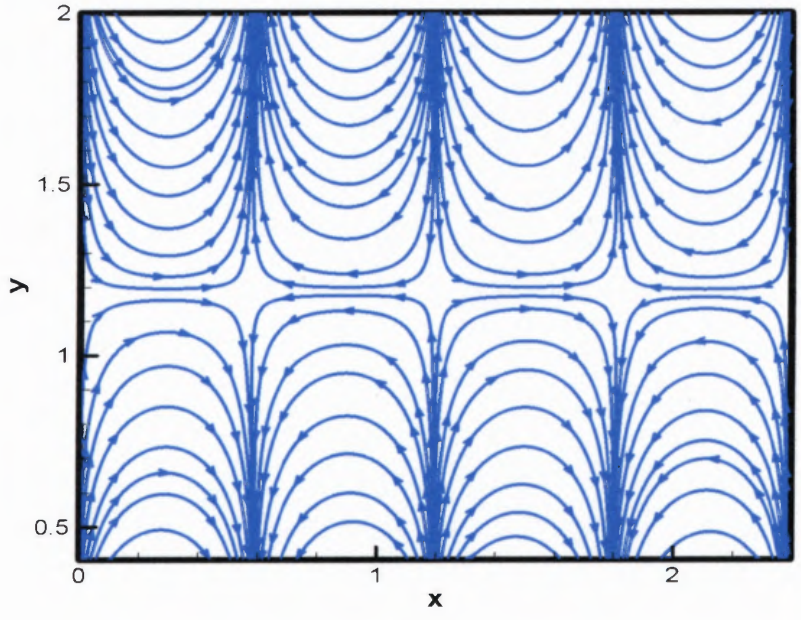

(b)

Figure 5.13 The solution of the Laplace equation. (a) Electric field **E** lines; (b) $\mathbf{E} \cdot \nabla \mathbf{E}$ (force) lines.

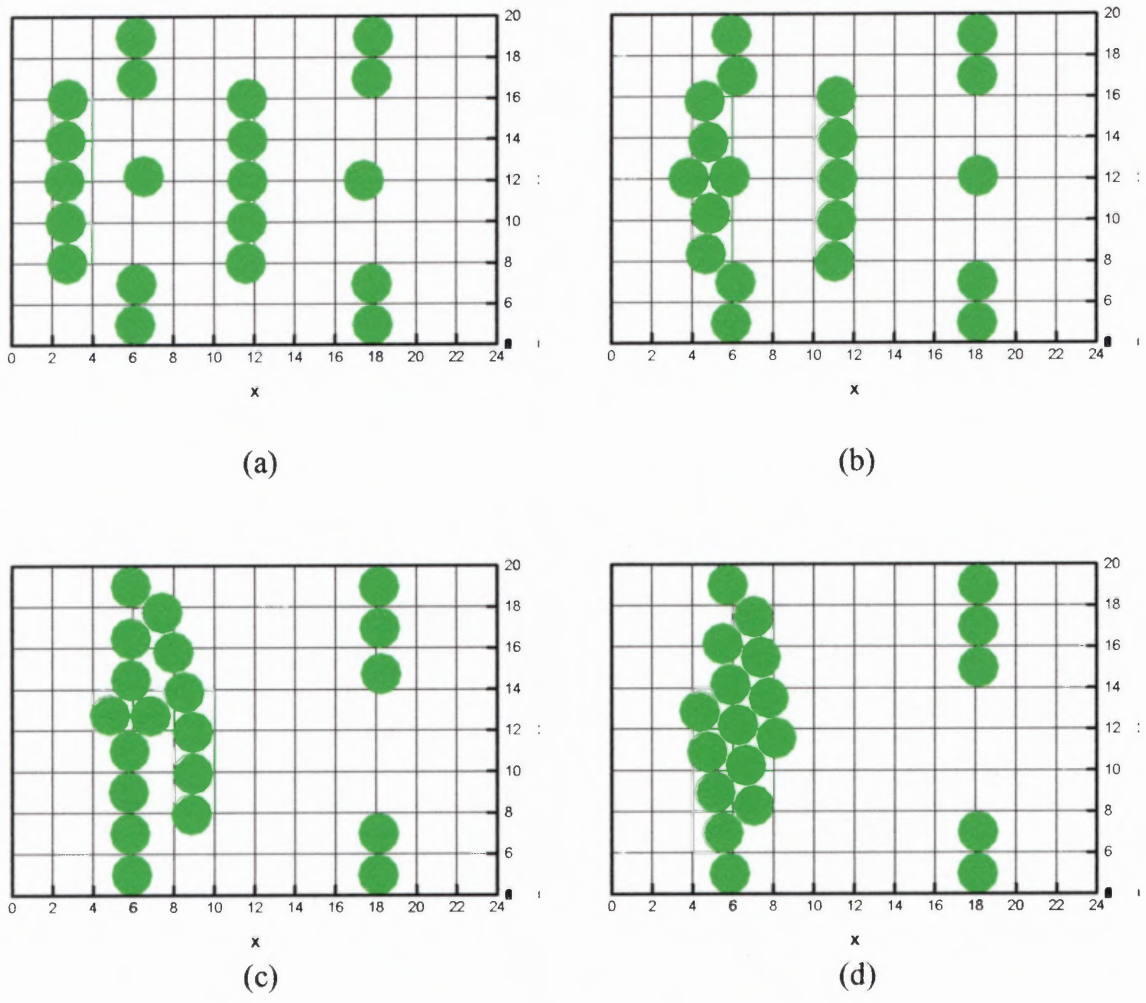

Figure 5.14 Instantaneous snapshots of the suspension structure with the inclusion of the near-field interactions (image method) without pressure driven flow at the various times: (a) t = 1s; (b) t = 3s; (c) t = 6s; (d) t = 10s.

Figure 5.14 (a)-(e) show the configuration of the suspension at various times. The instantaneous particles distributions were showed in Figure 5.14. At about time t = 1s, the particles in the left three columns gather together with the middle particle in their own column, and subsequently move to the middle of the first pair of electrodes. Note that the particles in the third column from the left, because they were placed initially slightly below the middle of the x direction, move to the middle of the first pair of electrodes. The

particles in the forth column, move to the second pair of electrodes. At time t = 6s, as shown in Figure 5.14(c), the particles in the left three columns start to aggregate along the middle line of the first pair of electrodes. Once the particles start to aggregate, they continue to do so as they undergo particle-particle interactions. At about time t = 8s, all particles are fully collected near the electrodes.

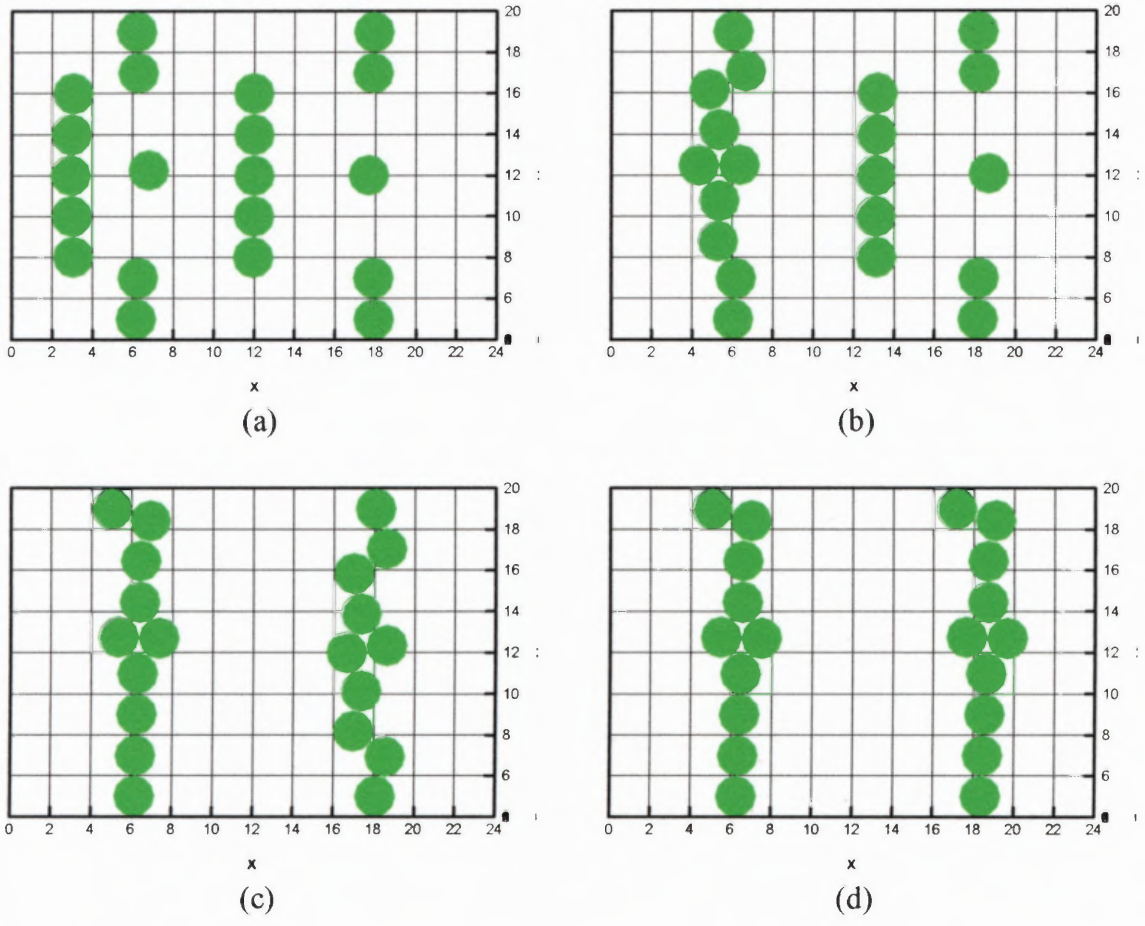

Figure 5.15 Instantaneous snapshots of the suspension structure, including the near-field interactions (image method) in presence of a pressure driven flow (dp/dx=10 pas./m) at various time: (a) t = 1s; (b) t = 3s; (c) t = 6s; (d) t = 10s.

5.2.3 Positive DEP with dp/dx≠0

In this section, the particles suspensions are studied in presence of different pressure gradients in the x direction. All other parameters are the same as in the previous section without the applied pressure gradient: the particle-to-fluid dielectric constant ratio is 2.0. The particles experience both a hydrodynamic force and an electrostatic force, where the latter includes the interaction between the field and the particles, as well as the interaction between the particles.

The first simulation of this section is performed with a pressure gradient of 10 pas./m (1 dyne/cm^3). The configurations of particles are shown in Figure 5.15 at the same times as those selected with no pressure gradient. Figure 5.15(a) shows that the configuration at time t = 1s is similar to that of Figure 5.14(a): the particles in the first and third columns move to the center due to the particle-particle interactions, and the particles in the second column move to the nearest electrodes. However, in the x direction, the particles in the third column move to the second pair of electrodes, instead of the first pair of electrodes due to the bulk fluid flow rate. As time increases, the particles in the first two columns continue to aggregate along the line connecting the centers of the first pair of electrodes. The third column continues to move toward the second pair of electrodes. Finally, one can observe two chains in the middle of the two pairs of electrodes at about t = 7s. At time t = 10s, the particles suspension has the similar structure, indicating that the two chains are stable after t = 7s.

The next simulation was performed with a pressure gradient of 20 pas./m (2 dyne/cm^3). All other parameters are kept the same. Simulations show that the suspension

has similar configurations as those previously described, but the different configurations occur at earlier times. Figure 5.16(c) and (d) show stable chains at about t = 6s.

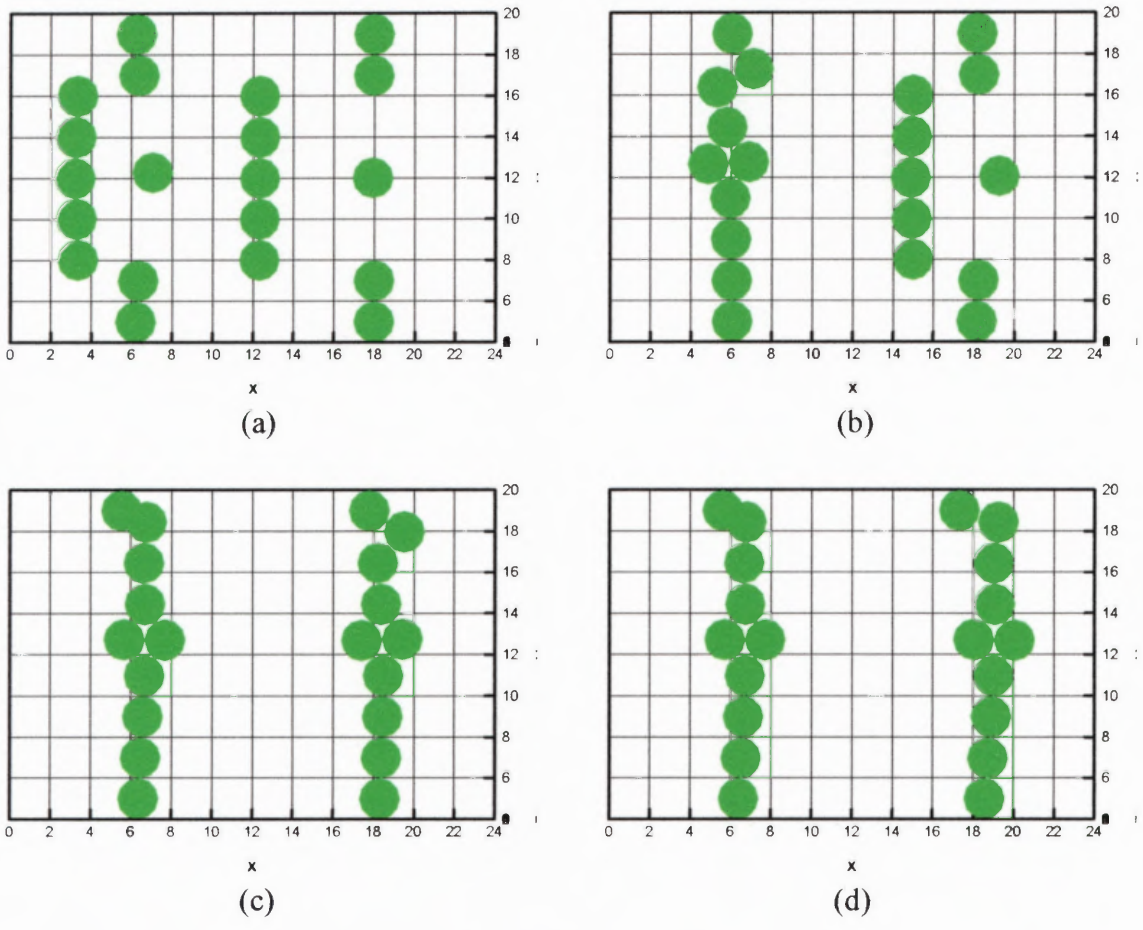

Figure 5.16 Instantaneous snapshots of the suspension structure, including the near-field interactions (image method) in presence of a pressure gradient (dp/dx=20 pas./m) at various times: (a) t = 1s; (b) t = 3s; (c) t = 6s; (d) t = 10s.

As the pressure gradient is further increased to 50 pas./m (5 dyne/cm^3), the simulation reported in Figure 5.17 shows that the particles are driven to the middle of the second and forth columns quickly, particularly due to the high flow velocity along the plane $y = 1/2l_y$. At about time t = 7.5s, these particles form two chains which eventually bend under the action of the flow velocity profile.

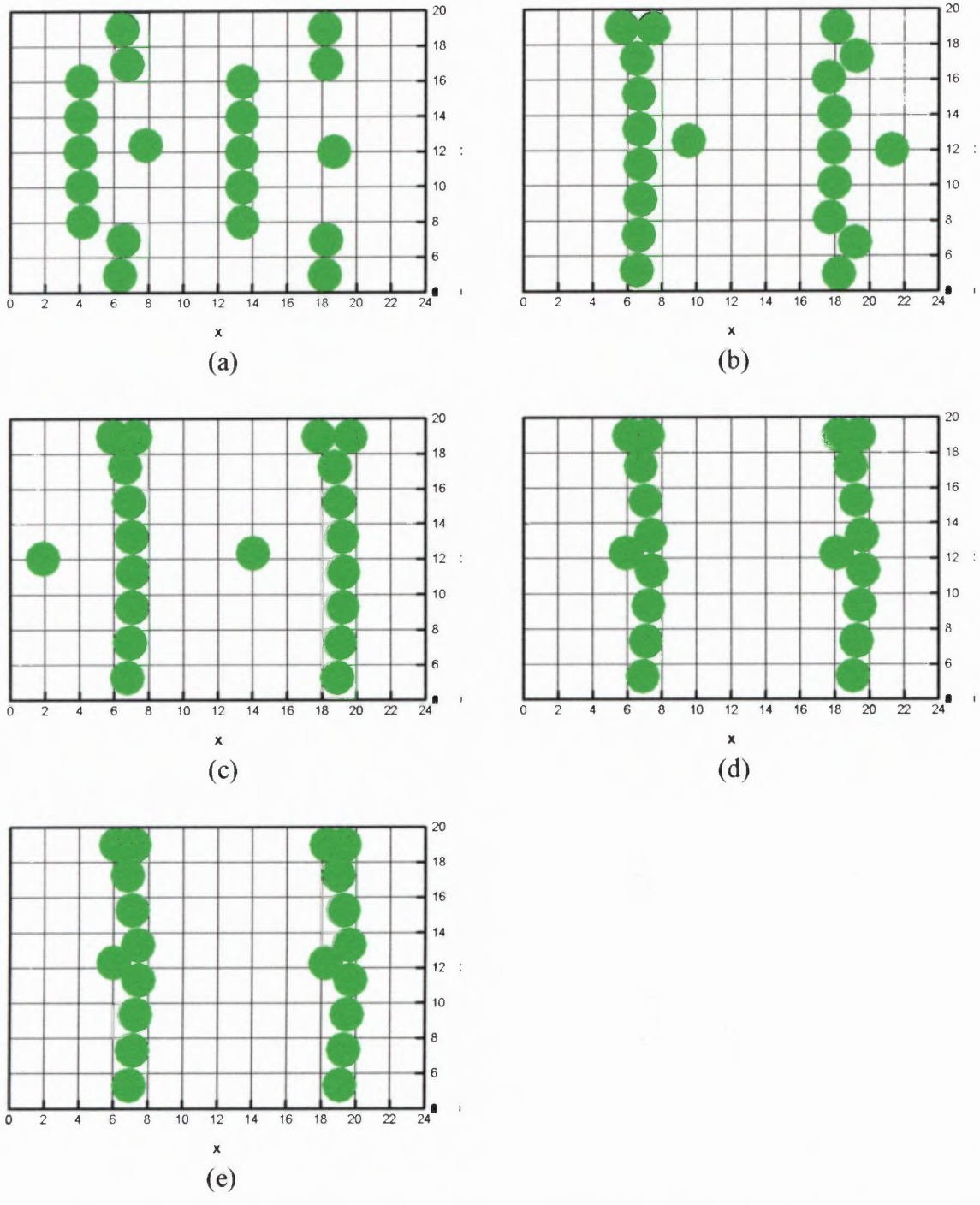

Figure 5.17 Instantaneous snapshots of the suspension structure, including the near-field interactions (image method) with the pressure driven flow (dp/dx=50 pas./m) at various times: (a) t = 1s; (b) t = 3s; (c) t = 6s; (d) t = 10s; (e) t = 15s.

5.2.4 Discussion

In this section multiparticles structures within suspensions subjected to a nonuniform electric field were studied numerically in the case where no pressure gradient was present as well as with an imposed pressure gradient. The effect of the strength of the latter was also investigated. The fluid velocity profile was assumed to be that of Poiseuille flow in a channel and thus the effect of the particles on the flow was neglected (this was justified by the fact that the suspension was very dilute (particles fraction less than 0.06)). In absence of pressure gradient, the three particles columns from the left were observed to chain together while the particles in the forth column was seen to chain separately. However, in presence of pressure gradients, the left two columns chained together, and so did the other two columns. The particles chained near the line connecting the middle points of the electrodes. The velocity of the fluid was seen to assist the forming of the chain structures.

5.3 Conclusions

In this Chapter, the multiparticles suspension structures were studied by means of a numerical method. The particles suspended in the fluid experienced both a hydrodynamic force and an electrostatic force. The hydrodynamic force consisted of Stokes viscous drag force, while the electrostatic force was computed from the differentiation of the electrostatic density of the system to include interactions both between the particles and the electric field, and between the particles. The near field effects were included by using the multiple image method applied to each pair of particles.

The simulations were performed with both positive and negative dielectrophoresis with or without the implied pressure gradient. The results showed that the fluid velocity assist the particles collecting or separating.

CHAPTER 6

CONCLUDING REMARKS AND RECOMMENDATIONS FOR FUTURE WORK

In this dissertation, a new numerical approach has been developed for simulating the motion of particles of suspensions subjected to spatially uniform and non uniform external electric fields. A suspended particle of the suspension experiences both hydrodynamic and electrostatic forces[100]. The former is calculated in the limit of zero Reynolds number by using the Stokes drag law, which assumes that the particle is isolated. The electrostatic force on a particle is determined by differentiating the electrostatic energy of the system with respect to the particle position. The integral form of the Laplace equation is first used to obtain the induced charges and dipole moments from the grand capacitance matrix, which are then used to obtain the electrostatic energy.

In the case of two particles placed in a uniform electric field, the electrostatic force acting on the particles is computed using the multiple image method and also by directly integrating the Maxwell stress tensor over the particles surfaces[101,105]. The latter requires the solution of the Laplace equation which is obtained in the bipolar coordinates. The force given by the two methods are found to be approximately equal, and also match the published values for a wide range of dielectric constant ratios.

In a nonuniform electric field, the total electrostatic force acting on a particle can be divided into two distinct contributions[43,100,102,105]. The first depends on the spatial non uniformity of the electric field and the second on the interactions among the polarized particles. The multiple image method is applied to obtain the dipole moments of the particles which are then used to construct the near field solution for two particles. This

multiple image near-field solution for two particles is used to account for the near-field effects in suspensions containing two or more particles. At present the multiple image method is not implemented to account for boundaries and electrodes. This, however, can be included and is essential when the particles approach the electrodes or the device walls.

The dynamical motion of particles suspended in a channel is simulated numerically for the cases when the channel is subjected to a pressure gradient and also when the pressure gradient is not applied[61,100]. Simulations show that when the applied pressure gradient is not zero the induced bulk fluid velocity in the channel reduces the time interval in which particles collect in the low or high electric field regions, depending on their dielectric constant relative to that of the fluid. In a nonuniform electric field, the particles form chains, which bend when a pressure gradient is applied.

In this dissertation, simulations were performed in a relatively simple geometry, i.e., in a channel with a rectangular cross-section. The electrodes were considered to be of the same size as the width of the channel. The approach developed in this dissertation, however, can be used in other more complex flow geometries that are of interest in various applications of dielectrophoresis.

In recent years, many new applications of dielectrophoresis have been developed, including in the areas of the biotechnology and nanotechnology[99,102-104]. The method developed in this dissertation will be helpful in both improving designs of dielectrophoretic devices, as well as for understanding the dynamical behavior of particles in these devices.

REFERENCES

[1] Winslow, W. M., 1949. Induced Fibration of Suspensions, *J. Appl. Phys.*, **20**, pp. 1137-1140.

[2] Pohl, H. A., 1978. *Dielectrophoresis*: The Behavior of Neutral Matter in Nonuniform Electric Fields, Cambrige(UK): Cambridge University Press.

[3] Jones, T. B., 1995. *Electromechanics of particles*, New York: Cambridge University Press.

[4] Wang, X-B, Huang, Y., Becker, F. F. and Gascoyne, P. R. C., 1991. A unified theory of dielectrophoresis and travelling wave dielectrophoresis. *J. physics D: applied physics*. **23**, pp. 1571-1574.

[5] Gascoyne, P. R. C. and Wang, X-B, 1997. Dielectrophoretic separation of cancer cells from blood. *IEEE transactions on industry applications*, **33**(3), pp. 670-678.

[6] Medoroy, G., N. Manaresiy, M. Tartagniz and R. Guerrieriz, CMOS-only sensors and manipulators for microorganisms, IEEE International Electron Devices Meeting (IEDM), December, 2000, pp. 415 -418.

[7] Ramos, A., Morgan, H., Green, N. G. and Castellanos, A., 1998. AC electrokinetics: a review of forces in microelectrode structures, *J. phys. D: applied physics*, **31**, pp. 2338-2353.

[8] Green, N. G., Ramos, A. and Morgan, H., 2000. AC electrokinetics: a survey of sub-micrometre particle dynamics, *J. phys. D: applied physics*, **33**, pp. 632-641.

[9] Dielectric material, Retrieved October 29, 2005 from the World Wide Web: http://whatis.techtarget.com/definition/0,,sid9_gci211945,00.html

[10] Dielectric Constant. Retrieved October 29, 2005 from the World Wide Web: http://scienceworld.wolfram.com/physics/DielectricConstant.html.

[11] Dipole Moment. Retrieved October 29, 2005 from the World Wide Web: http://hyperphysics.phy-astr.gsu.edu/hbase/electric/dipole.html.

[12] Morris, J.F., Brady, J.F., 1998. Pressure-driven flow of a suspension: buoyancy effects, *International Journal of Multiphase Flow*, **24**(1), pp. 105-130.

[13] Gast, A. P. and Zukoski, A. F., 1989. Electrorheological Fluids as Colloidal suspensions, *Advances in Colloid and Interface Science*, **30**, pp. 153-202.

[14] Parthasarathy, M., Klingerberg, D., 1996. Electrorheology: Mechanisms and models, *Materials Science and Engineering*, **R17**, pp. 57-103.

[15] Jordan, T. and Shaw, M., 1989. Electrorheology, *IEEE Transactions on Electrical Insulation*, **24**(5), pp. 849-878.

[16] Hao, T., 2002. Electrorheological Suspensions, *Advances in Colloid and Interface Science*, **97**, pp. 1-35.

[17] Rosensweig, R. E., 1985. *Ferrohydrodynamics*, Cambridge: Cambridge University Press, England.

[18] Bonnecaze, R. T., and Brady, J. F., 1992. Dynamic Simulation of an Electrorheological Fluid, *J. Chem. Phys.*, **96**(3), pp. 2183-2202.

[19] Batchelor, G.K., 1970, The stress system in a suspension of force-free particles, *J.Fluid Mech.*, **41**, 545-570.

[20] Batchelor, G.K., 1971. The stress generated in a non-dilute suspension of elongated particles by pure straining motion', *J.Fluid Mech.*, **44**, pp. 813-829.

[21] Uejima, H., 1972. Dielectric Mechanism and Rheological Properties of Electrofluids, *Japanese Journal of Applied Physics*, **11**, pp. 319–326.

[22] Marshall, L., J. W. Goodwin, and C. F. Zukoski, 1989. Effects of electric fields on the rheology of nonaqueous concentrated suspensions. *J. Chem. Sot. Faraday I* **85**, pp. 2785-2793.

[23] M. von Smoluchowski, 1916. Theoretische Bemerkungen uber die Viskositiit der Kolloide. *Kolloid. Zh.*, **18**, pp. 190-195.

[24] Klingenberg, D., Zukoski, C. and Hill, J., 1993. Kinetics of Structure formation in electrorheological suspensions. *J. Appl. Phys.* **73**(9), pp. 4644-4648.

[25] Bossis, G., Meunier, A., and Brady, J.F., 1991. Hydrodynamic stress on fractal aggregates of spheres. *J. Chem. Phys.* **94**, pp. 5064-5070.

[26] Bonnecaze, R.T. and Brady, J.F., 1992. Yield stresses in electrorheological fluids. *J. Rheol.* **36**, pp. 73-115.

[27] Brady, J. F., 1993. The rheological behavior of concentrated colloidal dispersions. *J. Chem. Phys.* **99**, pp. 567-581.

[28] Klingenberg, D., Zukoski, C., 1990. Studies on the Steady Shear Behavior of Electrorheological Suspensions," *Langmuir*, **6**, pp. 15-23.

[29] Klingenberg, D., Swol, F., and Zukoski, C., 1989. Dynamic simulation of electrorheological suspensions, *J. Chem. Phys.* **91**(12), pp. 7888-7895.

[30] Klingenberg, D., Swol, F., and Zukoski, C., 1991. The small shear rate response of electrorheological suspensions, I. Simulation in the point-dipole limit, *J. Chem. Phys.* **94**(9), pp. 6160-6169.

[31] Klingenberg, D., Swol, F., and Zukoski, C., 1991. The small shear rate response of electrorheological suspensions, II. Extension beyond the point-dipole limit, *J. Chem. Phys.* **94**(9), pp. 6170-6178.

[32] Anderson, R. A., 1994. Electrostatic Forces in an ideal spherical-particle electrorheological fluid, *Langmuir*, **10**, pp. 2917-2928.

[33] Whittle, M., 1990. Computer Simulation of an Electrorheological Fluid, *J. Non-Newtonian fluid mechanics*, **37**(2-3), pp. 233-263.

[34] Yu, K. W., and Wan, J. T. K., 2000. Interparticle force in polydisperse electrorheological fluids. *Computer physics communications*, **129**, pp. 177-184.

[35] Huang, J. P., Karttunen, M., Yu, K. W., Dong, L., and Gu, G. Q., 2004. Electrokinetic behavior of two touching inhomogeneous biological cells and colloidal particles: Effects of multipolar interactions, *Phys. Rev. E* **69**, 051402

[36] Gao, L., Huang, J. P., and Yu, K. W., 2003, Theory of ac electrokinetic behavior of spheroidal cell suspensions with an intrinsic dispersion, *Phys. Rev. E* **67**, 021910.

[37] Bonnecaze, R. T. and Brady, J. F., 1990. A Method for Determining the Effective Conductivity of Dispersions of Particles, *Proceedings: Mathematical and Physical Sciences*, **430**(1879), pp. 285-313.

[38] Bonnecaze, R. T. and Brady, J. F., 1991. The Effective Conductivity of Random Suspensions of Spherical Particles, *Proceedings: Mathematical and Physical Sciences*, **432**(1886), pp. 445-465.

[39] Davis, L., 1992. Finite-element analysis of particle-particle forces in electrorheological fluids. *Applied Physics Letters*, **60**(3), pp. 319-324.

[40] Davis, L., 1992. Polarization forces and conductivity effects in electrorheological fluids, *Journal of Applied Physics*, **72**(4), pp. 1334-1343.

[41] Anderson, R. A., 1991, in Electrorheological Fluids, Mechanisms, Properties, Structure, Technology, and Applications, *Proc. of the Int. Conf. on Electrorheological Fluids*, Carbondale, IL, World Scientific, Singapore, 1992. (Ed. by R. Tao)

[42] Jones, T.B., Kallio, G.A., 1979. Dielectrophoretic levitation of spheres and shells, *J. Electrostatics*, **6**, pp. 207-224.

[43] Kadaksham, J., Singh, P. and Aubry, N, 2005. Dielectrophoresis induced clustering regimes of viable yeast cells, Electrophoresis 26, pp. 3738-3744, 2005.

[44] Wu, C.W., and Conrad, H., 1997. Dielectric and conduction effects in ohmic electrorheological fluids, *J. Phys. D: Appl. Phys.* **30,** pp. 2634-2642.

[45] Felici, N., Foulc, J., and Atten, P., in Electrorheological Fluids, Mechanisms, Properties, Structure, Technology, and Applications, *Proc. of the Fourth Int. Conf. on Electrorheological Fluids*, Feldkirch, Austria, World Scientific, Singapore, 1993. (Ed. by R. Tao)

[46] Foulc, J., and Atten, P., and Felici, N., 1994. Macroscopic model of interaction between particles in an electrorheological fluid, *Journal of Electrostatics*, **33**(1), pp. 103-112.

[47] Melli-Huber, J., Weinberg, B., Fisch, A., Nikitczuk, J., Mavroidis, C., Wampler C., "Electro-Rheological Fluidic Actuators for Haptic Vehicular Instrument Controls", *Proceedings of the Eleventh Symposium on Haptic Interfaces for Virtual Environment and Teleoperator Systems*, March 22 and 23, 2003, Los Angeles, CA.

[48] Mannesmann VDO AG Information Systems, Programmable Rotating Actuator with Haptic Feedback, product description. Retrieved October 29, 2005, from the World Wide Web: www.vdo.com.

[49] Kuenzner, H. et al., Operating Device for Menu Controlled Functions of a Vehicle, US005,956,016, September 1999.

[50] Abu-Jdayil, B., Brunn, P., 2002. Effect of Electrode Morphology on the Behaviour of Electrorheological Fluids in Torsional Flow, *Journal of Intelligent Material Systems and Structures*, **13**(1), pp. 3-11.

[51] Sakaguchi, M. and Furusho, J., Force Display System Using Particle-Type Electrorheological Fluids. *Proceedings of the 1998 IEEE International Conference on Robotics and Automation,* Leuven, Belgium, May 1998a, pp. 2586-2590.

[52] Takesue, N., G. Zhang, J. Furusho and M. Sakaguchi, 1999. Precise Position Control of Robot Arms Using a Homogeneous ER Fluid, *IEEE Control Systems Magazine*, **19**(2), pp. 55-61.

[53] Choi, Y., Bitman, L., and Wereley, N., 2005. Nondimensional Analysis of Electrorheological Dampers using an Eyring Constitutive Relationship, *Journal of Intelligent Material Systems and Structures*, **16**(5), pp. 383-394.

[54] Voyles, R., Fedder, G., and Khosla, P., Design of a Modular Tactile Sensor and Actuator Based on an Electrorheological Gel, *In Proceedings of the 1996 IEEE International Conference on Robotics and Automation*, Minneapolis, MN, April 1996.

[55] Furusho, J. et al., Force Display Device Using ER Fluid, Retrieved October 29, 2005, from the World Wide Web: http://www-dyna.mech.eng.osaka-u.ac.jp/Lab/research/force_display-e.html

[56] Lou, Zheng; Ervin, Robert D.; Filisko, Frank E.; Winkler, Christopher B., 1999. Electrorheological rotary pure-shear damping devices, United States Patent 5992582.

[57] Tao, R., Electro- and Magneto-Rheological Fluid: A New Smart Fluid, The American Physical Society meeting, BAPSMAR97, 1997, Kansas City, MO.

[58] Smart Materials: A Technology & Market Assessment, Retrieved October 29, 2005, from the World Wide Web: http://bcc.ecnext.com/coms2/summary_0279-247344_ITM

[59] Jones, T.b., Electromechanics of Particles, Cambridge University Press, New York City, NY, 1995.

[60] Morgan, H., and N. G. Green. 1997. Dielectrophoretic manipulation of rod-shaped viral particles. *J. Electrostatics.* **42**, pp. 279-293.

[61] Kadaksham, J., Singh, P. and Aubry, N., 2004. Dynamics of electrorheological suspensions subjected to spatially nonuniform electric field, Journal of Fluids Engineering, **126**, pp. 170-179.

[62] Dong L., Huang, J.P., and Yu, K.W., 2004. Theory of dielectrophoresis in colloidal suspensions. *Journal of applied physics*, **95**(12), pp. 8321-8326.

[63] Jones, T. B., and Washizu, M., 1996. Multipolar Dielectrophoretic and Electrorotation Theory. *J. of Electrostatics*, **37**, pp. 121-134.

[64] Senda, M., J. Takeda, S. Abe and T. Nakamura, 1979. Induction of cell fusion of plant protoplasts by electrical stimulation. *Plant Cell Physiology,* **20**, pp. 1441-1445.

[65] Zimmermann, U., and J. Vienken, 1982. Electric field induced cell-to-cell fusion, *J. Membrane Biological*, **67**, pp. 165-182.

[66] Zimmermann, U., J. Vienken, and G. Pilwat, 1984, Electrofusion of cells, in Investigative Microtechniques in Medicine and Biology, New York: Marcel Dekker (ed. by J. Chayen and L. Bitensky).

[67] Zimmermann, U., 1986. Electrical Breakdown, Electropermeabilization and Electrofusion, *Rev. Physiol. Biochem. Pharmacol.*, **105**, pp. 175-256.

[68] Washizu, M., 1990. Electrostatic manipulation of biological objects. *J. Electrostatic*, **25**, pp. 109-123.

[69] Washizu, M., and O. Kurosawa. 1990. Electrostatic manipulation of DNA in microfabricated structures. *IEEE Trans. Ind. Appl.* **26**, pp. 1165-1172.

[70] Washizu, M., S. Suzuki, O. Kurosawa, T. Nishizaka, and T. Shinohara. 1994. Molecular dielectrophoresis of biopolymers. *IEEE Trans. Ind. Appl.* **30**, pp. 835-843.

[71] Washizu, M., O. Kurosawa, I. Arai, S. Suzuki, and N. Shimamoto. 1995. Applications of electrostatic stretch-and-positioning of DNA. *IEEE Trans. Ind. Appl.* **31**, pp. 447-456.

[72] Morgan, H., Hughes, M.P., and Green, N.G., 1999, Separation of Submicron Bioparticles by Dielectrophoresis, *Biophys J.*, 77(1), pp. 516-525.

[73] Abe, M., Orita, M., Yamazaki, H.,Tsukamoto, S., Teshima, Y., Sakai, T., Ohkubo, T., Momozawa, N., and Sakai, H., 2004, Three-Dimensional Arrangements of Polystyrene Latex Particles with a Hyperbolic Quadruple Electrode System, *Langmuir,* **20** (12), pp. 5046 -5051.

[74] Hughes, M.P., AC Electrokinetics: Applications for Nanotechnology, The Seventh Foresight Conference on Molecular Nanotechnology, 1999, Santa Clara, CA.

[75] Gascoyne, P.R.C., And Vykoukal, J.V., Dielectrophoresis-Based Sample Handling In General-Purpose Programmable Diagnostic Instruments, *Proceedings Of The IEEE*, **92**(1), 2004.

[76] Paradis, P., Yu, J., Ishikawa, T., and Yoda, S., 2004. Property Measurements and Solidification Studies by Electrostatic Levitation, *Ann. N.Y. Acad. Sci.* **1027,** pp. 464–473.

[77] Green, N.G., Morgan, H., 1997. Dielectrophoretic separation of nano-particles. *J. Phys. D: Appl. Phys.* **30**, pp. L41–L44.

[78] Green, N.G., Morgan, H., 1997. Dielectrophoretic investigations of sub-micrometre latex spheres. *J. Phys. D: Appl. Phys.* **30**, pp. 2626–2633.

[79] Green, N.G., Morgan, H., 1998. Separation of submicrometre particles using a combination of dielectrophoretic and electrohydrodynamic forces. *J. Phys. D: Appl. Phys.* **31**, pp. L25–L30.

[80] Morgan, H; Green, N. G., AC Electrokinetics: Colloids and Nanoparticles, 2003. Research Studies Press Ltd., Baldock, England.

[81] Dewarrat, F., M. Calame, C. Schönenberger, 2002. Orientation and Positioning of DNA Molecules with an Electric Field Technique, *Single Molecules*, **3**(4), pp. 189-193.

[82] Medoro, G., N. Manaresi, A. Leonardi, L. Altomare, M. Tartagni and R. Guerrieri, A Lab-on-a-chip For Cell Detection And Manipulation, IEEE Sensors Conference 2002, June, 2002.

[83] Medoro, G., N. Manaresi, M. Tartagni, L. Altomare, A. Leonardi and R. Guerrieri, A Lab-on-a-chip for Cell Separation Based on the Moving-Cages Approach, Eurosensors XVI, September, 2002.

[84] Manaresi, N., A Romani, G. Medoro, L. Altomare, A. Leonardi, M. Tartagni and R. Guerrieri, A CMOS Chip for Individual Cell Manipulation and Detection, ISSCC 2003, February, 2003, pp. 192-193, 487.

[85] Choi, S., and Park, J., 2005. Microfluidic system for dielectrophoretic separation based on a trapezoidal electrode array, *Lab on a Chip*, **5**(10), pp. 1161 – 1167.

[86] Hatfield, H.S., 1924. Dielectric separation: a new method for the treatment of ores, *Trans. Inst. Mining. Met. Engrs.*, **33**, pp. 335-342.

[87] K. Goossens, and L. Van Biesen, 1990. Dielectrophoretic Characterization of particles of geological origin, Inter. Geoscience and Remote Sensing Symposium IEEE-IGARSS, Washington (U.S.A.), May 20-24, pp. 999-1003.

[88] Lumsdon, S., Eric W. Kaler, and Orlin D. Velev, 2004. Two-Dimensional Crystallization of Microspheres by a Coplanar AC Electric Field, *Langmuir* **20**, pp. 2108-2116.

[89] Lumsdon, S. and Eric W. Kaler, Jacob P. Williams, Orlin D. Velev, 2003. Dielectrophoretic assembly of oriented and switchable two-dimensional photonic crystals, *Applied Physics Letters*, **2**(6), pp. 949-951.

[90] Washizu, M., Y. Iochi, H. Kurosawa, O. Aizawa, S.-i. Kudo, S. Magariyama, Y. Hotani, H., Dielectrophoretic measurement of bacterial motor characteristics, Industry Applications Society Annual Meeting, 1991, Conference Record of the 1991 IEEE, **1**, pp. 665-673.

[91] Reddy, N.J., Introduction to the Finite Element Method, McGraw-Hill Science/Engineering/Math, second edition, 1993.

[92] Silvester, P., 1969, High-order polynomial Triangular Finite Elements for Potential Problems, *Int. J. Engng. Sci.*, 7, pp. 849-861.

[93] Patankar, S. V., Numerical Heat Transfer and Fluid Flow, Hemisphere, Washington, DC, 1980.

[94] Patankar, S.V., 1981. A Calculation Procedure for Two-Dimensional Elliptic Situations, *Numer. Heat Transfer*, **4**, pp. 409-425.

[95] Jeffrey, D. J., 1973. Conduction Through a Random Suspension of Spheres, *Proceedings of the Royal Society of London. Series A, Mathematical and Physical Sciences*, **335**(1602), pp. 355-367.

[96] Jeffrey, D. J., 1974. Group Expansions for the bulk properties of a statistically Homogeneous, random suspension, *Proceedings of the Royal Society of London. Series A, Mathematical and Physical Sciences*, **338**(1615), pp. 503-516.

[97] Jackson, John David, Classical electrodynamics, New York: Wiley, c1999.

[98] O'Brien, R. W., 1979. A Method for the Calculation of the Effective Transport Properties of Suspensions of Interacting Particles, *J. Fluid Mech.*, **91**, pp. 17-39.

[99] Kadaksham, J., Singh, P. and Aubry, N., 2004. Dielectrophoresis of nanoparticles, *Electrophoresis*, **25**, pp. 3625-3632.

[100] Kadaksham, J., Singh, P. and Aubry, N., 2006. Manipulation of particles using dielectrophoresis, *Mechanics Research Communications*, **33**, pp. 108-122.

[101] Singh, P. and Aubry, N., 2005. Trapping force on a finite sized particle in a dielectrophoretic cage, *Physical Review E* **72**, 016602.

[102] Aubry, N. and Singh, P., 2005. Influence of particle-particle interactions and particle rotational motions in traveling wave dielectrophoresis, *Electrophoresis*, **26**.(To appear)

[103] Ben-Abdallah, P, Ni, B., Ould El Moctar, A., Aubry, N. and Singh, P., 2005. Tunneling control of neutral particles in suspension in nanofluidic flow, *Journal of Applied Physics*(To appear).

[104] Batton, J., Kadaksham, J., Nzihou, A., Singh, P. and Aubry, N., 2005. Trapping heavy metals by using calcium hydroxyapatite and dielectrophoresis, *Journal of Hazardous Materials*(To appear).

[105] Aubry, N. and Singh. P., Control of electrostatic particle-particle interactions in dielectrophoresis, Submitted, 2005.